

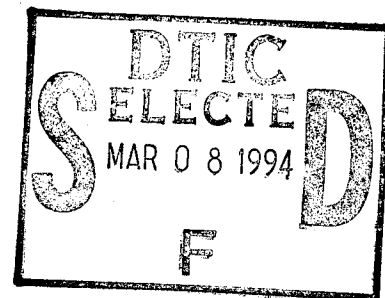
**AEDC-TR-94-16**



# **Cryogenic BRDF Measurements at 10.6 $\mu\text{m}$ and 0.63 $\mu\text{m}$ on Contaminated Mirrors**

**B. L. Seiber, R. J. Bryson, W. T. Bertrand, and B. E. Wood**  
Calspan Corporation/AEDC Operations

**February 1995**



**Final Report for Period October 1, 1993 through September 30, 1994**

Approved for public release; distribution is unlimited.

**19950303 068**

**ARNOLD ENGINEERING DEVELOPMENT CENTER  
ARNOLD AIR FORCE BASE, TENNESSEE  
AIR FORCE MATERIEL COMMAND  
UNITED STATES AIR FORCE**

THIS DOCUMENT CONTAINS

## NOTICES

When U. S. Government drawings, specifications, or other data are used for any purpose other than a definitely related Government procurement operation, the Government thereby incurs no responsibility nor any obligation whatsoever, and the fact that the Government may have formulated, furnished, or in any way supplied the said drawings, specifications, or other data, is not to be regarded by implication or otherwise, or in any manner licensing the holder or any other person or corporation, or conveying any rights or permission to manufacture, use, or sell any patented invention that may in any way be related thereto.

Qualified users may obtain copies of this report from the Defense Technical Information Center.

References to named commercial products in this report are not to be considered in any sense as an endorsement of the product by the United States Air Force or the Government.

This report has been reviewed by the Office of Public Affairs (PA) and is releasable to the National Technical Information Service (NTIS). At NTIS, it will be available to the general public, including foreign nations.

## APPROVAL STATEMENT

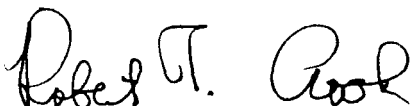
This report has been reviewed and approved.



JERRY F. FAIRCHILD, Capt, USAF  
Flight Dynamics Technology  
Applied Technology Division  
Test Operations Directorate

Approved for publication:

FOR THE COMMANDER



ROBERT T. CROOK  
Asst Chief, Applied Technology Division  
Test Operations Directorate

REPORT DOCUMENTATION PAGE			Form Approved OMB No. 0704-0188	
Public reporting burden for this collection of information is estimated to average 1 hour per response, including the time for reviewing instructions, searching existing data sources, gathering and maintaining the data needed, and completing and reviewing the collection of information. Send comments regarding this burden estimate or any other aspect of this collection of information, including suggestions for reducing this burden, to Washington Headquarters Services, Directorate for Information Operations and Reports, 1215 Jefferson Davis Highway, Suite 1204, Arlington, VA 22202-4302, and to the Office of Management and Budget, Paperwork Reduction Project (0704-0188), Washington, DC 20503.				
1. AGENCY USE ONLY (Leave blank)		2. REPORT DATE February 1995		3. REPORT TYPE AND DATES COVERED Final Report October 1993 - September 1994
4. TITLE AND SUBTITLE  Cryogenic BRDF Measurements at 10.6 $\mu\text{m}$ and 0.63 $\mu\text{m}$ on Contaminated Mirrors			5. FUNDING NUMBERS  0269	
6. AUTHOR(S) B. L. Seiber, R. J. Bryson, W. T. Bertrand, and B. E. Wood Calspan Corporation/AEDC Operations				
7. PERFORMING ORGANIZATION NAME(S) AND ADDRESS(ES) Arnold Engineering Development Center/DOT Air Force Materiel Command Arnold Air Force Base, TN 37389-9011			8. PERFORMING ORGANIZATION (REPORT NUMBER)  AEDC-TR-94-16	
9. SPONSORING/MONITORING AGENCY NAMES(S) AND ADDRESS(ES) Ballistic Missile Defense Organization (BMDO) through the Johns Hopkins Applied Physics Laboratory (JHU/APL) Johns Hopkins Road, Laurel, MD 29707, and Jet Propulsion Laboratory (JPL) Space Environmental Effects Program, 4800 Oak Grove Drive, Pasadena, CA 91109-8099			10. SPONSORING/MONITORING AGENCY REPORT NUMBER	
11. SUPPLEMENTARY NOTES Available in Defense Technical Information Center (DTIC).				
12A. DISTRIBUTION/AVAILABILITY STATEMENT Approved for public release; distribution is unlimited.			12B. DISTRIBUTION CODE	
13. ABSTRACT (Maximum 200 words)  Effects of contaminants on optical surface are concern for space-based systems. Many systems contain cryogenic optical systems that operate at temperatures where gases condense. This study presents experimental results of the effects of condensed gasses and spacecraft contaminants on highly polished (superpolished) mirror surfaces cooled, under vacuum to temperatures near 16 K and 70 K. After condensing contaminants on the mirror, the change in the bidirectional reflectance distribution function (BRDF) was obtained at wavelengths of 10.6 and 0.6328 $\mu\text{m}$ for various contaminant thicknesses up to 15 $\mu\text{m}$ . For a mirror surface of 16 K, BRDF changes for the following contaminant films were obtained: air, $\text{N}_2$ , $\text{O}_2$ , $\text{H}_2\text{O}$ , $\text{CO}$ , $\text{CO}_2$ , and Ar. For a mirror surface near 70 K, the BRDF changes from condensed films of the following outgassing effluents were measured: RS12M polycyanate, Nusil CV2500 silicone, Solithane 113/C113-300 urethane, RTV560 silicone, and $\text{H}_2\text{O}$ . In addition, using measured optical properties and the thin-film interference theory-based computer program CALCRT, the spectral reflectance of an 80 K aluminum mirror was calculated for $\text{H}_2\text{O}$ , $\text{CO}_2$ , and RTV560.  This report was sponsored by the Ballistic Missile Defense Organization (BMDO) through Johns Hopkins Applied Physics Laboratory (JHU/APL) and by the Jet Propulsion Laboratory (JPL) Space Environmental Effects Program.				
14. SUBJECT TERMS  BRDF                      superpolished mirror                      cryocontaminant			15. NUMBER OF PAGES  90	
			16. PRICE CODE	
17. SECURITY CLASSIFICATION OF REPORT  UNCLASSIFIED	18. SECURITY CLASSIFICATION OF THIS PAGE  UNCLASSIFIED	19. SECURITY CLASSIFICATION OF ABSTRACT  UNCLASSIFIED	20. LIMITATION OF ABSTRACT  SAME AS REPORT	

## PREFACE

The work reported herein was performed by the Arnold Engineering Development Center (AEDC), Air Force Materiel Command (AFMC) under Program Elements 921F01 (first phase) and 921E04 (second phase). The results were obtained by Calspan Corporation/AEDC Operations, support contractor for aerodynamic testing at the AEDC, AFMC, Arnold Air Force Base, TN 37389-4300, under AEDC Job Number 0269. The project was in two parts: the first sponsored by the Ballistic Missile Defense Organization (BMDO) through the Johns Hopkins Applied Physics Laboratory (JHU/APL) Laurel, Maryland, and the second part sponsored by Jet Propulsion Laboratory (JPL) Space Environmental Effects Program. Project Managers were Dr. Manuel Uy (JHU/APL), Jim Kenny (JPL), and Maj. Mark Briski and Capt. J. F. Fairchild (AEDC/DOT). The manuscript was submitted for publication on January 12, 1995.

The authors would like to thank Bill Hobbs and Winfred Johnson for their help with the Bidirectional Reflectance Distribution Function (BRDF) chamber operation and instrumentation.

Accession For	
NTIS   CRA&I	<input checked="" type="checkbox"/>
DTIC   TAB	<input checked="" type="checkbox"/>
Unannounced	<input type="checkbox"/>
Justification	
By _____	
Distribution /	
Availability Codes	
Dist	Avail and/or Special
A-1	

## CONTENTS

	Page
1.0 INTRODUCTION .....	7
2.0 EXPERIMENTAL TEST APPARATUS .....	8
2.1 BRDF Chamber .....	8
2.2 Contaminant Optical Properties (COP) Chamber .....	11
3.0 EXPERIMENTAL TEST PROCEDURE .....	14
3.1 BRDF Chamber Test Procedure .....	14
3.2 Contaminant Optical Properties (COP) Chamber Test Procedure .....	19
4.0 RESULTS AND DISCUSSION .....	20
4.1 Mirror Contamination Results Near 18 K (Sponsored by JHU/APL) .....	20
4.2 Mirror Contamination Results Near 68 K (Sponsored by JPL) .....	22
4.3 Mass Spectrometer and QCM Warmup Results .....	23
4.4 Contaminant Reflectance Results (Sponsored by JPL) .....	25
4.5 Data Uncertainty .....	26
5.0 CONCLUDING REMARKS .....	29
REFERENCES .....	31

## ILLUSTRATIONS

Figure	Page
1. BRDF Test Chamber .....	33
2. Close-Up View of Effusion Cell in BRDF Chamber .....	35
3. COP Test Chamber .....	36
4. Superpolished Mirror Degradation at Selected Air Film Thickness; 18 K Surface, 0.63- $\mu$ m Wavelength .....	38
5. Superpolished Mirror Degradation at Selected Air Film Thickness; 18 K Surface, 10.6- $\mu$ m Wavelength .....	39
6. Superpolished Mirror Degradation with Air Film Thickness; 18 K Surface, 6-deg Scatter Angle .....	40
7. Superpolished Mirror Degradation at Selected Nitrogen Film Thickness; 19 K Surface, 0.63- $\mu$ m Wavelength .....	41
8. Superpolished Mirror Degradation at Selected Nitrogen Film Thickness; 19 K Surface, 10.6- $\mu$ m Wavelength .....	42
9. Superpolished Mirror Degradation with Nitrogen Film Thickness; 19 K Surface, 6-deg Scatter Angle .....	43
10. Superpolished Mirror Degradation at Selected Oxygen Film Thickness; 15 K Surface, 0.63- $\mu$ m Wavelength .....	44
11. Superpolished Mirror Degradation at Selected Oxygen Film Thickness; 15 K Surface, 10.6- $\mu$ m Wavelength .....	45
12. Superpolished Mirror Degradation with Oxygen Film Thickness; 15 K Surface, 6-deg Scatter Angle .....	46

Figure	Page
13. Superpolished Mirror Degradation at Selected Water Film Thickness; 16 K Surface, 0.63- $\mu$ m Wavelength .....	47
14. Superpolished Mirror Degradation at Selected Water Film Thickness; 16 K Surface, 10.6- $\mu$ m Wavelength .....	48
15. Superpolished Mirror Degradation with Water Film Thickness; 16 K Surface, 6-deg Scatter Angle .....	49
16. Superpolished Mirror Degradation at Selected CO <sub>2</sub> Film Thickness; 17 K Surface, 0.63- $\mu$ m Wavelength .....	50
17. Superpolished Mirror Degradation at Selected CO <sub>2</sub> Film Thickness; 17 K Surface, 10.6- $\mu$ m Wavelength .....	51
18. Superpolished Mirror Degradation with CO <sub>2</sub> Film Thickness; 17 K Surface, 6-deg Scatter Angle .....	52
19. Superpolished Mirror Degradation at Selected CO Film Thickness; 15 K Surface, 0.63- $\mu$ m Wavelength .....	53
20. Superpolished Mirror Degradation at Selected CO Film Thickness; 15 K Surface, 10.6- $\mu$ m Wavelength .....	54
21. Superpolished Mirror Degradation with CO Film Thickness; 15 K Surface, 6-deg Scatter Angle .....	55
22. Superpolished Mirror Degradation at Selected Argon Film Thickness; 16 K Surface, 0.63- $\mu$ m Wavelength .....	56
23. Superpolished Mirror Degradation at Selected Argon Film Thickness; 16 K Surface, 10.6- $\mu$ m Wavelength .....	57
24. Superpolished Mirror Degradation with Argon Film Thickness; 16 K Surface, 6-deg Scatter Angle .....	58
25. Superpolished Mirror Degradation at Selected Water Film Thickness; 88 K Surface, 0.63- $\mu$ m Wavelength .....	59
26. Superpolished Mirror Degradation at Selected Water Film Thickness; 88 K Surface, 10.6- $\mu$ m Wavelength .....	60
27. Superpolished Mirror Degradation with Water Film Thickness; 88 K Surface, 6-deg Scatter Angle .....	61
28. Superpolished Mirror Degradation with RS12M Polycyanate Resin Effluent; 68 K Surface, 0.63- $\mu$ m Wavelength .....	62
29. Superpolished Mirror Degradation with RS12M Polycyanate Resin Effluent; 68 K Surface, 10.6- $\mu$ m Wavelength .....	63
30. Superpolished Mirror Degradation with Nusil CV2500 Silicone Effluent; 68 K Surface, 0.63- $\mu$ m Wavelength .....	64
31. Superpolished Mirror Degradation with Nusil CV2500 Silicone Effluent; 68 K Surface, 10.6- $\mu$ m Wavelength .....	65
32. Superpolished Mirror Degradation with Solithane 113/C113-300 Effluent; 68 K Surface, 0.63- $\mu$ m Wavelength .....	66
33. Superpolished Mirror Degradation with Solithane 113/C113-300 Effluent; 68 K Surface, 10.6- $\mu$ m Wavelength .....	67

Figure	Page
34. Superpolished Mirror Degradation with RTV560 Silicone Effluent; 68 K Surface, 0.63- $\mu$ m Wavelength .....	68
35. Superpolished Mirror Degradation with RTV560 Silicone Effluent; 68 K Surface, 10.6- $\mu$ m Wavelength .....	69
36. RS12M Polycyanate Resin Effluent Mass Spectrum .....	70
37. QCM and Superpolished Mirror Warmup, RS12M Polycyanate Resin .....	71
38. QCM Warmup with No Contaminant, sn 588 .....	72
39. Nusil CV2500 Effluent Mass Spectrum .....	73
40. QCM and Superpolished Mirror Warmup, Nusil CV2500 .....	74
41. Solithane 113/C113-300 Urethane Effluent Mass Spectrum .....	75
42. QCM and Superpolished Mirror Warmup, Solithane 113/C113-300 Urethane .....	76
43. QCM and Superpolished Mirror Warmup, RTV560 Silicone .....	77
44. Optical Properties of H <sub>2</sub> O Condensed on 80 K Germanium .....	78
45. Calculated Reflectance of 80 K Aluminum Mirror with H <sub>2</sub> O Contaminant Films .....	79
46. Optical Properties of CO <sub>2</sub> Condensed on 80 K Germanium .....	80
47. Calculated Reflectance of 80 K Aluminum Mirror with CO <sub>2</sub> Contaminant Films .....	81
48. Optical Properties for RTV560 Outgassing Products Condensed on 77 K Germanium ..	82
49. Calculated Reflectance of 77 K Aluminum Mirror with Condensed RTV560 Outgassing Products .....	83
50. Transmittance of 80 K Germanium Window with Condensed RS12M Polycyanate Outgassing Products .....	84
51. Transmittance 77 K Germanium Window with Condensed Solithane 113 Outgassing Products for Film Thickness of 0.12 and 0.87 $\mu$ m .....	86

## 1.0 INTRODUCTION

This report describes the effects of contaminant films on the reflecting properties of highly polished optical surfaces. For sensor systems that contain optical surfaces maintained at cryogenic temperatures, a major concern is that low-temperature contaminant films can condense on the mirror surface, altering the reflective properties. The property of most concern is the Bidirectional Reflectance Distribution Function (BRDF). BRDF describes the radiation that is scattered by the mirror into directions other than the specular. It is the major factor in determining whether optical systems are capable of differentiating between a weak target source and a much stronger nearby one.

The effects of contaminant films condensed on mirrors are of particular interest to the Midcourse Space Experiment (MSX) satellite personnel, since the cryogenic Spatial Infrared Radiometric and Interferometric Telescope III (SPIRIT III) will be kept at 15 - 20 K for approximately 18 months. At this temperature, the Spirit III primary mirror will freeze out any incident gas except for helium and hydrogen. The orbital contaminant gas sources can be trapped atmospheric gases (nitrogen, oxygen, water), gases from the orbit environment such as atomic oxygen, satellite material outgassing products (water, silicones, hydrocarbons), argon gas from the liquid-argon-cooled protective cover, or gases formed from the pyrotechnic explosives used for blowing the telescope cover (carbon dioxide and carbon monoxide). In addition, changes in mirror BRDF due to condensed films that might be caused by an accidental atmospheric leak during launch preparations need to be established for launch go/nogo Spirit III mirror criteria.

Many of the proposed satellite defense programs use cryogenically cooled optics for surveillance and tracking of targets. Typically, sensor systems are designed to operate between 60 and 100 K, with a few exceptions operating at or below 20 K. Alert, Locate, And Report Missiles (ALARM) and the Space and Missile Tracking System (SMTS) are systems that have been or will be designed to operate between 60 and 100 K. Measurement of the effects of condensed contaminants on optical systems at these temperatures is one of the objectives of the Air Force Space and Environmental Effects (SEE) Program (managed by the Jet Propulsion Laboratory). The results reported herein are in support of this program and were obtained for the most common contaminant condensables at these temperatures ( $H_2O$ ) and four satellite materials that are being used as components of these systems.

The results reported herein are in support of both the MSX and the SEE programs. Funding for this program was jointly provided by BMDO through the Johns Hopkins University Applied Physics Laboratory (JHU/APL) and by the Air Force Space Environmental Effects Program through the Jet Propulsion Laboratory (JPL). For these studies, contaminant films were condensed on a superpolished mirror surface. In the first phase (funded by JHU/APL), the mirror surface was cooled to temperatures as low as 15 K. The contaminant films investigated were air, nitrogen, oxygen, argon, carbon dioxide, carbon monoxide, and water. In the second phase (funded by JPL), the mirror was cooled to 68 K. The contaminant films investigated were water and condensed outgassing products from the following solid samples used as components in satellite systems: RS12M polycyanate resin, Nusil CV2500, Solithane 113/C113-300, and RTV560.



The film thicknesses were determined using a thin-film interference technique and ranged from zero to approximately 15- $\mu\text{m}$  thick. The scatter, or BRDF, was measured using a He-Ne laser that operated at 0.6328  $\mu\text{m}$  and a carbon dioxide laser that operated at 10.6  $\mu\text{m}$ . For each film thickness, the BRDF was obtained in both the visible and the infrared wavelengths. Previous work reporting the effects of condensed gases on the visible BRDF of cryogenic mirrors is presented in Ref. 1.

Additional work funded by JPL involved investigation of optical properties of contaminant films to predict the reflectance of these films on an aluminum mirror at 80 K.

## **2.0 EXPERIMENTAL TEST APPARATUS**

### **2.1 BRDF CHAMBER**

The BRDF chamber provides a technique for measuring the changes in the BRDF of a superpolished test surface in a vacuum environment as it is contaminated by condensed gases. The facility allows introduction of contaminant gas or the generation of outgassing products within the chamber. The thickness of the material is determined by counting the 0.6328- $\mu\text{m}$  laser interference fringes as the contamination layer is deposited. To aid in the determination of the mass and mass rate of material deposited, a quartz crystal microbalance (QCM) is mounted in the helium-cooled block next to the superpolished mirror. For the current measurements, various gases were condensed on the superpolished mirror surface, and the BRDF was measured at 0.6328  $\mu\text{m}$  and 10.6  $\mu\text{m}$ . The BRDF Chamber and associated BRDF equipment is shown in Fig. 1. Not shown is the carbon dioxide laser and its optics that were added for this investigation.

The BRDF Chamber vacuum is maintained by a turbomolecular pump. The chamber is also outfitted with a liquid-nitrogen-cooled liner and a gaseous-helium-cooled scavenger panel. The pressure in the chamber is measured with a Bayard-Alpert-type ion gage and can be maintained below  $1 \times 10^{-7}$  torr when the helium-cooled scavenger panel is used and the contaminant gas load is small. In the second phase when the scavenger panel was not used, the chamber pressure could be maintained below  $5 \times 10^{-6}$  torr with low contaminant load.

In addition to the scavenger panel, gaseous helium was used to cool the BRDF measurement sample and the QCM. The ultimate cryogenic temperature for the reflectance sample depended on the sample mounting configuration and on the helium refrigerator performance. A temperature as low as 15 K has been obtained.

#### **2.1.1 BRDF Measuring Apparatus**

The visible BRDF apparatus and measurement are described in Ref. 1. The BRDF measurement followed the technique described by Young (Ref. 2). The BRDF measurement apparatus for this work consisted of a helium-neon and a carbon dioxide laser and beam shaping optics exterior to the chamber. Inside the chamber, the laser beam irradiated the superpolished mirror surface at a near normal angle of incidence (less than 2 deg). Detector assemblies mounted on a computer-controlled rotary arm were used to measure the scattered light intensity as a function of the scattering angle. The system was calibrated using a gold diffuse scattering

sample of reflectance 0.94 at 10.6  $\mu\text{m}$  and a barium sulfate diffuse scattering sample of reflectance 0.98 at 0.632  $\mu\text{m}$  (Ref. 3) in place of the test mirror.

### 2.1.2 Test Mirrors

The superpolished test mirror was a 5.0-cm (2.0-in.) diam, nickel-coated, aluminum concave with a 52-cm focal length. The mirror was finished to provide a low scatter surface. The mirror had a measured BRDF rolloff beyond 6 deg that was proportional to  $\theta^{-x}$  where  $\theta$  is in degrees. The value for  $x$  was determined to be 1.5 at 0.63  $\mu\text{m}$  and 1.2 at 10.6  $\mu\text{m}$ . A foil resistance heater with Kapton<sup>®</sup> insulation was mounted to the mirror backside, and two temperature sensors were imbedded in holes drilled in the mirror sides. The mirror unit was mounted in an aluminum block, which could be cooled by flowing gaseous helium through it. The conduction path for cooling the mirror was through an aluminum donut mounted between the mirror and the aluminum cooling block. The donut was sized to obtain an optimum conductance, allowing heating by the heater and still minimizing the time required to cool the mirror. The mirror could be held at a temperature above the block temperature with the aid of a heater temperature controller that monitored a silicon-diode temperature sensor imbedded in the side of the mirror.

### 2.1.3 Gas Addition System

The gas addition system introduced the desired gases into the chamber for deposition on the superpolished samples. The system consisted of a contaminant gas source, a metering valve, and an injection tube inside the BRDF chamber that directed the gas flow in the direction of the superpolished sample. The contaminant sources were the purified gases argon, carbon dioxide, carbon monoxide, oxygen, and nitrogen, which were stored in pressurized steel bottles. The source for water vapor was a glass vial of deionized water that was valved into the gas addition system such that only the gas phase above the liquid was introduced. The metering valve was an adjustable vacuum leak valve used to obtain a convenient deposition rate on the superpolished sample. The metering valve was bypassed when water vapor was injected. The injection tube was 6-mm-diam stainless-steel tubing, protruding 60 cm into the chamber such that the superpolished sample surfaces were located in the gas plume exiting the injection tube.

### 2.1.4 Effusion Cell

The outgassing products from solid materials for contaminating the sample surface are generated using an effusion cell, shown in Fig. 2. The effusion cell has a cylindrical aluminum body 8.9 cm (3.5 in.) long with an internal bore 4.45 cm (1.75 in.) in diameter into which the material used to produce the outgassing flux is loaded. One end is closed, and the other end has a replaceable orifice plate located 35 cm (14 in.) from the front surface of the mirror. Two band heating elements clamped around the outside of the cylinder are used to heat the effusion cell to the desired temperature, usually 75°C or 125°C. A platinum resistance temperature detector (RTD) mounted in the effusion cell housing senses the effusion cell temperature. Output of the RTD feeds a proportional temperature controller, which varies the power applied to the heaters keeping the effusion cell temperature within 1°C of the set point. The controller has an analog output from which the effusion cell temperature is recorded. The effusion cell is capable of maintaining temperatures from ambient to 200°C.

An antechamber with a separate vacuum system is attached to the main chamber, separated by a gate valve. A push/pull rod mounts the effusion cell in the antechamber. This allows the effusion cell to be retracted into the antechamber for loading with contaminant material and then inserted in the main chamber when the contaminant source is desired. The antechamber allows the effusion cell to be cleaned and loaded without breaking the vacuum of the main chamber.

The effusion cell is lined with disposable aluminum foil liners. The effusion cell, liners, and aluminum foil sample boat are baked at 140°C for 24 hr before each material test, ensuring that the deposited contaminants come from the material being tested and not the peripheral components. New aluminum foil liners and boats are installed after each material test. To terminate the effusion cell contamination of the sample mirror, the effusion cell is retracted into the antechamber and the gate valve closed.

### 2.1.5 Film Thickness Apparatus

A portion of the BRDF apparatus was used to measure the cryofilm thickness. As the gas was deposited on the superpolished mirror, the specular component of the He-Ne laser beam reflected from the superpolished mirror and was monitored with a silicon solar cell mounted inside a beam dump. The electrical signal from the solar cell was amplified, rectified, and recorded on a strip chart. The reflected specular intensity variation with deposit thickness is described by thin-film interference theory. As the cryofilm thickness increases, the signal from the specular beam passes through maxima and minima. The thickness of the cryofilm,  $t$ , is determined from the thin-film interference equation for reflection maxima (Ref. 4). This equation is

$$t = \frac{m\lambda}{2n \sqrt{1 - \frac{\sin^2 \theta}{n^2}}} \quad (1)$$

where  $m = 1, 2, 3, \dots$  are the orders of interference maxima;  $n$  is the refractive index of the film;  $\theta$  is the angle of the incident beam measured from the surface normal; and  $\lambda$  is the wavelength of the incident light. The values used in Eq. (1) for the refractive index at 20 K and 77 K (Refs. 4 and 5) for a wavelength of 0.6328  $\mu\text{m}$  are listed below.

Gas	Temperature, K	Refractive Index	Thickness/ Fringe Maximum, $\mu\text{m}$
Air	20	1.23	0.257
Ar	20	1.23	0.257
CO <sub>2</sub>	20	1.28	0.247
CO	20	1.27	0.249
N <sub>2</sub>	20	1.26	0.251
O <sub>2</sub>	20	1.25	0.253
H <sub>2</sub> O	20	1.28	0.247
H <sub>2</sub> O	77	1.31	0.242

### **2.1.6 Quartz Crystal Microbalance (QCM)**

The QCM was mounted in the cooling block adjacent to the mirror and facing the contaminant source. The QCM was used as an aid in monitoring the mass and mass rate of the contaminant deposited on the mirror. After the contaminant deposit, the QCM could be warmed at a controlled rate, and the temperature that the components came off could be determined. The QCM is a cryogenic model capable of operating over the desired temperature range (15 to 320 K). An overview of QCM operation is presented in Ref. 1 and in detail in Refs. 6, 7, and 8.

### **2.1.7 Quadrupole Mass Spectrometer**

A quadrupole mass spectrometer, with its own vacuum pumping station, can be valved either into the antechamber to monitor the effusion cell output as it is warmed or into the main chamber (Fig. 1). The use in the main chamber is limited to chamber pressures above that of the mass spectrometer pumping system; hence, when the main chamber has the low pressures achieved by the helium cryopanel, mass spectra of the main chamber cannot be obtained using the present mass spectrometer pumping system. The mass spectrometer has a mass range of 1 to 600 amu. The operation and data acquisition of the mass spectrometer are controlled by an IBM® compatible personal computer.

### **2.1.8 Data Acquisition Systems**

The BRDF scattering measurements were recorded and reduced on the personal computer that controlled the BRDF apparatus, and the mass spectra were recorded on the personal computer that controlled the mass spectrometer. The thickness-related specular intensity information was recorded on a strip chart that monitored the maxima associated with the cryofilm. All other data were recorded on a separate system used for general housekeeping.

The housekeeping data system was based on a microcomputer tied by serial communication lines to several data units. A 64-channel data logger was used to read the analog data channels such as chamber pressures, temperatures from thermocouples, and the QCM oscillator and heater voltages. An 8-channel readout for silicon-diode temperature sensors was used to obtain temperatures of the cryopanel and the mounting block for the superpolished sample. The QCM controller was used to obtain the QCM frequency and temperature and control the mirror heater. At intervals set in the data logger, the microcomputer obtained data from the data logger and the remaining devices. In addition, when desired, the fixed angle scattering intensity from the BRDF scattering apparatus was also obtained. These data were displayed on a video terminal, printed, and recorded on a hard disk. The data were later reduced and plotted using various computers.

## **2.2 CONTAMINANT OPTICAL PROPERTIES (COP) CHAMBER**

Infrared transmittance measurements were made of satellite material outgassing contamination products on cryogenic surfaces in the AEDC COP Chamber (Fig. 3). The pumping system consisted of a turbomolecular pump with a mechanical forepump and a liquid-nitrogen (LN<sub>2</sub>)-cooled chamber liner. The turbopump and cryopanel were necessary to provide

a near contaminant free vacuum. With this pumping system a vacuum in the mid  $10^{-7}$  torr range could be routinely achieved. Thermocouple and ion gauges were used to monitor the chamber pressure. An effusion cell heated the materials to  $125^{\circ}\text{C}$  to provide the source of contamination. The test surface was a germanium window mounted in the center of the chamber. It was cooled to near 77 K with a constant flow of  $\text{LN}_2$ . The germanium window temperature was monitored by platinum resistors embedded in the surrounding housing. The thin-film interference model on which the optical property determinations were based required that only the front surface be coated by the contaminant material. Therefore, special precautions were taken to ensure that nothing deposited on the rear surface. Two  $\text{LN}_2$ -cooled baffles were located behind the rear surface to scavenge any gases that otherwise would be incident on it. One was a rectangular flat plate located directly behind the germanium surface when it was in position for film deposition. The other was a hollow  $\text{LN}_2$ -cooled cylinder that shielded the rear surface when it was rotated into the infrared (IR) transmittance measurement position. The IR beam used in making the transmittance measurements passed through the center of the hollow tube.

### 2.2.1 Effusion Cell

The outgassing products for contaminating the sample surface were generated using an effusion cell. It had a cylindrical aluminum body 8.9 cm. (3.5 in.) long with an internal bore diameter of 4.45 cm (1.75 in.). The material used to produce the outgassing flux was loaded into the closed end of the effusion cell, and the outgassing products exited through the open end. A Teflon<sup>®</sup>-coated heating element covered most of the outside surface of the cylinder. A temperature-controlled power supply was used to maintain the temperature of the cell at a constant value (usually  $125^{\circ}\text{C}$ ). Cell temperatures were sensed by a thermocouple and controlled within  $\pm 1^{\circ}\text{C}$  of the set point. The effusion cell exit was positioned 5.1 cm (2.0 in.) from the germanium window and QCM. The centerline of the effusion cell was located midway between the centers of the germanium window and the QCM so that the deposition rates on the two were equal. This allowed film density measurements to be made.

The effusion cell was lined with disposable aluminum foil liners. The liners and aluminum foil sample boat were baked out at  $125^{\circ}\text{C}$  for 24 hr before each material test. This ensured that the deposited contaminants came from the material being investigated and not the peripheral components. New aluminum foil liners and boats were installed for each material investigated.

### 2.2.2 Germanium Window Deposition Surface

Germanium was picked for the deposition surface because it had good thermal conductance and a flat transmittance spectrum over the 700 to  $4000\text{ cm}^{-1}$  ( $14 - 2.5\text{ }\mu\text{m}$ ) wavenumber range. The window was 67.0 cm (2.75 in.) square and was 4.0 mm (0.16 in.) thick. Nominally, the transmittance of the window (at room temperature) was 47 - 48 percent over most of the wavenumber range. At 77 K the transmittance increased to about 49 percent in the flat portion of the spectrum. The refractive index of germanium (Ref. 9) is given by

$$n_g(v) = A + BL + CL^2 + Dv^{-2} + Ev^{-4} \quad (2)$$

where

$$\begin{aligned} v &= \text{wavenumber} \\ A &= 3.88 \\ B &= 0.391707 \\ C &= 0.163492 \\ D &= -0.000006 \\ E &= 0.000000053 \\ L &= (v^{-2} - 0.028)^{-1} \end{aligned}$$

### 2.2.3 Infrared Transmittance Measurement Equipment

A commercially made Michelson interferometer was used in making IR transmittance measurements of the deposited contaminant film on the germanium window. A graphite radiation source was located inside the interferometer housing. The interferometrically modulated IR beam was collimated and allowed to pass through a housing port. The exit beam was then passed through a KBr window on the chamber port, through the germanium test window, through another KBr window on the opposite side of the chamber, and finally to a box containing the detector optics and detector. The detector was Hg-Cd-Te, which was sensitive to wavelengths from 4000 - 450  $\text{cm}^{-1}$  (2.5 - 22.2  $\mu\text{m}$ ). Typically, 32 scans were co-added for both the sample and reference measurements with a resolution of 2  $\text{cm}^{-1}$ . A reference measurement was made before each sample measurement. Data were initially stored on the system hard disk and magnetic tape.

### 2.2.4 Film Thickness Apparatus

The thin-film thickness measurement technique has been described previously (Refs. 4 and 5) and will only be reviewed here. To make accurate  $n$ ,  $k$  measurements, the transmittance must be measured for carefully determined film thicknesses. The thin-film interference technique provided a method for calculating these discrete thicknesses. As a thin film forms on a reflecting (or transmitting) substrate, a reflected or transmitted beam of radiation will exhibit a sinusoidally varying signal. Using the thin-film interference equations, the maxima and minima locations can be used to accurately calculate the thin-film thickness using Eq. (1). However, to make these calculations, the film refractive index  $n$  must be known for the incident wavelength. The He-Ne laser wavelength of 0.6328  $\mu\text{m}$  was used. Since germanium does not transmit this wavelength, the technique was used in the reflective mode. Two He-Ne laser beams were incident at two angles (24.0 and 67.5 deg), and interference fringes were observed as the contaminant film was deposited. The refractive index at 0.6328  $\mu\text{m}$  was determined from the interference patterns observed on a strip chart recorder trace for the two laser-solar cell outputs. This was done by fringe (interference maxima or minima) counting for each of the incidence angles and using the following equation from Ref. 10:

$$n = [\{ \sin^2 \theta_1 - (m_1/m_2)^2 * \sin^2 \theta_2 \} / (1 - (m_1/m_2)^2)]^{0.5} \quad (3)$$

where  $\theta_1$  and  $\theta_2$  were the two incidence angles, and  $m_1$  and  $m_2$  were the numbers of interference peaks counted for the angles  $\theta_1$  and  $\theta_2$ , respectively.

### 3.0 EXPERIMENTAL TEST PROCEDURE

#### 3.1 BRDF CHAMBER TEST PROCEDURE

The experiment consisted of two phases. Initially, the mirror was cooled to the vicinity of 18 K, and BRDF measurements were made of the following films: air, N<sub>2</sub>, O<sub>2</sub>, CO<sub>2</sub>, CO, Ar, and H<sub>2</sub>O. The second phase was conducted with the mirror at higher temperatures. The chamber cooling was reconfigured to use liquid nitrogen only, and the mirror was cooled to 88 K for H<sub>2</sub>O contamination measurements. Then to get lower mirror temperatures, the refrigerator was operated at 55 K, and the mirror was cooled to near 68 K for the contamination measurements using the effusion cell as the contaminant source.

##### 3.1.1 Superpolished Mirror and QCM Preparation

On receipt, the BRDF of the superpolished mirror was measured in a clean room environment, then covered with a metal cap until ready for use. This measurement was used as a baseline to evaluate the deterioration of the mirror BRDF with use.

A foil resistance heater and platinum resistance temperature sensor were bonded to the back of the mirror before installation in a helium-cooled mounting block in the BRDF Chamber. This allowed limited heating of the mirror for deposit removal. The mirror was kept covered when not in use, with the cover being removed only after the chamber was under vacuum and then reinstalled on chamber opening.

Before each contamination test, the superpolished mirror and the QCM were heated to 320 K to remove contaminant films and kept warm until the mounting block was cooled to proceed with the contamination test.

##### 3.1.2 Gas Addition System Preparation

Contamination gases were supplied to the chamber by connecting the desired gas bottle to the gas addition system. The lines up to the gas bottle were evacuated by the vacuum system to remove trapped gas. When ready for gas addition, the lines were valved to the chamber, and the leak valve was opened until the desired flow rate was obtained. The flow rate indication was taken from the QCM frequency shift, the change in the interference fringe maxima and minima, and in the case of the gases, the change in the chamber pressure.

For water vapor addition, the procedure was slightly different. The glass water vapor flask was partially filled with water and partially evacuated with a vacuum pump to remove most of the air. The flask with a partial vacuum was then valved shut. The flask was attached to the gas addition system, and the lines were evacuated, as with the bottled gas, to remove entrapped air. During water addition, the temperature of the gas injection tube was monitored, and heat was added to the injection tube as necessary to keep the water in the gas phase.

##### 3.1.3 BRDF Measurement

Nicodemus (Refs. 11, 12, and 13) defined the BRDF of an opaque, reflective surface in terms of the incident irradiance,  $E_i$  (W/m<sup>2</sup>), and the reflected radiance,  $L_r$  (W m<sup>-2</sup> sr<sup>-1</sup>), in the differential form

$$\text{BRDF} = \frac{dL_r}{dE_i}, \text{sr}^{-1} \quad (4)$$

Using the technique described by Young (Ref. 2), the following expression can be obtained:

$$\text{BRDF}_s = \rho \left( \frac{V_s}{V_{\text{ref}}} \right) \left( \frac{1}{\pi \cos \theta_s} \right), \text{sr}^{-1} \quad (5)$$

where

$\rho$  is the reflectance of the reference diffuser at the scattering wavelength,

$V_{\text{ref}}$  is the detector voltage from the reference diffuser,

$V_s$  is the detector voltage from the superpolished sample, and

$\theta_s$  is the reflecting/scattering angle measured between the direction of the specularly reflected radiation and the scattered radiation (i.e., the angle between the detector arm and the specular reflection from the mirror), deg.

The basic BRDF technique used is summarized in more detail in Refs. 1 and 2.

The basic BRDF degradation measurement proceeded as follows:

1. A gold diffuser ( $\rho = 0.94$  at  $10.6 \mu\text{m}$ ) was used as the reference diffuser in the infrared. At  $0.63 \mu\text{m}$ , a barium sulfate diffuser ( $\rho = 0.98$  at  $0.63 \mu\text{m}$ ) was used as reference.
2. The superpolished sample (mirror) and the reference diffuser (gold diffuser) were installed in the BRDF chamber.
3. The BRDF chamber was closed and pumped down, and the mirror cover was removed.
4. Under vacuum, the reference diffuser was inserted into the laser beam. The optics and detector were aligned, and several measurements were made of the scattered radiation near specular along with the laser output power. This was used as the scattering reference signal.
5. The superpolished sample mirror was inserted into the laser beam. With the detector shutter closed, the positions of the specular reflection and the detector were adjusted such that the entrance aperture of the detector would be centered on the specular reflection when the detector arm was at an angle of zero deg scattering angle (measured from specular). The laser output power and the detector output were measured as the detector was stepped through set angles from 2 deg through 30 deg. This became the sample scattering signal. In the case of the  $\text{CO}_2$  laser, the laser was turned on and allowed to stabilize for 3 hr before measurements were made, and the



laser was checked to ensure that it was operating at 10.6  $\mu\text{m}$  before each measurement scan.

6. The BRDF was calculated using the data obtained in steps 4 and 5.
7. Because of movement of the specular beam as the sample mounting block was cooled with gaseous helium, the alignment of the specular beam to the detector entrance aperture (step 4) was repeated when the mounting block was cold. Experience showed that the alignment did not change as long as the mounting block remained at cryogenic temperatures.
8. A contaminant film was allowed to condense on the superpolished mirror; the BRDF detector scan was made of the contaminated mirror, and the new BRDF was calculated.
9. For measurements of the contaminant films of a given thickness, the BRDF profiles were taken in the order: visible, infrared, visible to check for possible effects on the scattering surface by the  $\text{CO}_2$  laser heating.

#### **3.1.4 Contamination Test with the Mirror Near 18 K (Sponsored by JHU/APL)**

The 18 K contamination tests with the superpolished mirror were conducted as follows. The BRDF Chamber was evacuated to approximately  $1 \times 10^{-5}$  torr, and the liquid nitrogen liner was then cooled to approximately 80 K and maintained at this temperature for the duration of the test. As the nitrogen liner approached its final temperature, the gaseous helium refrigerator was used to simultaneously cool the helium cryopanel in the top of the BRDF Chamber. The chamber pressure would then decrease to  $1 \times 10^{-7}$  torr. The helium system was kept cold for the duration of the contamination test; in some cases, this lasted for more than one day. The superpolished mirror resistance heater was kept on until just before the contamination to minimize the condensing of air and water films on the mirror. When ready to proceed, the mirror mounting block was cooled, and the clean mirror BRDF scans were made (at this point, mirror temperature could be maintained at about 60 K). Next, the mirror heat was turned off and as the mirror approached its final temperature, in the vicinity of 18K, the contaminant gas was injected into the chamber until an interference maximum was obtained. The gas injection was turned off, and a BRDF scan was taken of the contaminated surface. The gas injection was restarted, and gas was added until the next interference maximum was reached. The gas was again turned off and a BRDF scan made. The process was repeated until the desired maximum thickness was obtained. After the last BRDF scan, the mirror heater was turned on, and the mirror was warmed at a rate of 2.5 K/min. Above 65 K, the helium refrigerator was turned off and the mounting/ cooling block allowed to warm along with the mirror. After the helium system temperature was considerably above the nitrogen liner temperature, the nitrogen liner was allowed to warm. The object was to minimize additional contamination to the superpolished mirror as the helium panel and nitrogen panel dumped their cryogenic load. Arnold (Ref. 14) had encountered residue remaining on a sample surface after cryofilms had evaporated. This residue was removed by heating the surface above 330 K. These same effects were observed in these studies, so the superpolished mirror and QCM were heated to 320 K, which removed the remaining residue of contaminant.

### 3.1.5 Contamination Test with the Mirror Near 68 K (Sponsored by JPL)

#### 3.1.5.1 Water Contaminant on an 88 K Mirror

The chamber cooling was reconfigured to use LN<sub>2</sub> cooling for the cryopanel and the mirror block. With this configuration the chamber could reach approximately  $5 \times 10^{-6}$  torr with small contaminant loads. With nitrogen cooling on the mirror mounting block, the mirror would reach about 88 K. The contaminant addition was similar to that in the first-phase experiments using water.

#### 3.1.5.2 Sample Preparation for the Effusion Cell

The effusion cell samples were prepared as listed in the following table. Two of the samples, RS12M and RTV560, were received from the Jet Propulsion Laboratory pre-cured. The other material samples were mixed to the specified mass ratio of curing agent to resin by adding the components to a clean pre-weighed mixing container and measuring the mass of the container as each component was added. The mass was measured on a calibrated balance with resolution to 0.0001 gm. The samples were cured as specified by the instructions in a timed, temperature-controlled oven. After cure, all material samples were cut into pieces of about 1 cm maximum dimension and put in the 50-percent relative humidity container for 24 hr before installation in the effusion cell. The effusion cell sample mass was measured immediately before installation in the effusion cell and again after the contamination test was completed. The total mass loss (TML) was determined from the pretest mass after 24 hr at 50-percent relative humidity, and the posttest mass measured immediately on removal from the chamber. Normally, TML is determined after the material sample is held at 125°C for 24 hr. This deviates from the standard definition for TML in that the material outgassing was not made for the standard 24-hr period at 125°C.

Material	Mass Mixing Ratio; Hardener/Resin	Cure	Effusion Cell Sample Size, gm	Effusion Cell Temp, °C	TML, percent
RS12M Polycyanate Resin	Pre-cured	Pre-cured	72	75, 125	NA
Nusil CV2500 Silicone	0.100	25°C (77°F) for 24 hr	14.50	75, 125	0.041
Solithane 113/C113-300 Polyurethane	0.7402 PR5-22-1	65.5°C (150°F) for 7 hr	52.47	75, 125	0.115
RTV560 Silicone	Pre-cured	Pre-cured	57.06	75	1.237

### 3.1.5.3 Effusion Cell Contaminants on a 68 K Mirror

The refrigerator was operated at 55 K, and the mirror was held near 68 K during the contamination using the effusion cell. At this temperature, the main chamber pressure was about  $5 \times 10^{-6}$  torr with small gas loads. The basic chamber operation and BRDF measurements were similar to the first experimental portion with the following exceptions involving the effusion cell. All BRDF measurements were made with the effusion cell retracted into the antechamber. The 68 K mirror BRDF degradation measurements proceeded as follows:

1. The effusion cell was baked overnight at 140°C.
2. The antechamber was valved off from the main chamber and was brought to atmosphere with dry nitrogen gas, and a new foil liner was installed.
3. The prepared sample was installed in the effusion cell, and the antechamber evacuated using the antechamber vacuum pumps.
4. The effusion cell was heated to 75°C.
5. While the effusion cell was heating to 75°C, mass spectra were taken of the effusion cell effluent.
6. When the effusion cell reached 75°C, the valve between the antechamber and the main chamber was opened, and the effusion cell was positioned in front of the mirror to start contaminating the mirror.
7. After contaminating the mirror about 18 to 24 hr, the effusion cell was retracted, and a set of BRDF scans was made.
8. The effusion cell was again inserted in the chamber and the contamination was resumed. Depending on the outgassing rate observed, the effusion cell was left at 75°C or raised to 125°C.
9. After a period of time, the effusion cell was retracted, and a set of BRDF scans was made.
10. At the end of the contamination, mass spectra were again taken in the antechamber with the effusion cell maintained at its current temperature.
11. The mirror and QCM were warmed to 320 K as the mirror scatter and QCM frequency were recorded.
12. The gaseous helium cooling and the liquid nitrogen cooling were terminated after the mirror and QCM reached 320 K.

## 3.2 CONTAMINANT OPTICAL PROPERTIES (COP) CHAMBER TEST PROCEDURE

### 3.2.1 Procedure to Predict the Infrared Reflectance

Using the procedure described in Ref. 15, the COP Chamber was used to obtain the transmission of contaminant films on the 80 K germanium window at various contaminant film thicknesses. The transmission data over the 700 to 4000  $\text{cm}^{-1}$  range were input into the TRNLIN computer code, which was based on thin-film interference with a germanium window as substrate (Ref. 4). Using this program, the refractive ( $n$ ) and absorptive ( $k$ ) indices of the contaminant films were determined. Once determined, these  $n$  and  $k$  values were used to calculate the reflectance of an aluminum mirror with three thicknesses of contaminant films, using another computer program CALCRT. The reflectance was calculated assuming normal incidence and an aluminum mirror with an uncontaminated reflectance of 0.98.

### 3.2.2 Procedure to Obtain Contaminant Film Transmittance Data

After the test material had been preconditioned, the boat containing the sample material was inserted into the effusion cell and installed in the COP chamber. He-Ne laser alignment checks were carried out to ensure that the laser beams reflected from the germanium window were incident on the solar cell detectors. Also, the transmittance of the germanium window was inspected to ensure that no contaminant film had remained after cleaning. The housekeeping data program was started for monitoring the effusion cell temperatures, the solar cell outputs for the two incidence angles, and the germanium window temperatures. The chamber was evacuated using a mechanical pump and a turbomolecular pump. Once the chamber pressure was reduced to the  $10^{-5}$  torr level, the chamber liner was cooled to  $\text{LN}_2$  temperature. After the liner reached  $\text{LN}_2$  temperature, the liquid nitrogen flow to the germanium window was started. When the chamber pressure reached the high  $10^{-7}$  torr range, heating of the effusion cell was started. The effusion cell was thermostatically controlled to 125°C, and the outgassed components were condensed on the germanium window and the QCM. The solar cell outputs were documented versus time, using a strip chart recorder. As the outgassed products condensed on the germanium window, the thin-film interference caused the solar cell outputs to exhibit sinusoidally varying values. Deposition continued until the first interference minimum (quarter-wavelength film thickness) occurred. The transmittance of the germanium window with the deposited film was then measured. This required rotating the germanium out of the deposition position into the transmittance measurement position. In making the transmittance measurement, a set of 32 scans was taken with the germanium rotated out of the IR interferometer beam. This was the 100-percent transmittance, or reference, beam. The germanium window was then rotated into position so the interferometer beam was incident normal to it, and another 32 scans were taken. The transmittance was determined by a ratio of the Fourier transforms of the two sets of interferograms.

Once the transmittance measurements were completed, the germanium was rotated back into deposition position, and the film buildup and transmittance measurements continued. This procedure was repeated for as many thicknesses as could be obtained before the deposition rate decreased to a minimal value. Transmittance measurements were made for as many thicknesses as possible to maximize the accuracy of the  $n$ ,  $k$  calculations.

## 4.0 RESULTS AND DISCUSSION

### 4.1 MIRROR CONTAMINATION BRDF NEAR 18 K (SPONSORED BY JHU/APL)

#### 4.1.1 Air Contaminant

Selected 0.63- $\mu\text{m}$  (visible) and 10.6- $\mu\text{m}$  (IR) BRDF profiles for air contaminant films condensed on the 18 K mirror are presented in Figs. 4 and 5, respectively. The scatter angle presented is measured from the direction of the specular reflected ray. The sinusoidal fluctuations in the visible BRDF profiles are attributed to scattering interference noted by Smith (Ref. 16). The crossing of some of the IR profiles beyond 15 deg (such as the 10- and 15- $\mu\text{m}$  thickness profiles) may, also, be scattering interference. Before the measurements, there was some concern that heating by the relatively high irradiance from the carbon dioxide laser might remove the contaminant film or cause a phase change. Comparing the visible BRDF profiles made before (marked pre) and after (marked post), the corresponding IR measurements show that, within experimental error, the  $\text{CO}_2$  laser incident power did not change the film scatter. This is seen in Fig. 4 where, for both the 5- $\mu\text{m}$  and 15- $\mu\text{m}$  film thickness, the pre and post profiles appear to be one curve. The visible BRDF contours become more diffuse with thickness (become more flat), whereas the infrared does not show much change. For a scattering angle near 6 deg, the BRDF change with air film thickness is more easily seen in Fig. 6. The visible BRDF increases approximately two orders of magnitude as the film thickness increases to 15  $\mu\text{m}$ ; the infrared BRDF increases much more slowly, by about a factor of three over the same thickness range.

#### 4.1.2 $\text{N}_2$ Contaminant

Selected BRDF profiles for nitrogen contaminant films on the 19 K mirror surface are presented in Figs. 7 and 8. Figure 9 presents the change in BRDF with nitrogen film thickness at a scattering angle near 6 deg. Again, the sinusoidal structure of the visible profiles (Fig. 7) is attributed to scatter interference. For the 2.5-, 5-, and 10- $\mu\text{m}$   $\text{N}_2$  film thickness, the corresponding visible profiles before and after the infrared measurement show that the effect of the  $\text{CO}_2$  laser heating on the BRDF is less than the experimental error. The visible scatter from the nitrogen film increases faster than that observed previously (Refs. 1 and 17). For example, with 5- $\mu\text{m}$  nitrogen film thickness and a scatter angle of 20 deg, the BRDF in the present study was more than twice that observed in Ref. 17. This may be due to the fact that different surfaces were used; one, a superpolished mirror and the other a superpolished QCM crystal surface. As the nitrogen film thickness approaches 10  $\mu\text{m}$ , the visible BRDF profile flattens, and the film acts as a diffuser with low reflectance. As with air films, the  $\text{N}_2$  film infrared BRDF profiles change slowly with film thickness. At a 6-deg scatter angle (Fig. 9), the visible scatter increases a factor of ten as the film thickness increases to 10  $\mu\text{m}$ , whereas the IR scatter only increases a factor of three over the same film thickness range.

#### 4.1.3 $\text{O}_2$ Contaminant

The BRDF profiles for  $\text{O}_2$  contaminant films condensed on the 15 K mirror surface are presented in Figs. 10 and 11. The visible scatter profiles made before and after the  $\text{CO}_2$  laser

measurements are presented for 5- and 12- $\mu\text{m}$  film thicknesses. The before and after profiles lie over each other within the measuring instrument's experimental error. The visible scatter profiles of the  $\text{O}_2$  films are flat with some indication of scatter interference. The visible scatter increased more than two orders of magnitude for the 1- $\mu\text{m}$  oxygen film thickness. This is consistent with previous measurements (Ref. 17). The infrared scatter profiles show a smooth increase in scatter with oxygen film thickness. For a 10- $\mu\text{m}$  film thickness, the IR BRDF is an order-of-magnitude more than that of the clean mirror. The IR profiles also become more flat or diffuse as the film thickness increases. The change in BRDF near 6 deg with oxygen film thickness is presented in Fig. 12.

The BRDF at 10.6- $\mu\text{m}$  wavelength increases an order of magnitude as the film thickness increases to 10  $\mu\text{m}$ ; the BRDF at 0.63- $\mu\text{m}$  wavelength increases much faster and levels off after a three-order-of-magnitude increase at 5- $\mu\text{m}$  film thickness. The slight drop in the 6-deg angle visible BRDF for a film thickness beyond 5- $\mu\text{m}$  is attributed to the fact that the surface is becoming more like a perfect diffuser and scattering an increasing fraction of the light to the larger angles.

#### 4.1.4 $\text{H}_2\text{O}$ Contaminant

Selected BRDF profiles for water films condensed on the 16 K mirror are presented in Figs. 13 and 14. The scatter change as the thickness increases is presented in Fig. 15 for a 6-deg scattering angle. The visible scatter increased about a factor of two as the film thickness increased to 0.5  $\mu\text{m}$ . Beyond 3- $\mu\text{m}$  film thickness, there was a two-order-of-magnitude increase in the visible scatter. This large increase is attributed to an effect noted by Arnold (Ref. 14) as shattering or fracturing of the contaminant film surface. This shattering that was observed to occur at temperatures near 20 K is typical for water (ice) films. Fracture of the condensed film was observed on all the water deposition runs at these low temperatures. The film thickness where fracture has been observed varied between 0.5 and 4  $\mu\text{m}$ .

The scattering at a wavelength of 10.6  $\mu\text{m}$  actually decreased by a factor of two as the film thickness increased to 3  $\mu\text{m}$ . When the film thickness passed 3  $\mu\text{m}$  and the film fractured, the infrared scatter increased three orders of magnitude. The initial slight decrease in the infrared scatter with film thickness is attributed to some absorption of the 10.6- $\mu\text{m}$  laser light by the absorption band of water. There are noticeable jumps in the visible scatter between the pre and post visible profiles for the film thicknesses of 1.9, 3.0, and 4.1  $\mu\text{m}$ . These jumps in the visible BRDF are obvious in Fig. 15. Apparently, in the case of water films, the 10.6- $\mu\text{m}$   $\text{CO}_2$  laser scan can change the visible scatter by causing a partial amorphous-to-crystalline phase change.

#### 4.1.5 $\text{CO}_2$ Contaminant

Selected BRDF profiles for  $\text{CO}_2$  contaminant applied to a 17 K mirror are presented in Figs. 16 and 17. The BRDF change with film thickness for a scatter angle near 6 deg is presented in Fig. 18. The visible pre and post profiles for 1.24- and 4.94- $\mu\text{m}$  carbon dioxide film thickness indicate that, within experimental error, the  $\text{CO}_2$  laser did not change the film scatter. The visible scatter increases smoothly with film thickness to 1.2  $\mu\text{m}$ , then increases two orders of magnitude

as the film increases to 2.5  $\mu\text{m}$ . This indicates that the film fractured for a film thickness somewhere beyond 1.2  $\mu\text{m}$ . The IR scatter increased less than a factor of two until the 2.5- $\mu\text{m}$  film thickness was passed, then it increased almost three orders of magnitude. The film fracture appears to have increased the visible scatter first at 1.2  $\mu\text{m}$ , but an increase in the IR scatter was not observed until the texture of the fracture became more coarse (increased film thickness).

#### **4.1.6 CO Contaminant**

Selected BRDF profiles for CO contaminant applied to a 17 K mirror are presented in Figs. 19 and 20. The BRDF change with film thickness for a 6-deg scatter angle is presented in Fig. 21. Comparisons of the visible pre and post profiles for the carbon monoxide film thickness of 2.5, 5.0 and 10.3  $\mu\text{m}$  indicate that, within experimental error, the  $\text{CO}_2$  laser did not change the CO film scatter. The visible scatter increases smoothly with contaminant thickness with a rate that is slightly greater than that presented for air and nitrogen films. The visible scatter profile shows the structure attributed to scatter interference and shows the flat profile typical of a diffuse scattering surface. The infrared scatter also increased smoothly with the CO film thickness and at a rate slightly greater than the air and nitrogen films. With a 12- $\mu\text{m}$  CO film thickness, the IR scatter increased about a factor of two over that of a clean mirror.

#### **4.1.7 Ar Contaminant**

Selected BRDF profiles for argon contaminant films applied to a 16 K mirror are presented in Figs. 22 and 23. The BRDF change with film thickness for a 6-deg scatter angle is presented in Fig. 24. Comparison of the visible pre and post profiles for the Ar film presented in Fig. 22 for a thickness of 12.5  $\mu\text{m}$  indicates that, within experimental error, the  $\text{CO}_2$  laser did not change the Ar film scatter. The visible scatter profiles show the structure attributed to scatter interference, and the profiles tend toward a flat diffuse profile as the film thickness increases. Compared to the clean mirror, the infrared BRDF increased about a factor of three with a 12.5- $\mu\text{m}$  Ar film. The rate of the visible and infrared scattering increase is about the same as for nitrogen films.

### **4.2 MIRROR CONTAMINATION RESULTS NEAR 68 K (SPONSORED BY JPL)**

#### **4.2.1 H<sub>2</sub>O Contaminant**

Selected BRDF profiles for water films condensed on the 88 K mirror are presented in Figs. 25 and 26. The BRDF change with film thickness is presented in Fig. 27. Within the instrument error, there is no noticeable change in the visible BRDF until the contaminant film fractures at 8.5- $\mu\text{m}$  thickness, then there is a two-order-of-magnitude increase in the BRDF. At 10.6  $\mu\text{m}$  the BRDF decreases until the surface fractures at a film thickness near 8.5  $\mu\text{m}$ , then the BRDF increases about three orders of magnitude. Comparing the results obtained for the surface temperature of 88 K to that obtained below 20 K, the water film on the warmer surface reached more than twice the thickness before fracture occurred.

#### **4.2.2 RS12M Polycyanate Resin**

The BRDF profiles obtained after the 68 K mirror was exposed to RS12M polycyanate resin effluent are presented in Figs. 28 and 29. The mirror was exposed for 18 hr with the effusion cell

at 75°C (approximate contaminant film thickness 0.03  $\mu\text{m}$ ), then another 6 hr with the effusion cell at 125°C (approximate contaminant film thickness 0.06  $\mu\text{m}$ ). The differences between the BRDF profiles for the clean mirror and the mirror exposed to the contaminant are within the instrument noise.

#### 4.2.3 Nusil CV2500 Silicone

The BRDF profiles obtained after the 68 K mirror was exposed to the effluent from CV2500 are presented in Figs. 30 and 31. The effusion cell was held at 75°C for 20 hr (approximate contaminant film thickness 0.014  $\mu\text{m}$ ) and an additional 4 hr at 125°C (approximate contaminant film thickness 0.019  $\mu\text{m}$ ). The differences between the BRDF profiles for the clean mirror and the mirror exposed to the contaminant are within the instrument noise.

#### 4.2.4 Solithane 113/C113-300 Urethane

The BRDF profiles obtained after the 68 K mirror was exposed to the effluent from solithane 113/C113-300 urethane are presented in Figs. 32 and 33. The effusion cell was held at 75°C for 25 hr (contaminant film thickness 0.19  $\mu\text{m}$ ) and an additional 18 hr at 125°C (contaminant film thickness 0.26  $\mu\text{m}$ ). Comparing the pre and post visible profiles indicates that the CO<sub>2</sub> laser did not cause significant changes. The visible BRDF increased over one order of magnitude with the 75°C effusion cell effluent, then dropped to within a factor of two of the clean mirror after exposure to the effluent from the 125°C effusion cell. The cause of the change in the visible BRDF is not known. Examination of strip chart traces of the 6-deg BRDF indicates that the scatter increased for the first 10 hr, leveled off, and started a slow decrease after 15 hr. The 75°C BRDF was taken at 22 hr. After the BRDF profile was taken, the 6-deg BRDF continued to decline until the 125°C BRDF profile was taken at 42 hr. Examination of the QCM frequency showed continual increase in deposit throughout the duration of the exposure to the effusion cell effluent, indicating that the deposit was not coming back off the surfaces. Similar results were observed on a second contamination run with solithane. The infrared BRDF is essentially that of the clean mirror.

#### 4.2.5 RTV560 Silicone

The BRDF profiles obtained after the 68 K mirror was exposed to the effluent from RTV560 are presented in Figs. 34 and 35. The effusion cell was held at 75°C for 22 hr (contaminant film thickness 2.3  $\mu\text{m}$ ) and an additional 20 hr at 125°C (contaminant film thickness 3.1  $\mu\text{m}$ ). The measured film thickness was 2.3  $\mu\text{m}$  after the 75°C exposure and 3.1  $\mu\text{m}$  after the 125°C exposure, which is the most contamination caused by any of the samples tested. The visible BRDF change was less than a factor of two increase even after the 125°C exposure with the 3.1- $\mu\text{m}$  film thickness. The infrared BRDF change was less than the instrument could measure.

### 4.3 MASS SPECTROMETER AND QCM WARMUP RESULTS

While the outgassing sample was being heated to 75°C in the antechamber, mass spectrometer spectra were taken of the effusion cell effluents. Again after the mirror



contamination with the effusion cell at 125°C, the effusion cell was retracted into the antechamber, and mass spectra were taken. Samples of these spectra are presented in the following sections.

After the mirror and QCM were contaminated, they were heated to room temperature. The change in the visible scatter from the mirror at an angle of 10 deg and the change in the QCM frequency were recorded along with the corresponding temperatures. These results are also presented in the following sections.

#### 4.3.1 RS12M Polycyanate Resin

The mass spectrum taken as the RS12M polycyanate was warmed to 75°C is presented in Fig. 36a. Since the chamber background varies with pressure, the effusion cell background was not subtracted from the spectra. Because of this, the spectrum shows water and air constituents (nitrogen 14, 28 amu; oxygen 16, 32 amu; and water 17 (OH), 18 amu). The peaks at 12, 14, 16, and 17 amu are elevated from normal, which could indicate the presence of hydrocarbons and nitrogen bearing compounds. The peak corresponding to CN (26 amu) does not show on either mass spectrum. The small peak at 27 amu may be from HCN. The peaks at 28 and 44 amu are enhanced above the normal air background and could be from the presence of CO and CO<sub>2</sub>. The source of the peak at 19 amu is in the effusion cell background and may indicate the presence of fluorine from the effusion cell heater wires. After being at 125°C, the mass spectrum (Fig. 36b) shows mostly water and air. The mass spectrometer scans only show relative intensity of components within a scan and because of scale factor changes cannot be used to compare intensities between figures.

The warmup of the QCM and the mirror is presented in Fig. 37. Both show a drop in the 150 to 160 K range. For the chamber pressure of  $5 \times 10^{-6}$  torr, the visible scattering and frequency drop indicates the presence of water which, depending on the other contaminant film components, can come off between 150 and 180 K. The change in the QCM frequency beyond 180 K is primarily due to the temperature characteristics of the QCM (Fig. 38).

#### 4.3.2 Nusil CV2500 Silicone

The mass spectra of CV2500 effluents at 75°C and 125°C are presented in Fig 39. From the manufacturer's material safety data sheet (MSDS) for CV2500, one would expect in addition to water and air, silicon compounds (including silicon, 28 amu; SiO, 44 amu; CO, 28 amu; CO<sub>2</sub>, 44 amu) and hydrocarbons. The spectrum obtained at 75°C shows mainly air and water with the possibility of silicon or CO in addition to nitrogen at 28 amu. The peak at 29 amu may be HCO or one of the many hydrocarbon fragments that show up at 28 and 29 amu. The spectrum after the effusion cell was heated to 125°C has more peaks but, in general, is related to the previously listed products. The peaks at 58 and 59 amu can come from many compounds with components of the form C<sub>x</sub>H<sub>y</sub>O<sub>z</sub>, C<sub>x</sub>H<sub>y</sub>N<sub>z</sub>, or C<sub>x</sub>H<sub>y</sub>F<sub>z</sub> where x, y, and z represent positive integers.

Warmup of the QCM is presented in Fig. 40. The frequency may have a slight change near 150 K where water starts to come off but has no other distinctive changes, indicating a specific

component coming off. The visible mirror scatter also had no definite change.

### 4.3.3 Solithane 113/C113-300 Urethane

The mass spectra of Solithane 113/C113-300 are presented in Fig. 41. The mass spectrum of the 75°C effluent indicates the presence of hydrocarbon components in addition to air and water. The mass spectrum of the effluents after 125°C indicates the presence of more constituents that may be carbon compounds.

The warmup of the QCM and the mirror is presented in Fig. 42. The QCM has a small frequency change near 80 K and a large frequency drop in the 160 - 180 K region. There is a large visible BRDF change near 80 K and another in the 160 - 180 K region. The change near 80 K may be from the CO<sub>2</sub> component of the contaminant, and the change in the 160 - 180 K region indicates water is present in the contaminant film. There are other changes in the 200 to 250 K region that are from unidentified components (these may be of hydrocarbon origin). The QCM frequency change above 250 K is primarily due to temperature effects on the QCM used.

### 4.3.4 RTV560 Silicone

Because the mass spectrometer was adversely affected by the large effluent containing silicones, no usable mass spectra were obtained of the RTV560.

The warmup is presented in Fig. 43. The only obvious change in the QCM frequency occurs near 210 K. Since there is no drop in the 160 - 180 K region, no appreciable amount of water came off. The components coming off above 210 K are probably some of the various silicone products from RTV560. The visible BRDF increases smoothly until near 190 K, then it drops erratically until 250 K is reached, when there is another scatter increase. The specific RTV560 components causing this behavior are unidentified.

## 4.4 CONTAMINANT REFLECTANCE RESULTS (SPONSORED BY JPL)

### 4.4.1 Reflectance of H<sub>2</sub>O Films on 80 K Aluminum Mirror

The optical properties ( $n$ ,  $k$ ) of H<sub>2</sub>O films at 80 K have been previously determined (Ref. 18) and are presented in Fig. 44. Using these optical properties and assuming an aluminum mirror, 80 K, reflectance of 0.98, and normal incidence, CALCRT was used to calculate the reflectance for H<sub>2</sub>O contaminant film thicknesses of 0.0, 0.25, 1.0, and 4.0  $\mu\text{m}$ . (Fig. 45). These results assume that the contaminant film has not shattered and become more diffuse. This appears reasonable based on past experience with water films at this temperature.

### 4.4.2 Reflectance of CO<sub>2</sub> Films on 80 K Aluminum Mirror

The optical properties ( $n$ ,  $k$ ) of CO<sub>2</sub> films at 80 K also have been previously determined (Ref. 18) and are presented in Fig. 46. Using these optical properties and assuming an aluminum mirror, 80 K, reflectance of 0.98, and normal incidence, CALCRT was used to calculate the

reflectance for CO<sub>2</sub> contaminant film thicknesses of 0.0, 0.25, 1.0, and 4.0  $\mu\text{m}$  (Fig. 47).

#### **4.4.3 Reflectance of RTV560 Films on 80 K Aluminum Mirror**

Optical properties ( $n$ ,  $k$ ) of RTV560 films at 80 K also have been previously determined (Ref. 19) and are presented in Fig. 48. Using these optical properties and assuming an aluminum mirror, 80 K, reflectance of 0.98, and normal incidence, CALCRT was used to calculate the reflectance for RTV560 contaminant film thicknesses of 0.0, 0.25, 1.0, and 4.0  $\mu\text{m}$  (Fig. 49).

#### **4.4.4 Transmission of RS12M Polycyanate Film on 80 K Germanium Window**

Transmission measurements were made of RS12M polycyanate contaminant films on an 80 K germanium window, but the contaminant film thickness was insufficient to obtain reliable  $n$  and  $k$  values. The transmission results are presented in Fig. 50 with a typical transmission spectrum for a water film of 1.0  $\mu\text{m}$  on a germanium window. The similarity between the two spectra indicates that a major portion of the RS12M polycyanate contaminant is water. The presence of water as a major component agrees with the results of the BRDF mirror warmup and the QCM warmup discussed earlier.

#### **4.4.5 Transmission of Solithane 113 Film on 80 K Germanium Window**

Transmission measurements were previously made of Solithane 113 contaminant films on an 80 K germanium window (Ref. 20), but the contaminant film thickness was insufficient to obtain reliable  $n$  and  $k$  values. The transmission results are presented in Fig. 51.

#### **4.4.6 Transmission of Nusil CV2500 Silicone**

Insufficient material was available to obtain a transmission spectrum of the Nusil CV2500 silicone outgassing products.

### **4.5 DATA UNCERTAINTY**

#### **4.5.1 BRDF Determination**

The BRDF was obtained using Eq. (5). This method required a detector voltage measurement with a known diffuser in the sample position. Then, measurements were made of detector voltage at different angles with the superpolished mirror in the sample position. The errors in this technique were discussed by Young (Ref. 2) and for this chamber in Ref. 1.

In general, the major source of error in BRDF measurements is caused by stray light. Some of the causes of the stray light in the BRDF chamber and the steps taken to reduce the stray light effects were discussed in Ref. 1. The error contribution from stray light sources is difficult to quantify. To see if significant stray light sources remained, comparisons were made between measurements made on the superpolished mirror *before* installation in the BRDF chamber (using a different measuring apparatus) and measurements made in the BRDF chamber after installation. Then different beam dump and baffle configurations were tried to achieve the results

made out of the chamber. The comparison in the final configuration did not indicate any major stray light problems for the 18 K mirror phase but indicated reflected stray light when baffles had to be removed to insert the effusion cell. Since the stray light showed only at 18 deg, data were not taken about this angle for the second phase of the experiment.

Detector linearity for a similar detector and amplifier system was investigated in Ref. 2. The conclusion was that the maximum deviation from linearity was less than 8 percent.

The diffuser reference method for determining the BRDF of the mirror requires knowledge of the reflectance of the reference diffuser near normal. The uncertainty in the reflectance is estimated to be within 10 percent of the actual value. However, when one is interested in the BRDF change with contamination this error has a much smaller effect.

The laser power drift was monitored by measuring the laser power output before each BRDF scan and comparing it to the laser power when the reference diffuser was measured. After time was allowed for the laser to reach operating temperature, the power change was less than the 5 percent repeatability of the power measurement.

The scattering angle was measured from specular, which required the detector arm position to be referenced to the center of the specularly reflected laser beam. This was accomplished by closing the detector shutter and rotating the detector arm until the specular beam was centered on a small bull's-eye marked on the shutter. The bull's-eye location matched the center of the detector assembly entrance aperture when the shutter was closed. That position was designated as the zero scatter angle. An estimated upper limit of the uncertainty for determining this position is 0.3 deg. For large angles, this had an insignificant effect compared with other sources of error. However, with a low scatter mirror like the superpolished mirror, the BRDF changes rapidly with angle as the specular position is approached. For example, in Ref. 1, moving from 4.7 to 5.0 deg caused the BRDF to decrease approximately 10 percent, but in going from 1.7 to 2.0 deg, the BRDF decreased approximately 80 percent.

From the comparisons between different BRDF measurements of the superpolished mirror and the effects of detector arm positioning on the BRDF of a superpolished mirror, the total uncertainty of the BRDF of a superpolished surface is estimated to be less than 80 percent for angles less than 3 deg, 30 percent for angles between 3 and 10 deg, 15 percent for angles between 10 and 20 deg, and 30 percent for angles greater than about 25 deg. All of this uncertainty is a bias error (in contrast to random error).

#### **4.5.2 Thickness Measurement**

The relation to obtain the film thickness from the interference fringe maxima was given by Eq. (1). The dominating quantities, when near normal laser beam incidence, are the film refractive index and the location of the interference fringe maxima. The refractive index has a reported error of 2 percent (Ref. 4). By examining the interference fringe cycles of the specular beam intensity recorded on the strip chart recorder, it was estimated that an interference fringe maxima could be located to within 5 percent of a cycle (Ref. 1). From Eq. (1), one interference fringe

cycle was calculated to be approximately  $0.25\ \mu\text{m}$ , giving an estimated uncertainty of  $0.013\ \mu\text{m}$  in locating the interference fringe maximum. Since the fringe maximum is a periodic function, the relative error in the thickness from locating the maximum will decrease inversely proportional to the number of maxima used. For example, using two fringe maxima would give approximately 2.5 percent error from locating the fringe maximum, whereas using 10 fringe maxima reduces this source of error to approximately 0.5 percent. Combining the two errors, from refractive index and fringe maximum location, and using the root sum squares gives an estimate of the total uncertainty for the thickness. Expressed in percent, these bias errors are 2-percent error for a total film thickness of  $0.5\ \mu\text{m}$  (2 fringe maxima) and 2-percent error for a total film thickness of  $2.5\ \mu\text{m}$  (10 fringe maxima).

### 4.5.3 Superpolished Mirror Surface Temperature

The silicon-diode temperature sensor for the superpolished mirror was epoxied in a hole in the side of the mirror, and the mirror heater was attached to the rear surface of the mirror.

The silicon-diode temperature sensor used in the mirror had an error specified by the manufacturer as the greater of  $\pm 1.5\ \text{K}$  or  $\pm 1.5$  percent of the temperature. This corresponds to an error of  $\pm 1.5\ \text{K}$  at  $20\ \text{K}$  and an error of  $\pm 4.5\ \text{K}$  at  $300\ \text{K}$ . This is the dominant contributor to the uncertainty when the mirror is at steady-state conditions, and it is a bias error.

When large temperature gradients occur in the mirror during heating or cooling, errors can arise because the temperature sensor is located near the center of the mirror rather than being on the front mirror surface. Calculated estimates of possible temperature gradients in the mirror indicate that at the maximum heating rate (about  $20\ \text{W}$  input power), the upper limit to the difference in the front mirror surface temperature and the temperature near the sensor is about  $0.6\ \text{K}$  with the temperature sensor being warmer than the front surface. During the maximum cooling rate (about  $110\ \text{W}$  heat removal), the estimated upper limit to the temperature difference is  $3.5\ \text{K}$  with the temperature sensor being cooler than the front mirror surface.

### 4.5.4 QCM Crystal Surface Temperature

Temperature differences can exist between the sensing crystal surface temperature and the QCM temperature sensor. Both quartz crystals, the silicon-diode temperature sensor, and the heater are mounted together in the crystal pack. The front sensing crystal makes contact with its copper mounting plate around the outer edge. This mount produces a poor thermal path. The silicon-diode temperature sensor is mounted in a copper plate in the center of the crystal pack, and the heater is mounted in a copper plate at the rear of the crystal pack. Glassford (Ref. 7) analyzed a QCM of similar design in the vicinity of  $100\ \text{K}$  that was assumed to be in thermal equilibrium. Glassford evaluated the heat loss from the crystal by radiation to the cold chamber wall and by evaporation of the contaminant. He estimated a  $0.1\ \text{K}$  temperature gradient existed between the temperature sensor and crystal surface. For the BRDF Chamber, the situation was more complex. The BRDF Chamber had a helium-cooled cryopanel at approximately  $15\ \text{K}$  in the first experiments and  $55\ \text{K}$  in the second experiments, a nitrogen-cooled liner at approximately  $77\ \text{K}$ , and the BRDF arm assembly and mounting plate that had temperatures varying between

180 and 300 K. The QCM sense crystal, near 15 K, exchanged radiation with these surfaces. During steady state, the temperature difference should still be less than 1 K. When the QCM is being cooled or heated at rates greater than 1 K/min, larger temperature differences between the sensor and crystal surface could exist. The silicon-diode temperature sensor is rated by the manufacturer to have less than 1.5 K error for the 10 to 100 K range, the main region of interest. Calibration of the QCM Research model 1819 QCM controller was adjusted to be within 0.8 K. For equilibrium, the root sum square of the error contributions gave an estimated uncertainty for the QCM surface temperature of 2 K, all of which is a bias error.

#### 4.5.5 QCM Frequency

The QCM frequency measurement depended on the amplitude and shape of the QCM output waveform. As the contaminant film built up on the QCM sense crystal, the amplitude of the output signal decreased, requiring additional amplification to operate the frequency counter. A point would be reached where the signal-to-noise ratios of the signal decreased so much that the frequency measurement became unreliable. At temperatures near 20 K, this point did not occur until the contaminant film fractured or the mass built up so much that the QCM quit operating. When the QCM was used for the second phase of the experiment with a 65 K base temperature, the QCM used was not as well behaved. The QCM signal had less amplitude and had significant frequency components other than the fundamental QCM signal, resulting in a waveform that in some regimes could give a factor of two error. This error was eliminated by monitoring the waveform on an oscilloscope and correcting the measured frequency when the distorted signal occurred. The estimated uncertainty in the QCM frequency when below 100 kHz is 1 percent, all bias.

### 5.0 CONCLUDING REMARKS

Experiments have been performed under vacuum to measure the degradation of the 0.6328- $\mu\text{m}$  and 10.6- $\mu\text{m}$  bidirectional reflectance distribution function (BRDF) of a superpolished mirror with condensed contaminant films. Sequential measurements were made on the same film in the order visible, infrared, then visible. The studies were divided into two phases. In the first phase sponsored by JHU/APL, the contaminant films studied were air, nitrogen, oxygen, water vapor, carbon dioxide, carbon monoxide, and argon deposited on a mirror surface below 20 K. In the second phase, sponsored by JPL, contaminant films from outgassing products of RS12M polycyanate resin, Nusil CV2500 silicone, Solithane 113/C113-300 urethane, and RTV560 silicone condensed on a 68 K mirror were investigated. In addition, water condensed on an 88 K mirror was investigated.

An investigation was performed to obtain optical properties ( $n$ ,  $k$ ) of various contaminant film at 80 K. Then using these optical properties as inputs to the thin-film theory-based computer program CALCRT, the reflectance spectra of an 80 K aluminum mirror were calculated for film thicknesses of 0.25, 1.0, and 4.0  $\mu\text{m}$ . Reflectance spectra for the following films were presented: water,  $\text{CO}_2$ , and RTV560. In addition, raw transmittance spectra were presented for solithane 113 and RS12M polycyanate on a germanium window.

The following conclusions are drawn from the data obtained:

1. The CO<sub>2</sub> infrared laser heating had negligible effects on the measured BRDF for most of gases studied, the exception being water where the CO<sub>2</sub> laser may have had an effect as the contaminant film appears to have undergone a phase change.
2. Air, nitrogen, argon and carbon monoxide contaminant films had the least effect on the scatter for the temperature (15 - 19 K) and the film thickness range (to beyond 10  $\mu\text{m}$ ) studied. The scatter increased a factor of two to three in the infrared and a factor of 10 to 30 in the visible.
3. Oxygen contaminant films at 15 K increased the scatter the most of the films that did not fracture. The visible scatter increased two orders of magnitude and had a flat diffuse profile with a 1.2- $\mu\text{m}$  film thickness, while the infrared scatter increased one order of magnitude with the much thicker 12- $\mu\text{m}$  film thickness.
4. Carbon dioxide contaminant films at 17 K had a small infrared and visible scattering change until the film fractured. After fracture, both the infrared and visible scatter increased several orders of magnitude.
5. Water contaminant films at 16 K, before fracture, had a small scatter increase in the visible and a small scatter decrease, because of absorption, in the infrared. After fracture, the visible scatter increased about two orders of magnitude and the infrared scatter about three orders of magnitude.
6. As reported earlier by Smith (Ref. 16), the fracture of water occurred at different film thicknesses. Other than temperature, the causes of this variation are uncertain.
7. For the MSX program, and in particular for the Spirit III telescope, the only two gases that can make an appreciable change in mirror infrared BRDF for the contaminant film thicknesses expected (less than 1  $\mu\text{m}$ ) will be water and oxygen. H<sub>2</sub>O films, with the potential for shattering, still appear to be possibly the most damaging.
8. RS12M polycyanate resin and the Nusil CV2500 silicone contaminant films produced little effect on the visible and the infrared BRDF of the mirror.
9. Solithane 113/C113-300 urethane showed an order-of-magnitude BRDF change in the visible with a contaminant film thickness about 0.1  $\mu\text{m}$ . As the film thickness increased, the visible BRDF decreased to within a factor of two of the clean mirror value. The infrared BRDF change was less than the instrument could measure.
10. RTV560 silicone contaminant film, even though it built up relatively large thickness (2 to 3  $\mu\text{m}$ ), caused less than a factor of two change in the visible BRDF and a change in the infrared BRDF that was less than the instrument could measure.

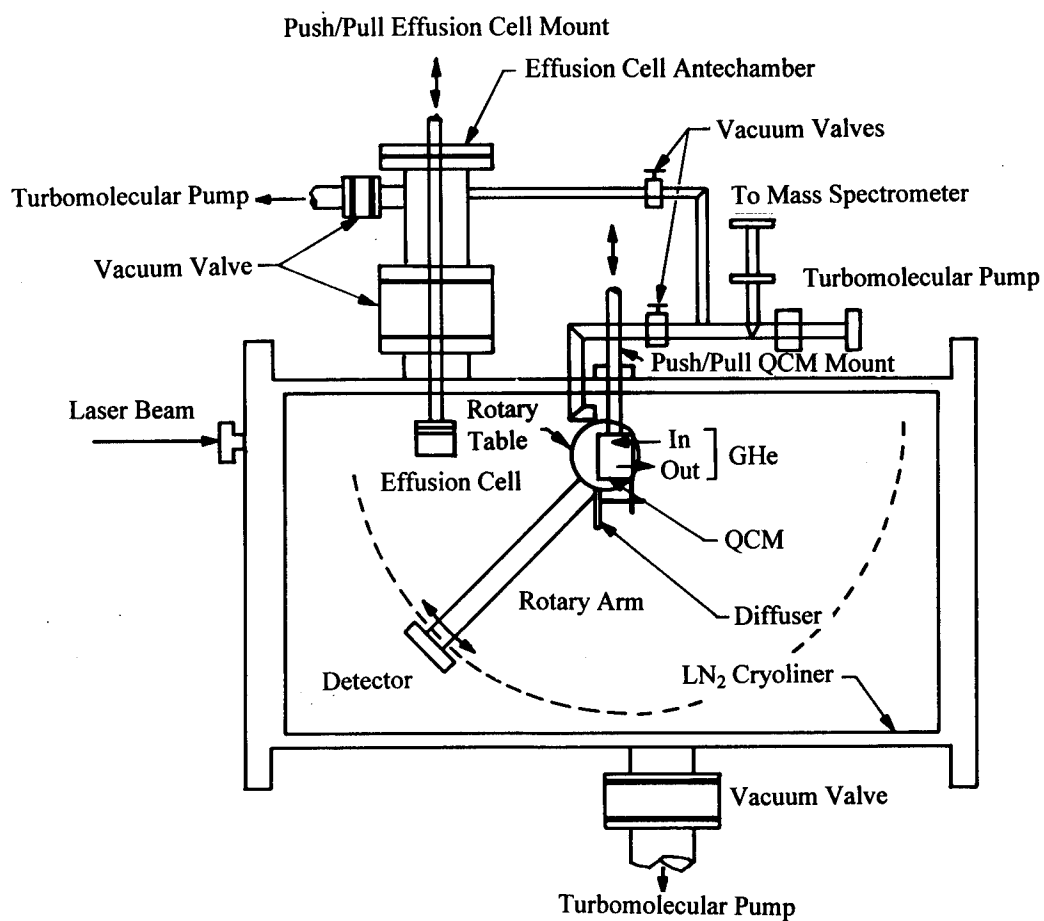
11. Solithane 113 and RTV560 had large visible BRDF increases when the mirror was warmed (the infrared BRDF was not monitored during warmup but was presumed to increase also).
12. Calculated reflectance spectra for an aluminum mirror with H<sub>2</sub>O, CO<sub>2</sub>, and RTV560 condensed films had major reflectance dips in their spectra.
13. RS12M polycyanate and Solithane 113 produced insufficient contaminants for determination of optical properties but did produce measurable transmission spectra. Solithane 113 spectra indicated a major water component.
14. Nusil CV2500 had the fewest condensable outgassing products and did not produce measurable transmission spectra for the sample quantities normally used.

### REFERENCES

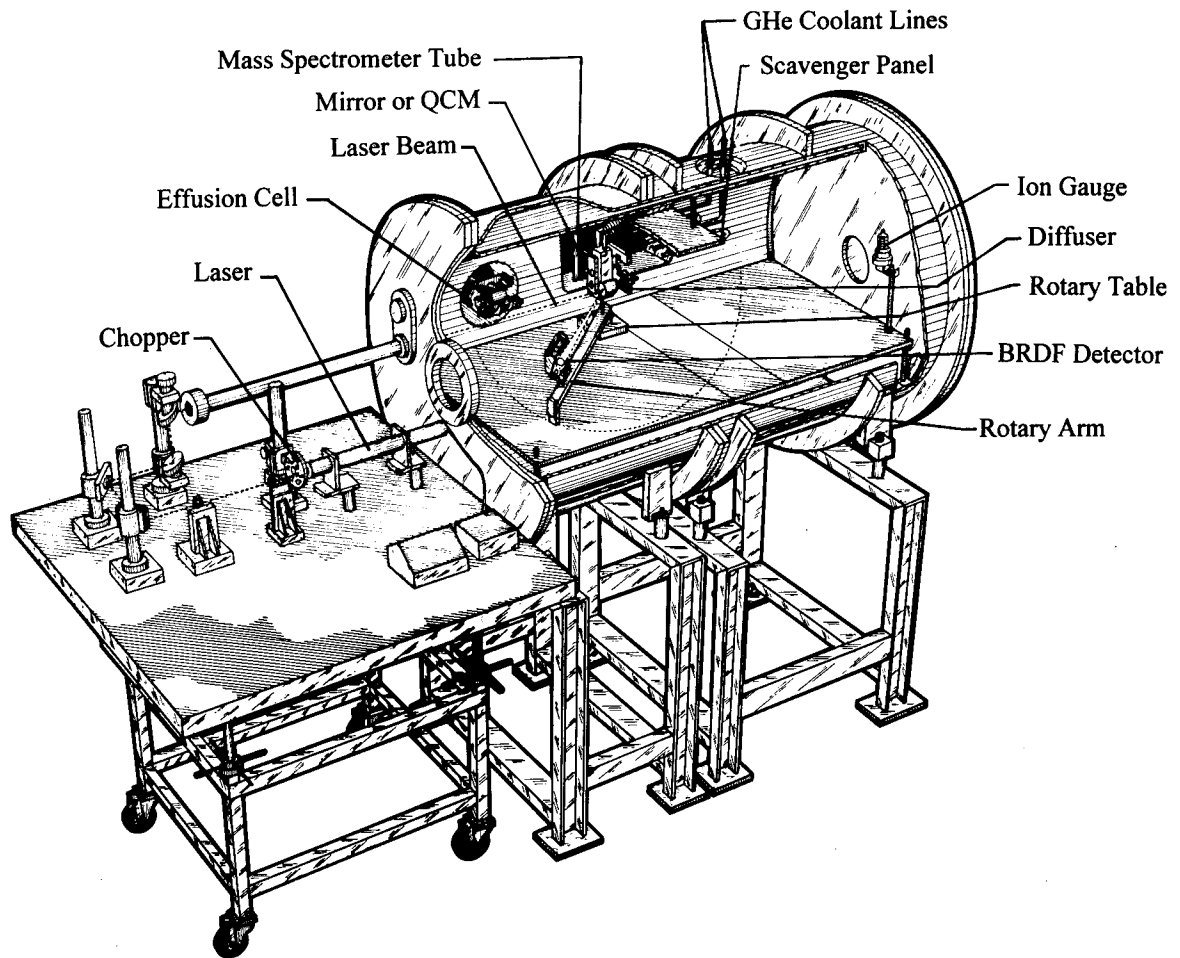
1. Seiber, B. L., Bryson, R. J., Young, R. P., Sr., and Wood, B. E. "Effects of Cryocontaminants on Cryogenic Superpolished Mirror and Quartz Crystal Microbalance." AEDC-TR-92-5 (AD-A255972), September 1992.
2. Young, R. P., Sr. "Metal Optics Scatter Measurements." SPIE Proceedings Vol. 65. Design, Manufacture and Application of Metal Optics, August 19 - 20, 1975. San Diego, CA (ISBN 0-89252-077-9), pp. 57-62.
3. Grum, F. and Luckey, G. W. "Optical Sphere Paint and a Working Standard of Reflectance." *Applied Optics*, Vol. 7, November 1968, pp. 2289-94.
4. Wood, B. E. and Roux, J. A. "Infrared Optical Properties of Thin H<sub>2</sub>O, NH<sub>3</sub>, and CO<sub>2</sub> Cryofilms." *Journal of the Optical Society of America*, Vol. 72, No. 6, June 1982, pp. 720-28.
5. Roux, J. A., et. al. "Infrared Optical Properties of Thin CO, NO, CH<sub>4</sub>, HCl, N<sub>2</sub>O, O<sub>2</sub>, N<sub>2</sub>, Ar, and Air Cryofilms." AIAA Progress Series, Spacecraft Contamination: Sources and Prevention, Eds. J. A. Roux and T. D. McCay, 1984, pp. 139-161.
6. Operation Manual for Quartz Crystal Microbalance, QCM Sensor Mark 16, QCM Research Laguna Beach, CA.
7. Glassford, A. P. M. "Analysis of the Accuracy of a Commercial Quartz Crystal Microbalance." AIAA Paper 76-438, AIAA 11th Thermophysics Conference, July 14-16, 1976.
8. Wallace, D. A. and Wallace, S. A. "Realistic Performance Specifications for Flight Quartz Crystal Microbalance Instruments for Contamination Measurement on Spacecraft." AIAA Paper 88-2727, Presented at AIAA Thermophysics, Plasmadynamics and Lasers Conference, June 27-29, 1988, San Antonio, TX.



9. Herzberger, M. and Salzberg, C. D. "Refractive Indices of Infrared Optical Materials and Color Correction of Infrared Lenses." *Journal of the Optical Society of America*, Vol. 52, Number 4, April 1962, pp. 420-427.
10. Wood, B. E. and Smith, A. M. "Infrared Reflectance of Condensed Gas Films." AIAA Progress in Astronautics and Aeronautics: Thermophysics and Thermal Control, Vol. 65, Ed. Raymond Viskanta, 1979, pp. 22-38.
11. Nicodemus, F. E. "Directional Reflectance and Emissivity of an Opaque Surface." *Applied Optics*, Vol. 4, No. 7, July 1965, pp. 767-73.
12. Nicodemus, F. E. "Reflectance Nomenclature and Directional Reflectance and Emissivity." *Applied Optics*, Vol. 9, No. 6, June 1970, pp. 1474-75.
13. Nicodemus, F. E., et. al. "Geometrical Considerations and Nomenclature for Reflectance." NBS Monograph 160, October 1977.
14. Arnold, F. "Degradation of Low-Scatter Metal Mirrors by Cryodeposit Contamination." AEDC-TR-75-128 (AD-B007022L), October 1975.
15. Wood, B. E., et al. "Satellite Material Contaminant Optical Properties." SPIE Proceedings, Vol 1165. Scatter from Optical Components, August 8-10, 1989, San Diego, CA (ISBN 0-8194-021-x), pp 392-400.
16. Smith, A. M., Tempelmeyer, K. E., Muller, P. R., and Wood, B. E. "Angular Distribution of Visible and Near IR Radiation Reflected from CO<sub>2</sub> Cryodeposits." *AIAA Journal*, Vol. 7, No. 12, December 1969, pp. 2274-2280.
17. Seiber, B. L., et al. "Effect of Cryocontaminants on Cryogenic Superpolished Mirror and Superpolished Quartz Crystal Microbalance." SPIE Proceedings, Vol. 1754, Optical System Contamination, July 23 -24, 1992, San Diego, CA (ISBN-89252-077-9), pp 215-225.
18. Roux, J. A., Wood, B. E., and Smith, A. M. "IR Optical Properties of Thin H<sub>2</sub>O, NH<sub>3</sub>, and CO<sub>2</sub> Cryofilms." AEDC TR 79-57 (AD-A074913), September 1979.
19. Wood, B. E., et al. "Surface Effects of Satellite Material Outgassing Products." AEDC TR 89-2 (AD-B133593), June 1989.
20. Wood, B. E., et al. "Surface Effects of Satellite Outgassing Products." AEDC TR 87-8 (AD-B115252), September 1987.



a. Plan view of BRDF chamber  
 Figure 1. BRDF Test Chamber.



**b. Three-dimensional view of chamber**  
**Figure 1. Concluded.**

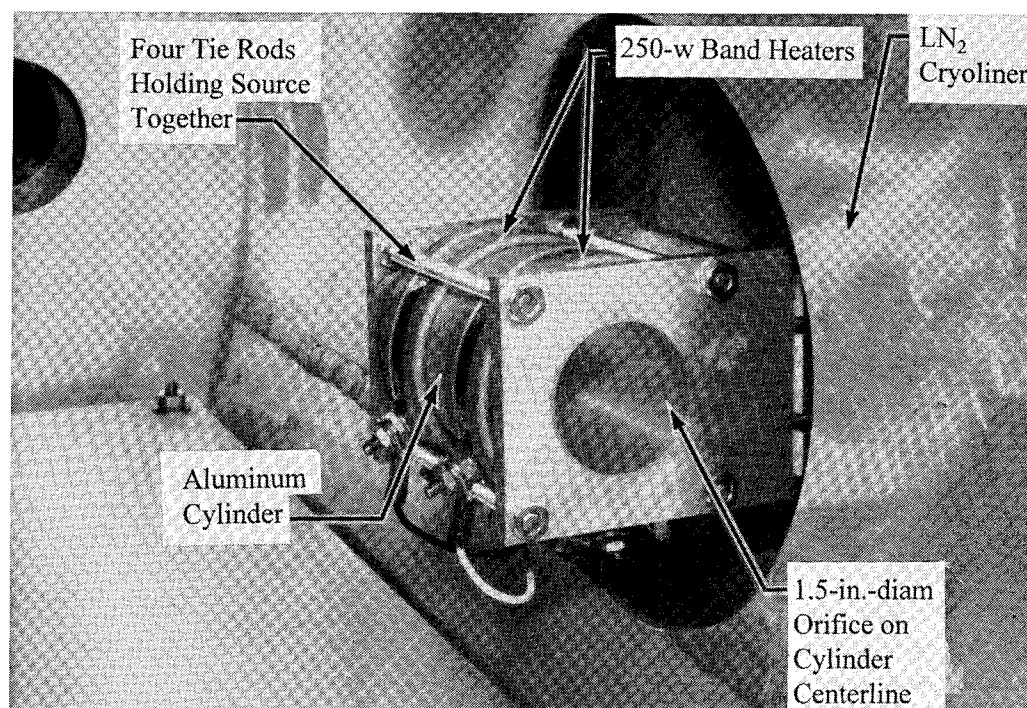
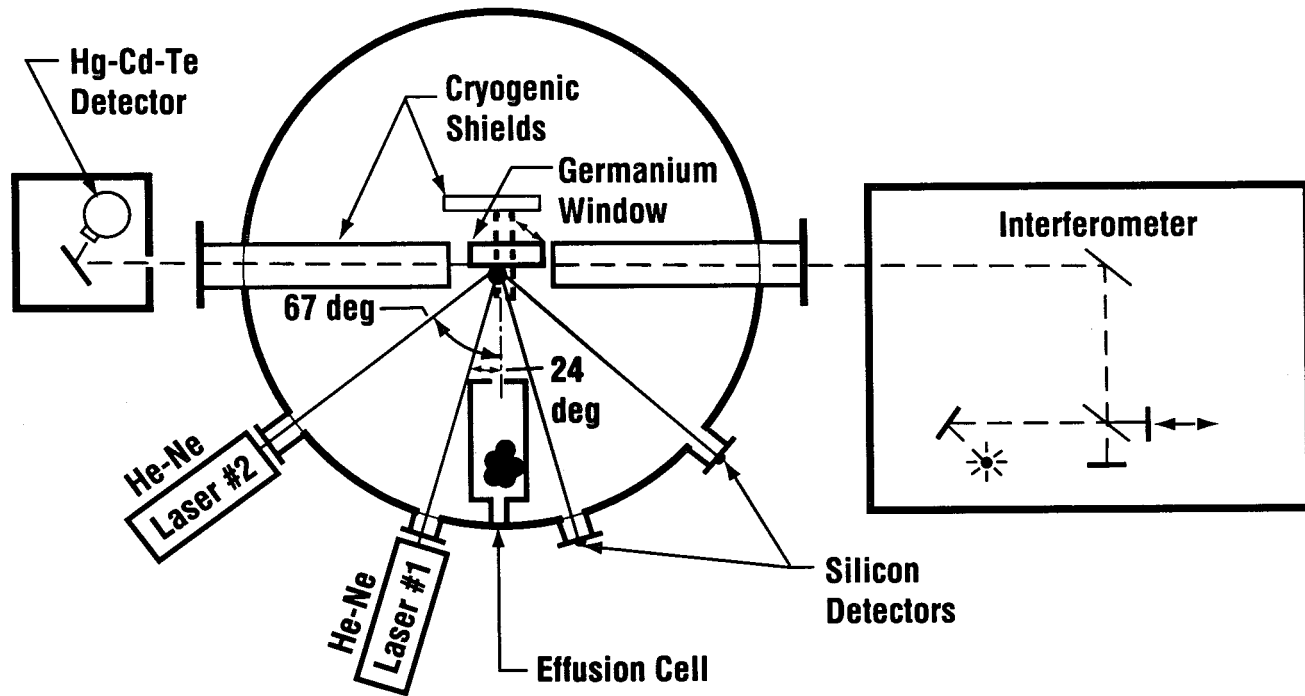
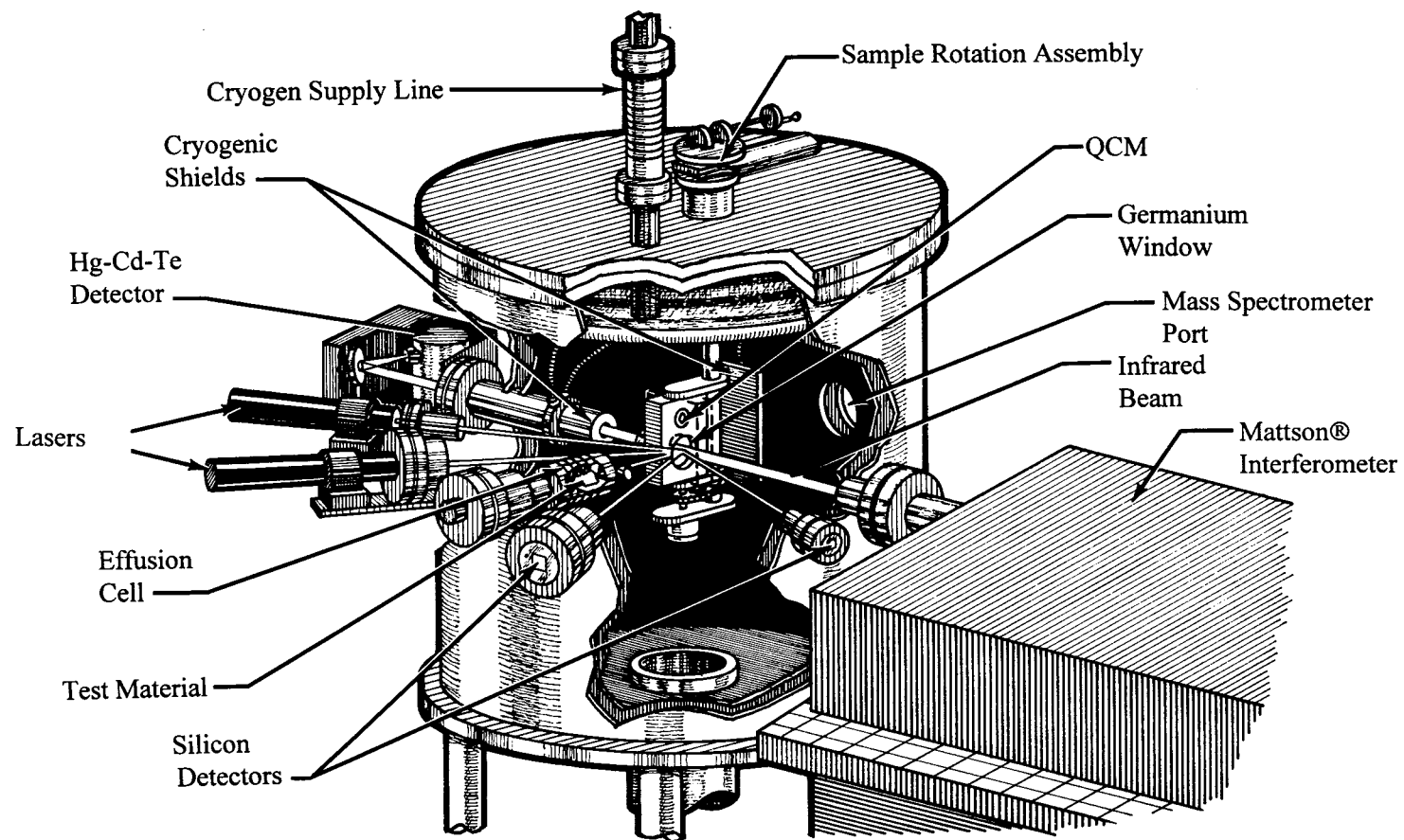


**Figure 2. Close-up view of effusion cell in BRDF chamber.**



a. Plan view of COP chamber  
Figure 3. COP Test Chamber.



**b. Three-dimensional view of COP chamber.**  
**Figure 3. Concluded.**

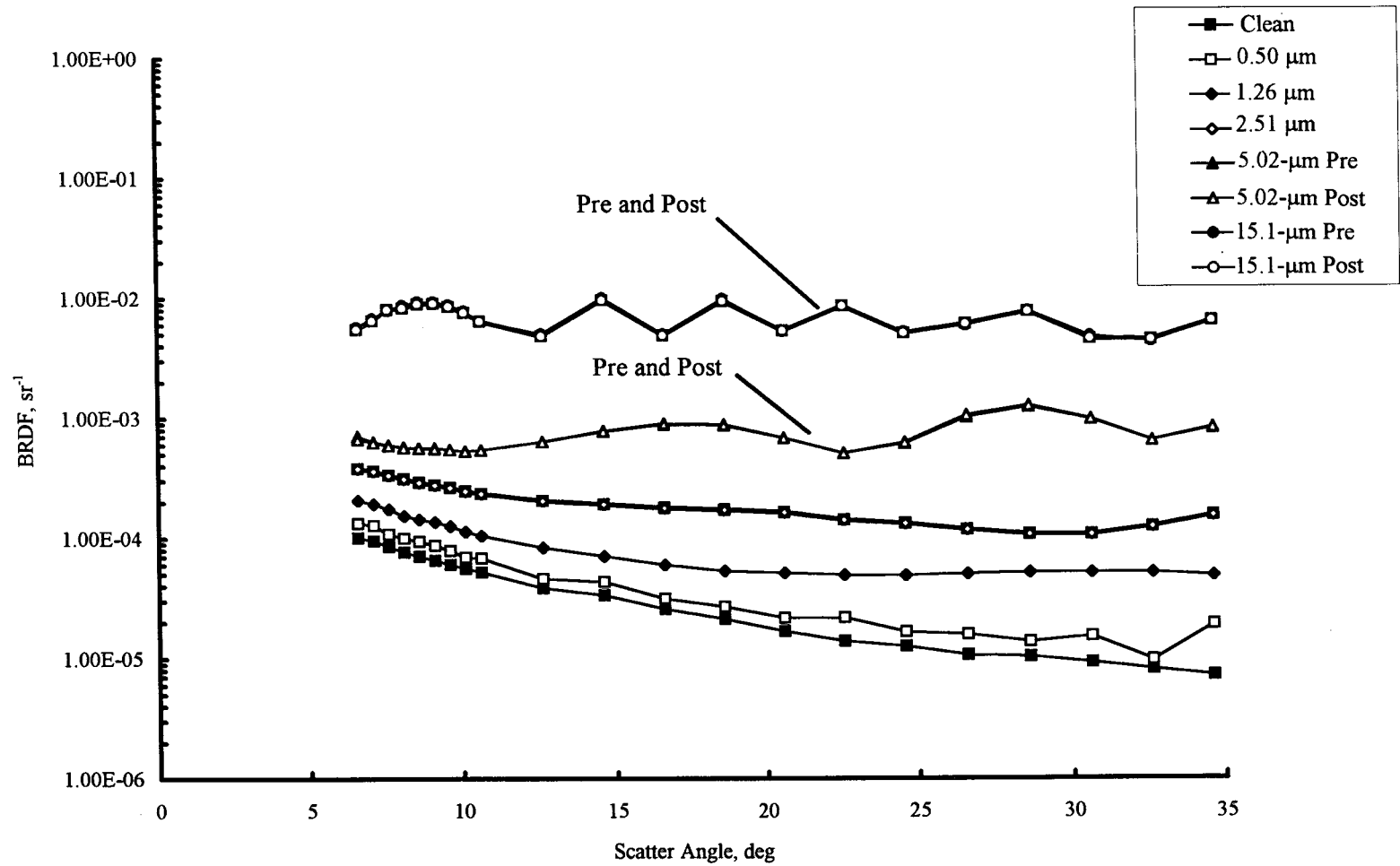


Figure 4. Superpolished mirror degradation at selected air film thickness;  
18 K surface, 0.63-μm wavelength.

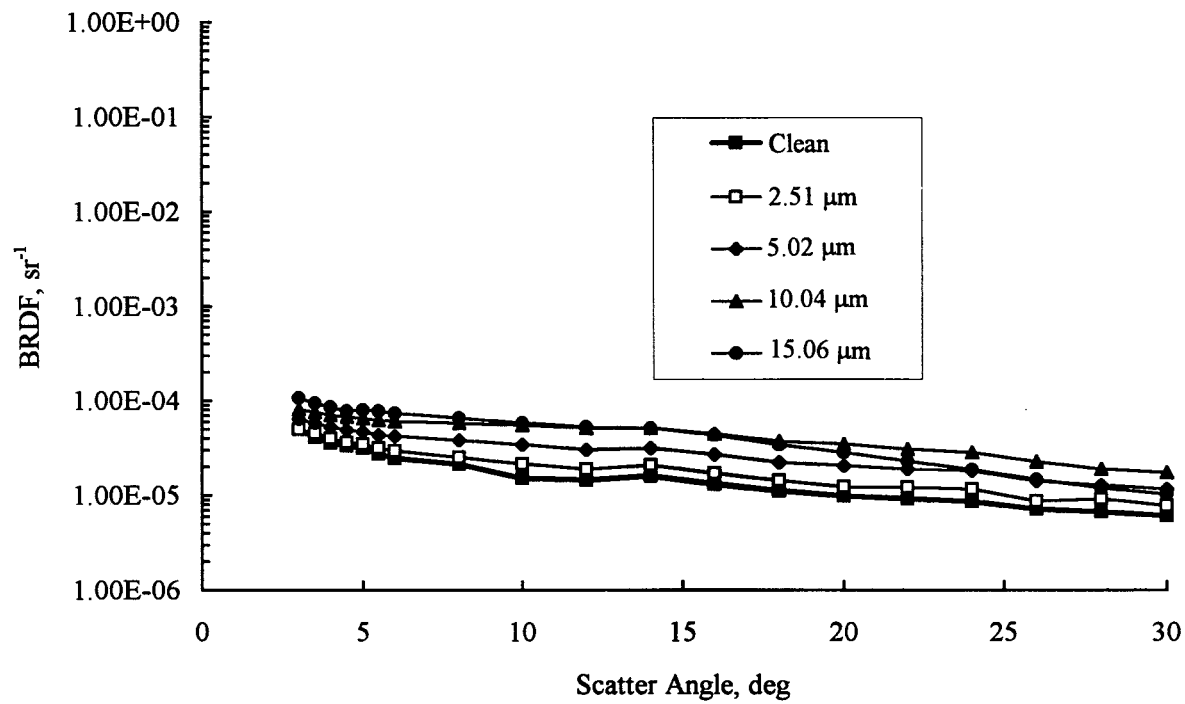
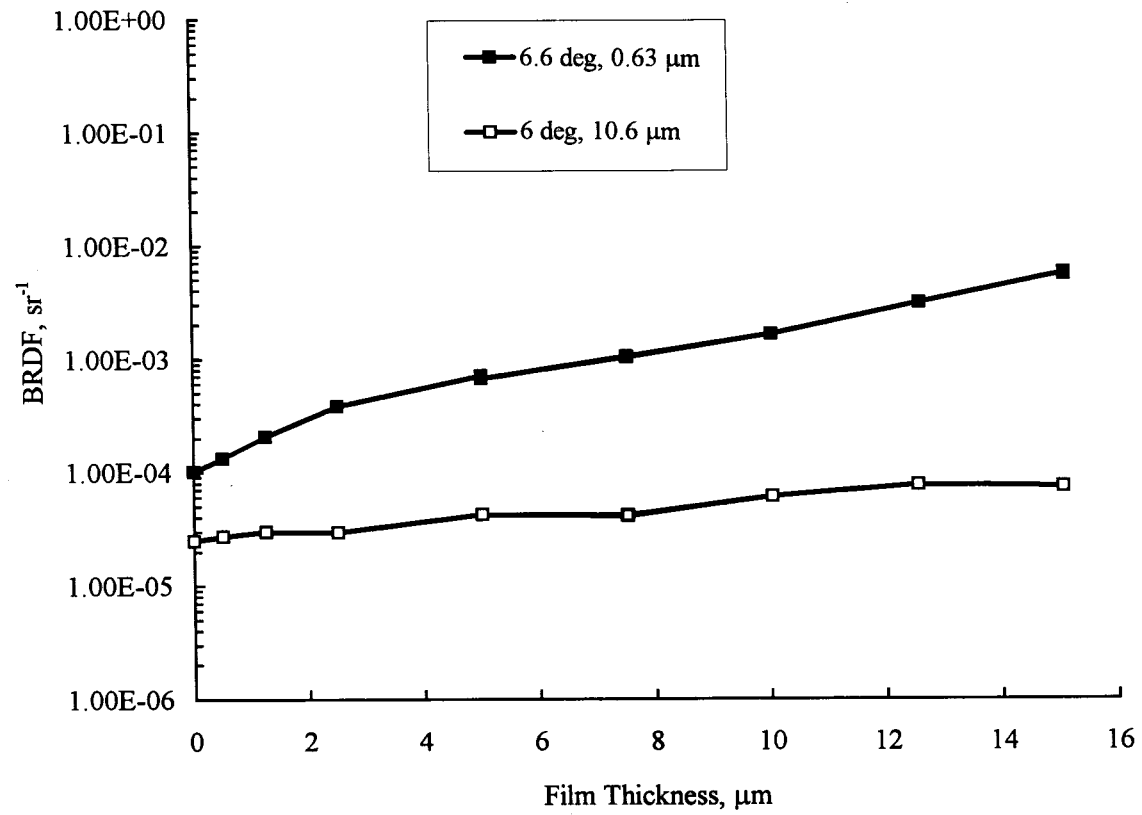


Figure 5. Superpolished mirror degradation at selected air film thickness; 18 K surface, 10.6-μm wavelength.





**Figure 6. Superpolished mirror degradation with air film thickness; 18 K surface, 6-deg scatter angle.**

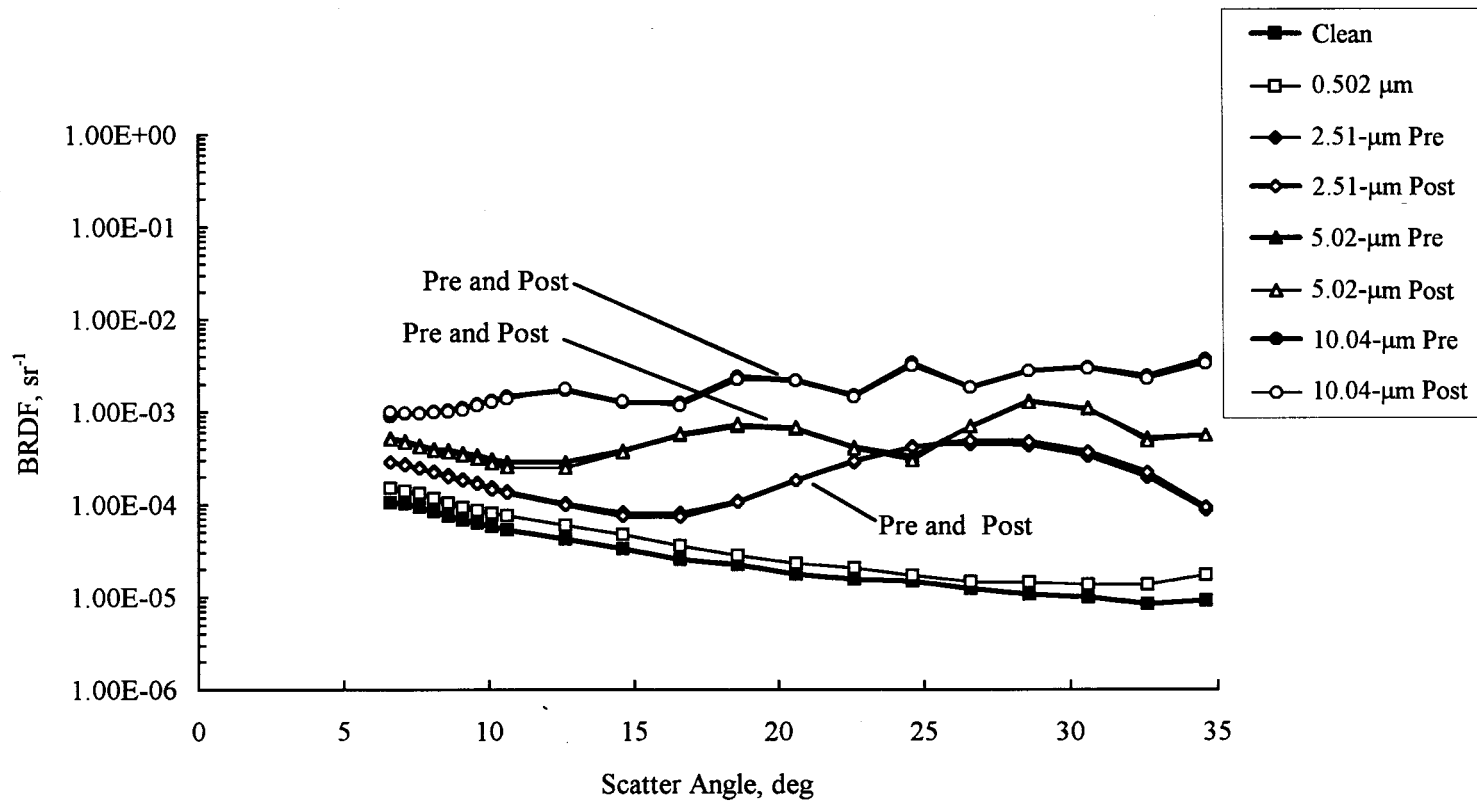
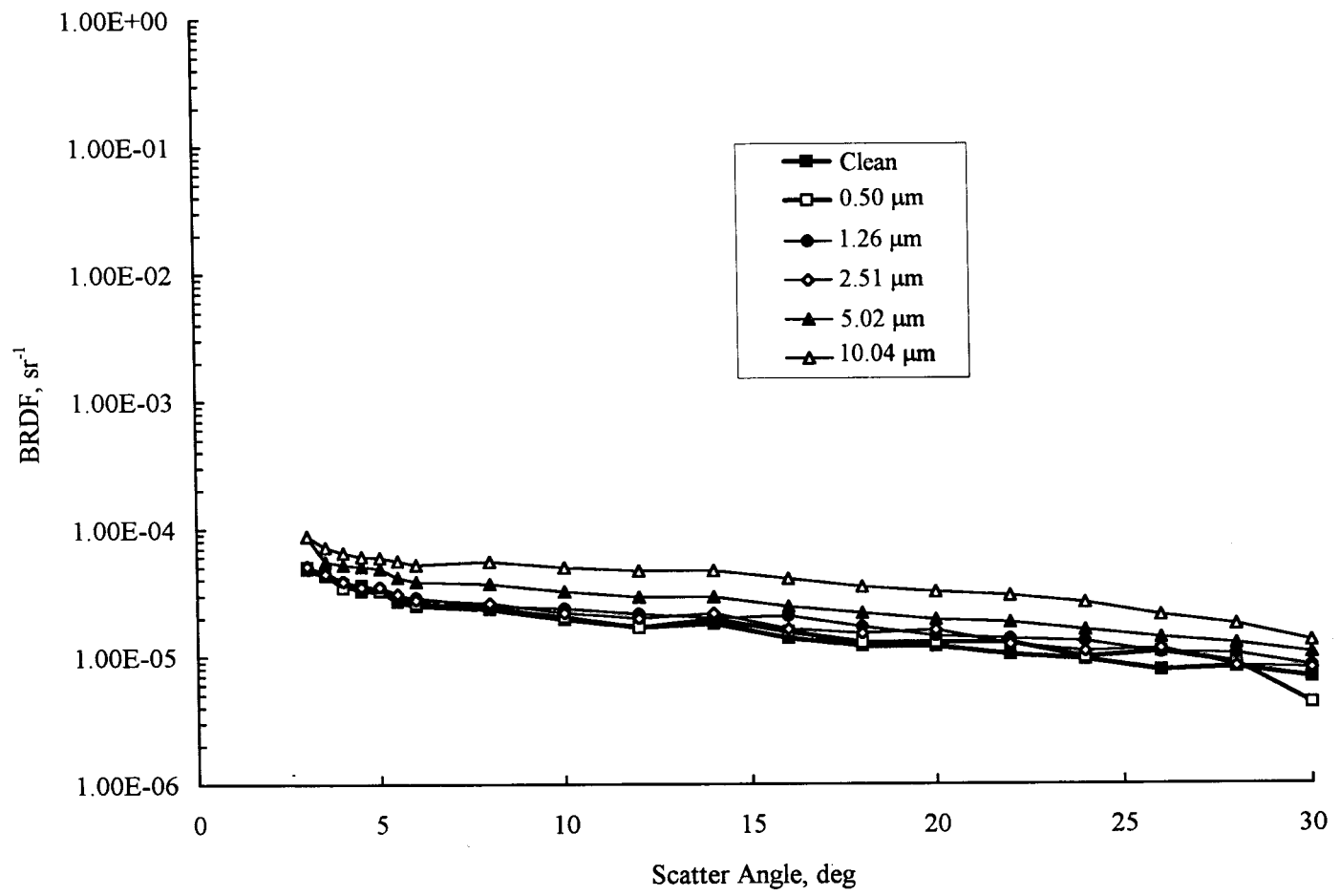


Figure 7. Superpolished mirror degradation at selected nitrogen film thickness;  
19 K surface, 0.63-μm wavelength.



**Figure 8. Superpolished mirror degradation at selected nitrogen film thickness;  
19 K surface, 10.6-μm wavelength.**

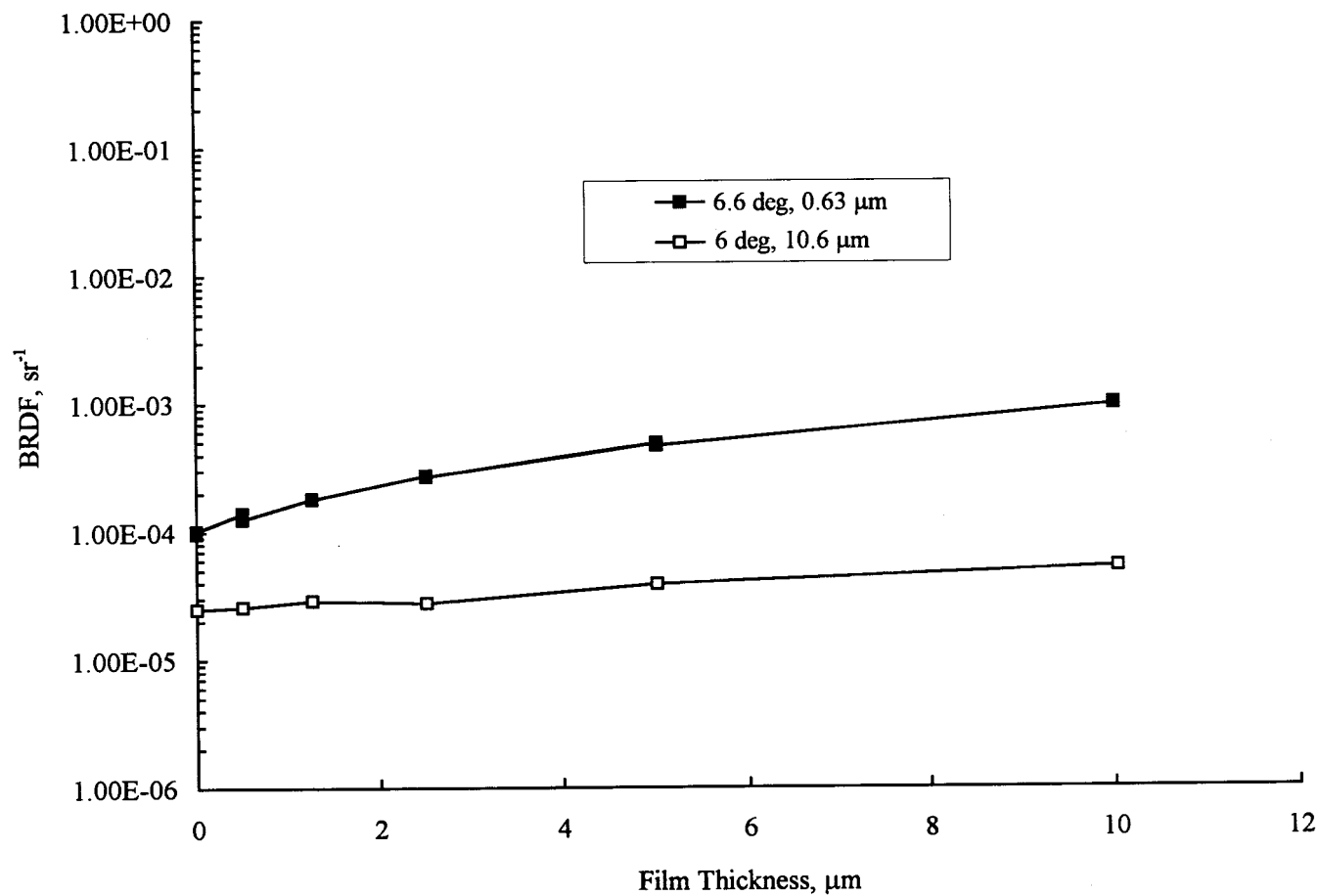


Figure 9. Superpolished mirror degradation with nitrogen film thickness; 19 K surface, 6-deg scatter angle.

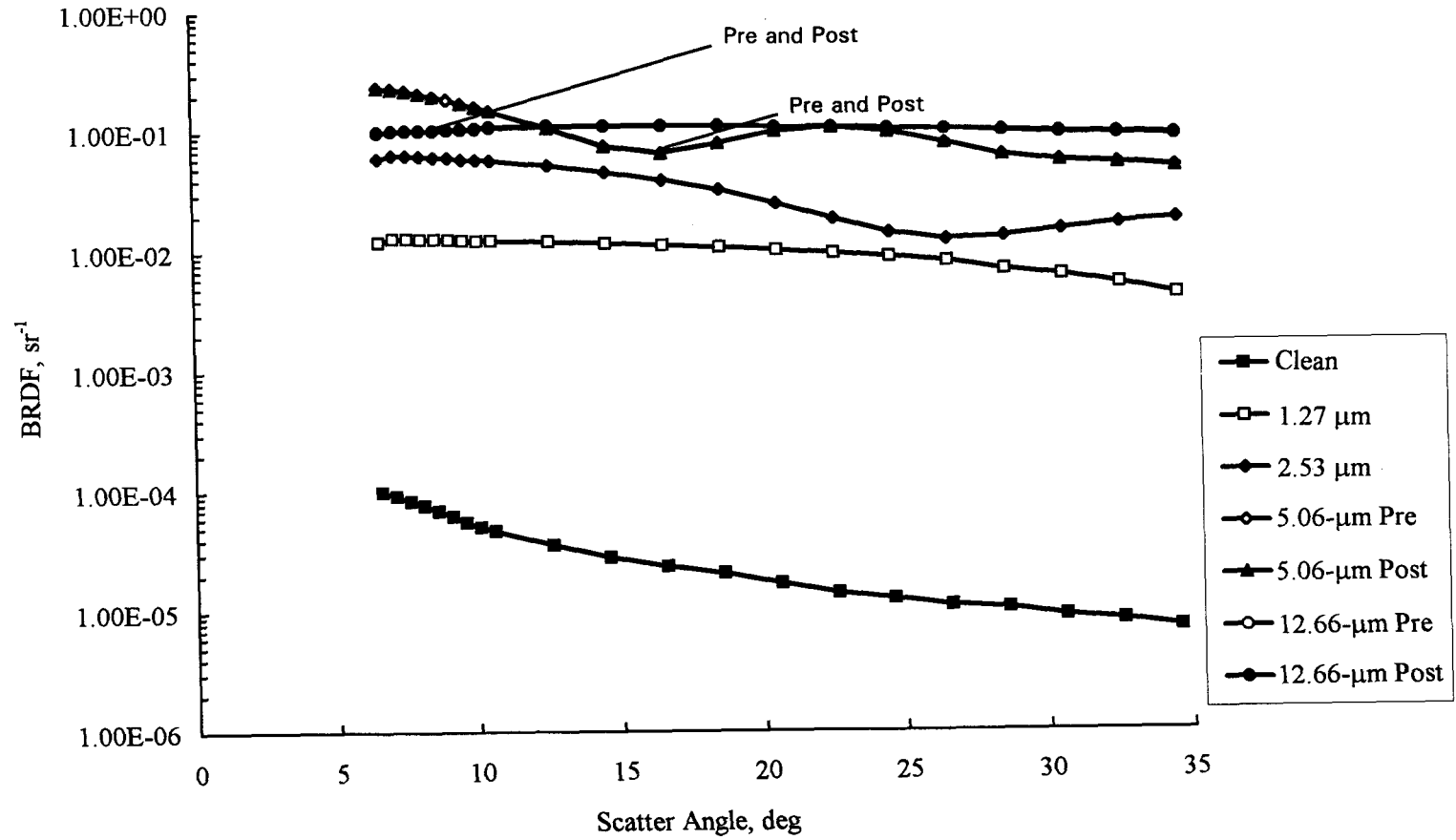


Figure 10. Superpolished mirror degradation at selected oxygen film thickness; 15 K surface, 0.63-μm wavelength.

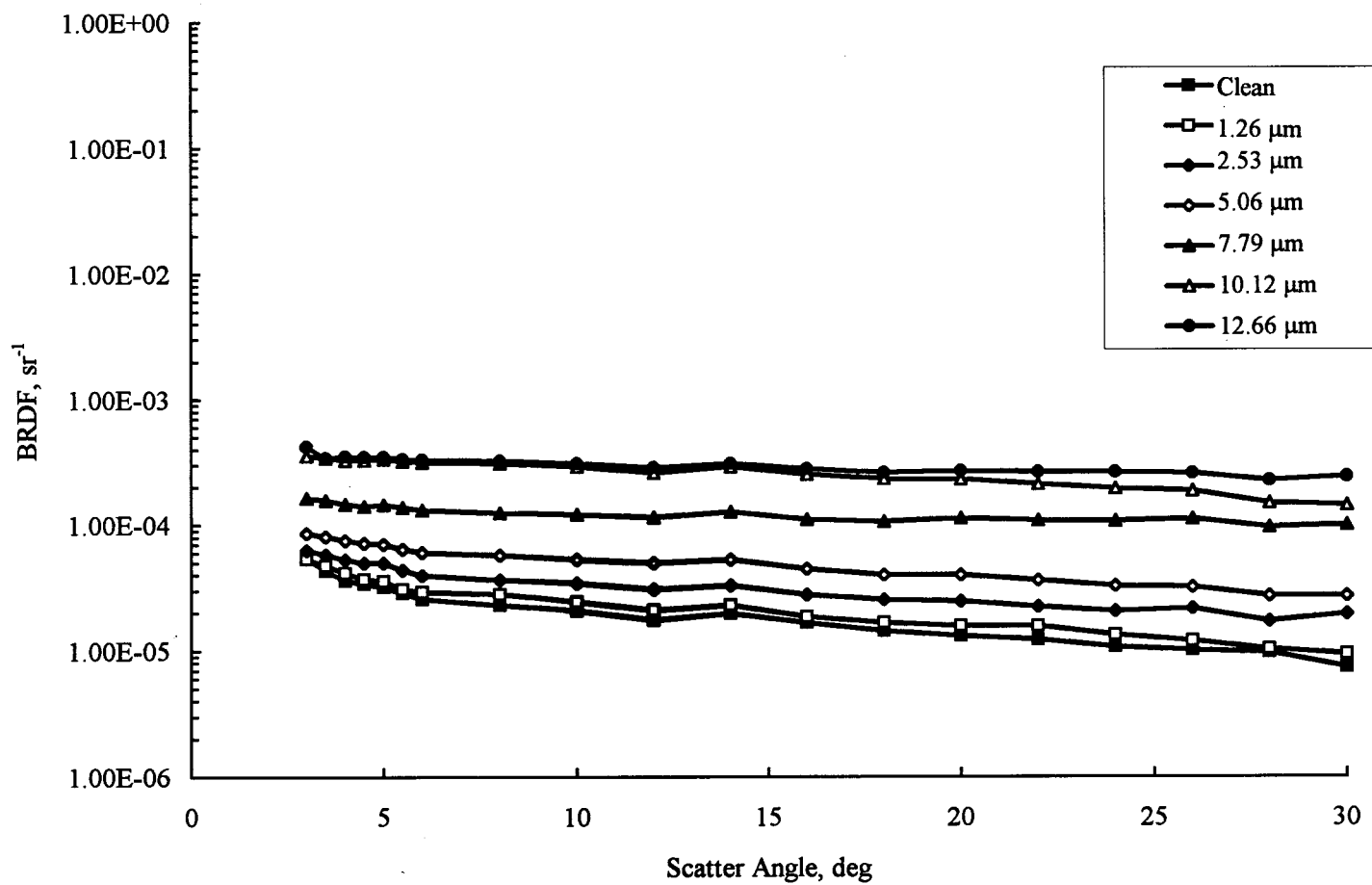


Figure 11. Superpolished mirror degradation at selected oxygen film thickness; 15 K surface, 10.6-μm wavelength.

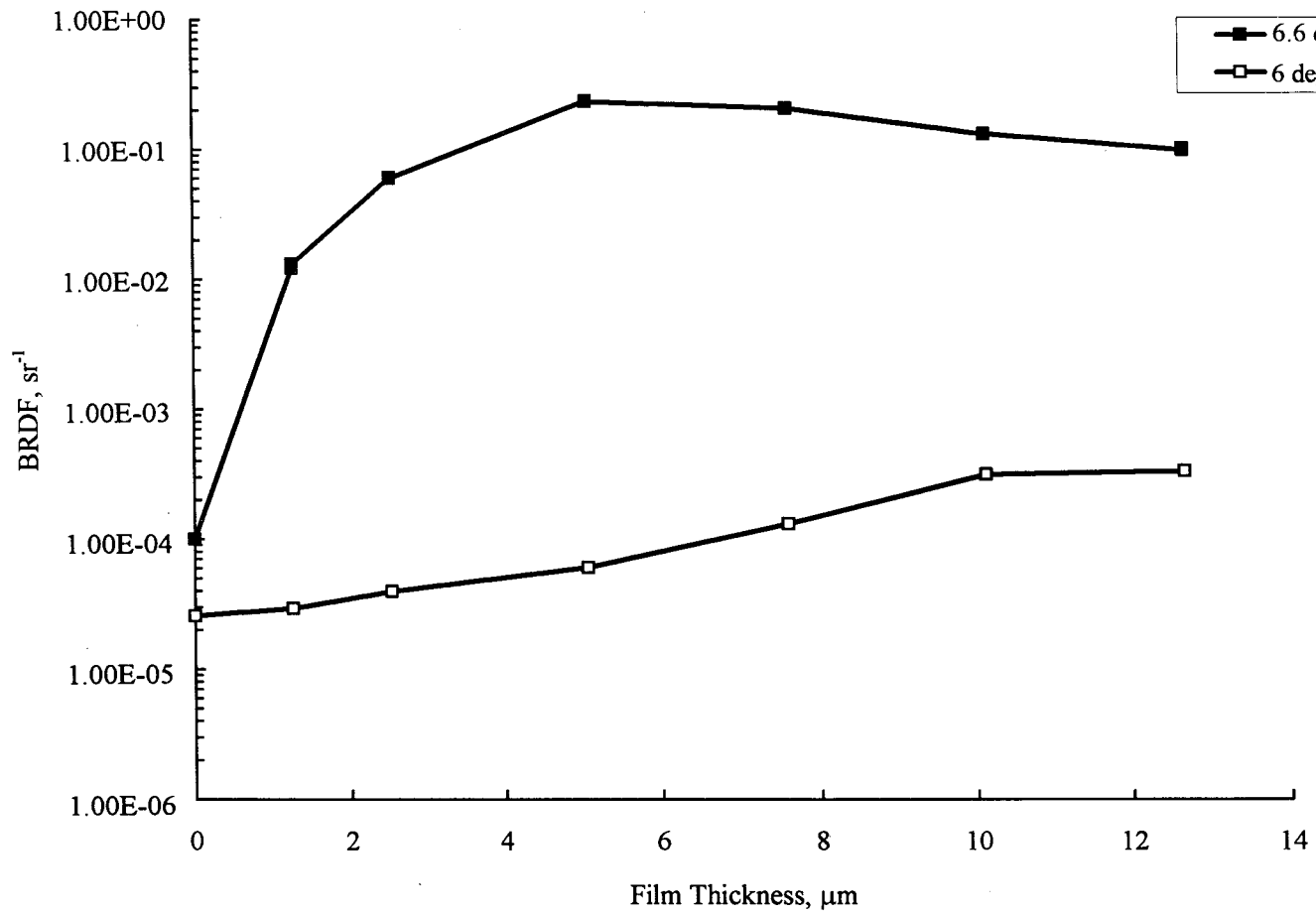


Figure 12. Superpolished mirror degradation with oxygen film thickness; 15 K surface, 6-deg scatter angle.

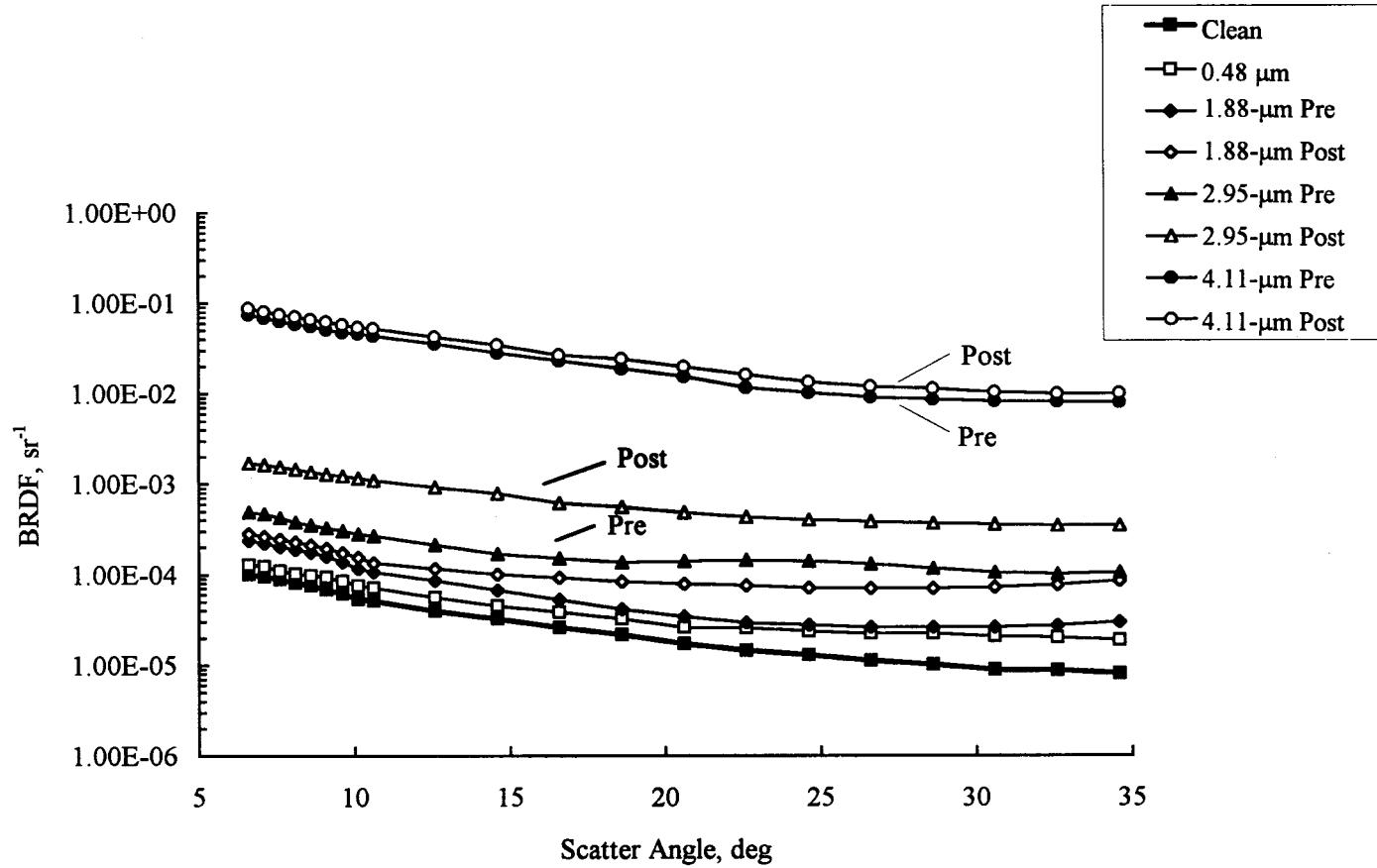
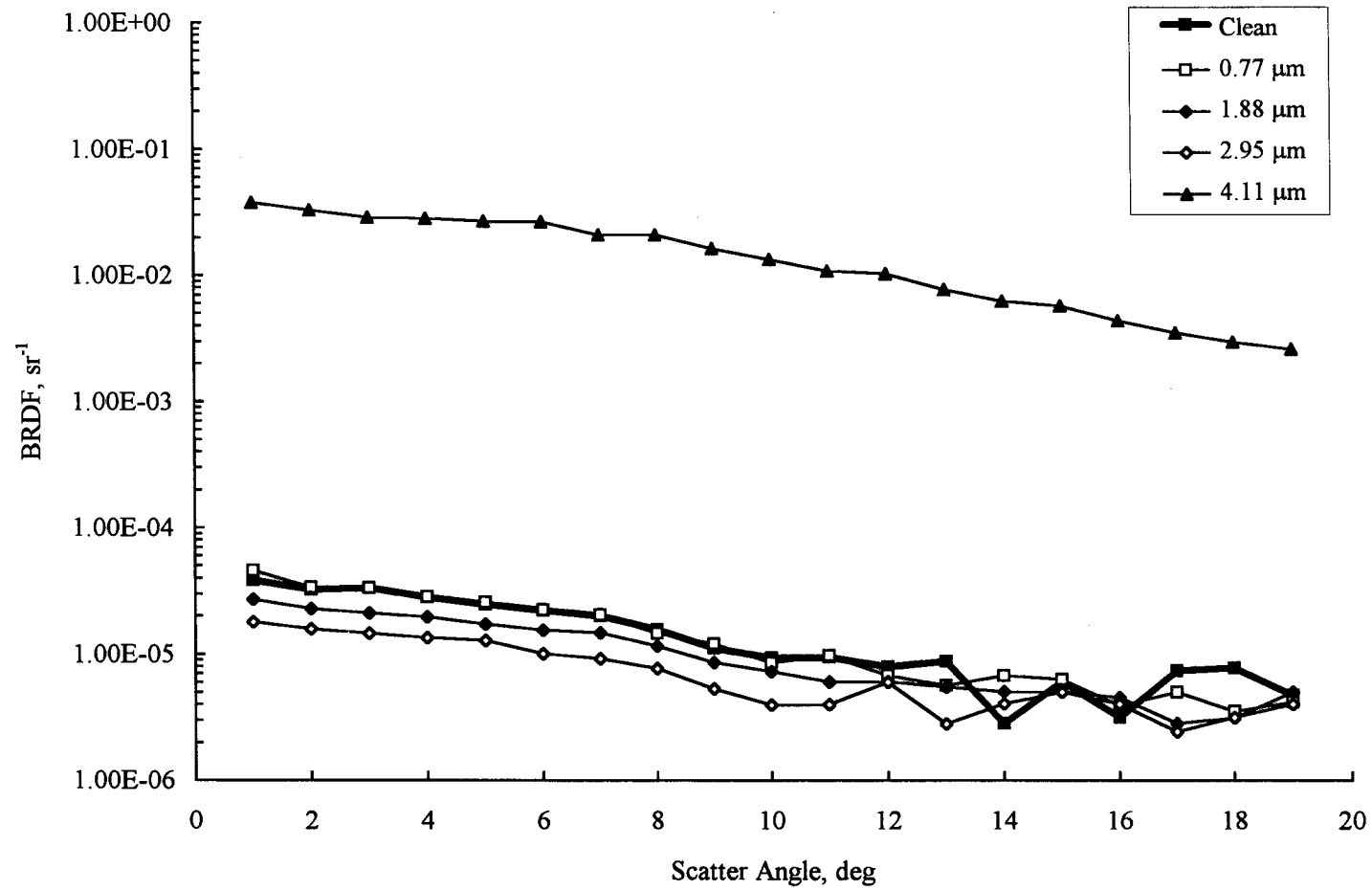


Figure 13. Superpolished mirror degradation at selected water film thickness; 16 K surface,  $0.63\text{-}\mu\text{m}$  wavelength.





**Figure 14. Superpolished mirror degradation at selected water film thickness; 16 K surface, 10.6- $\mu\text{m}$  wavelength.**

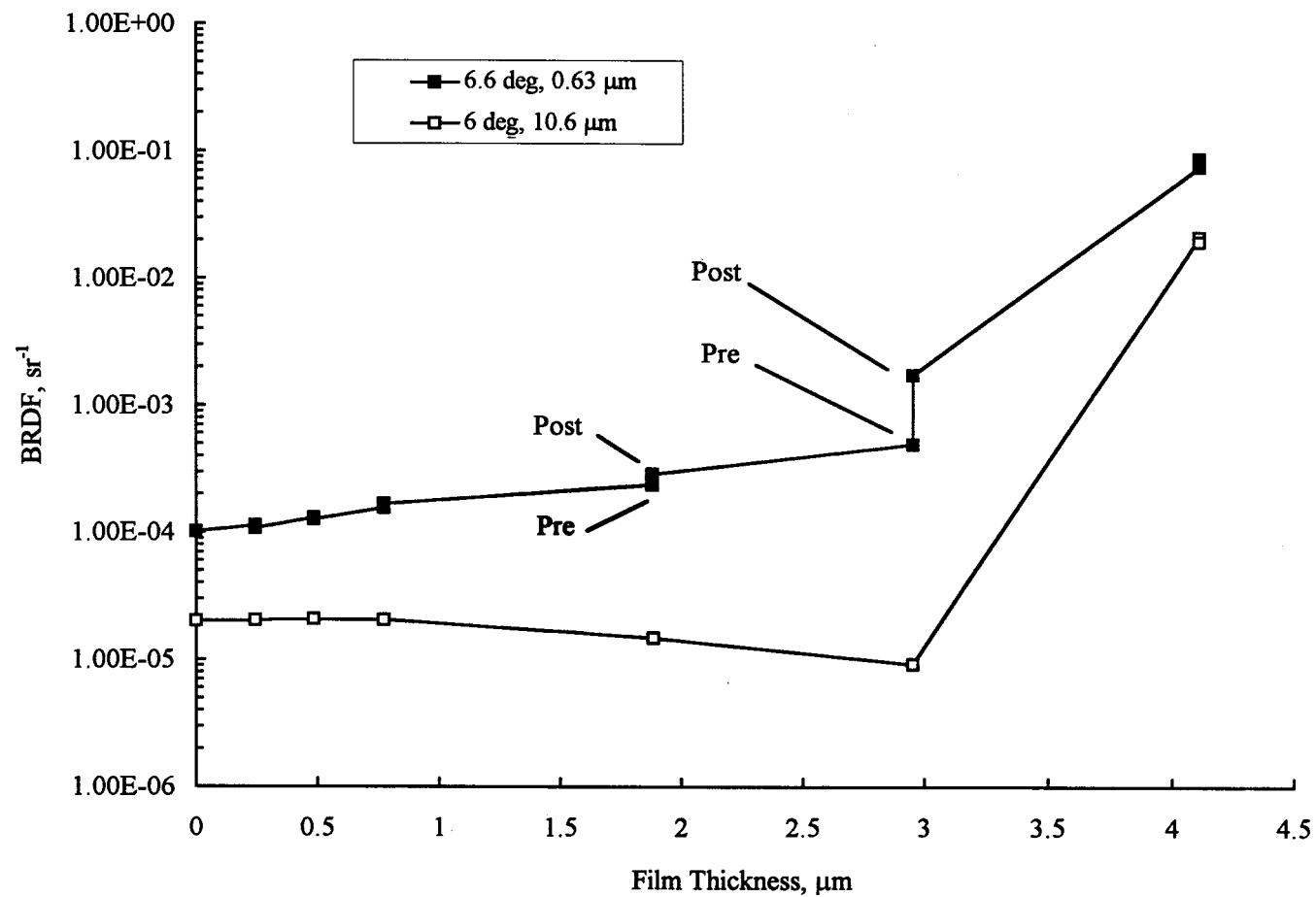


Figure 15. Superpolished mirror degradation with water film thickness; 16 K surface, 6-deg scatter angle.

50

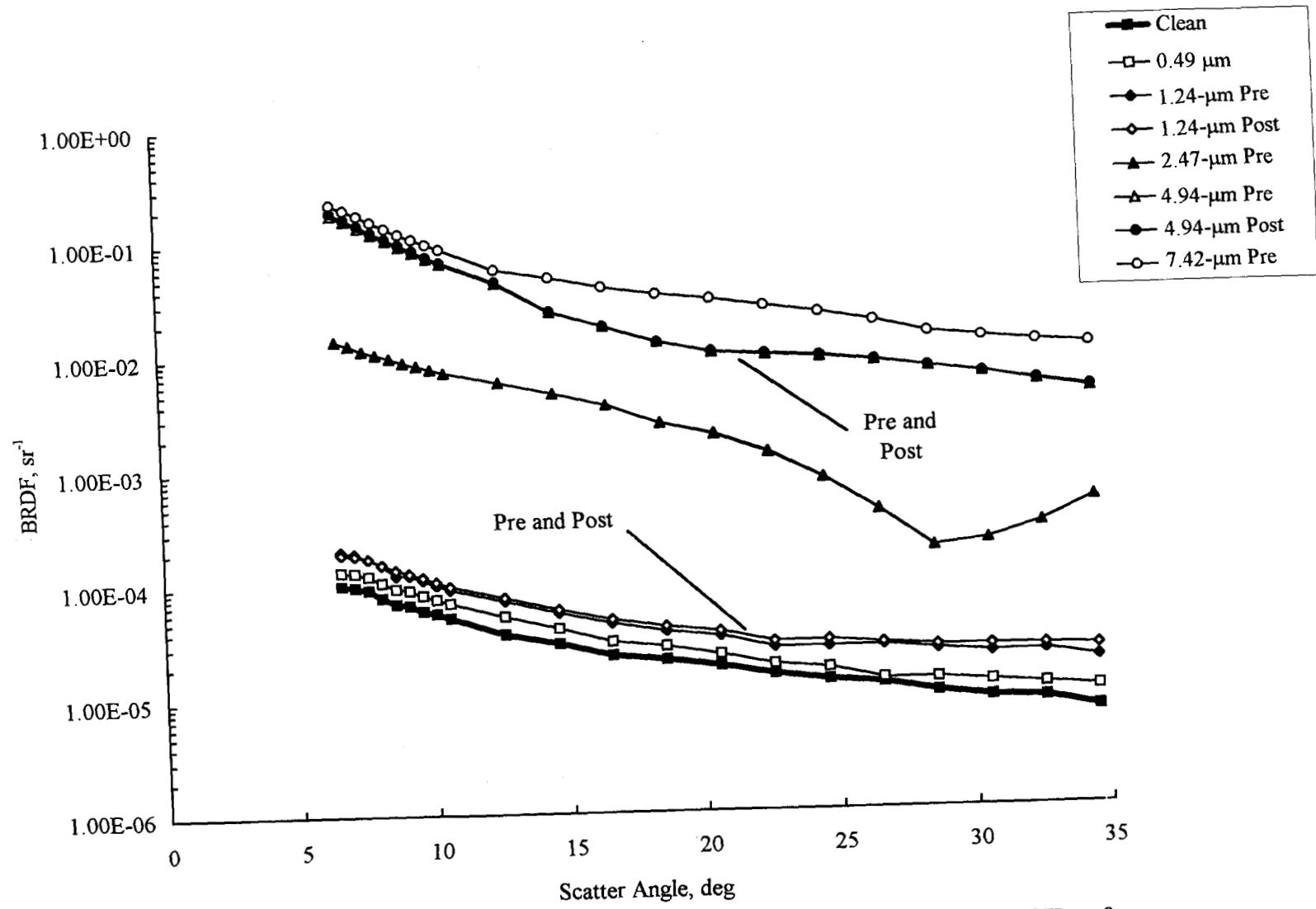


Figure 16. Superpolished mirror degradation at selected CO<sub>2</sub> film thickness; 17 K surface, 0.63- $\mu\text{m}$  wavelength.

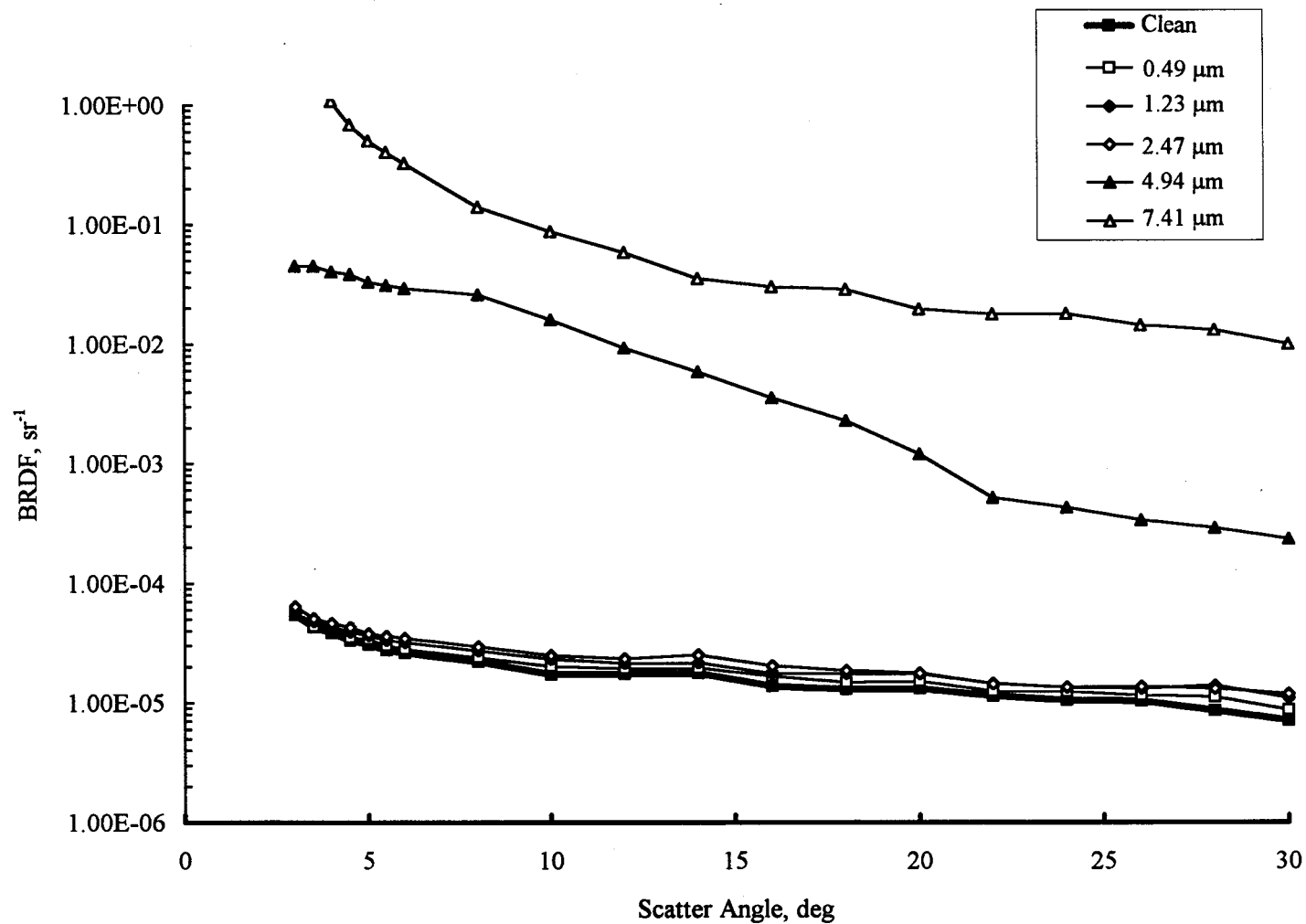


Figure 17. Superpolished mirror degradation at selected CO<sub>2</sub> film thickness; 17 K surface, 10.6-μm wavelength.

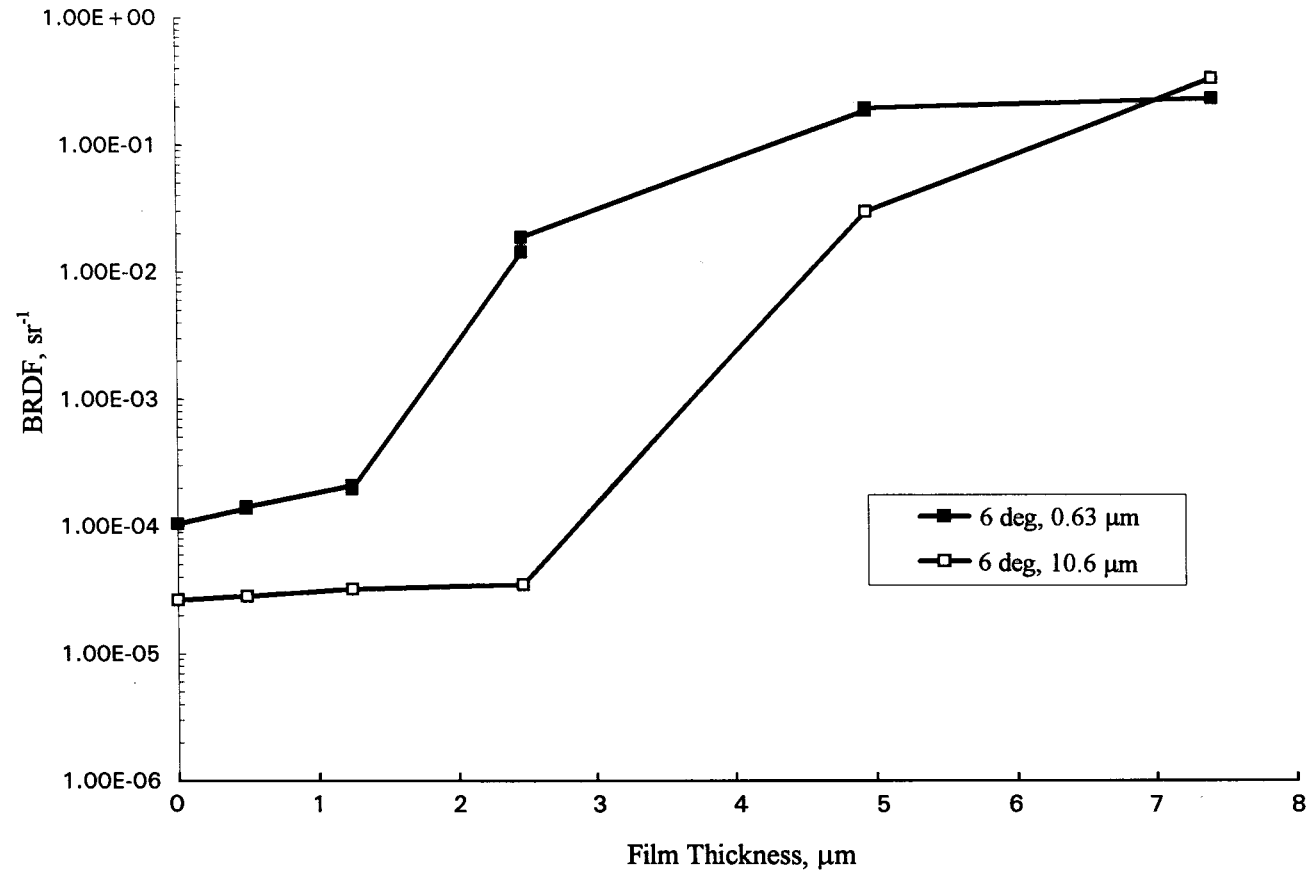


Figure 18. Superpolished mirror degradation with CO<sub>2</sub> film thickness; 17 K surface, 6-deg scatter angle.

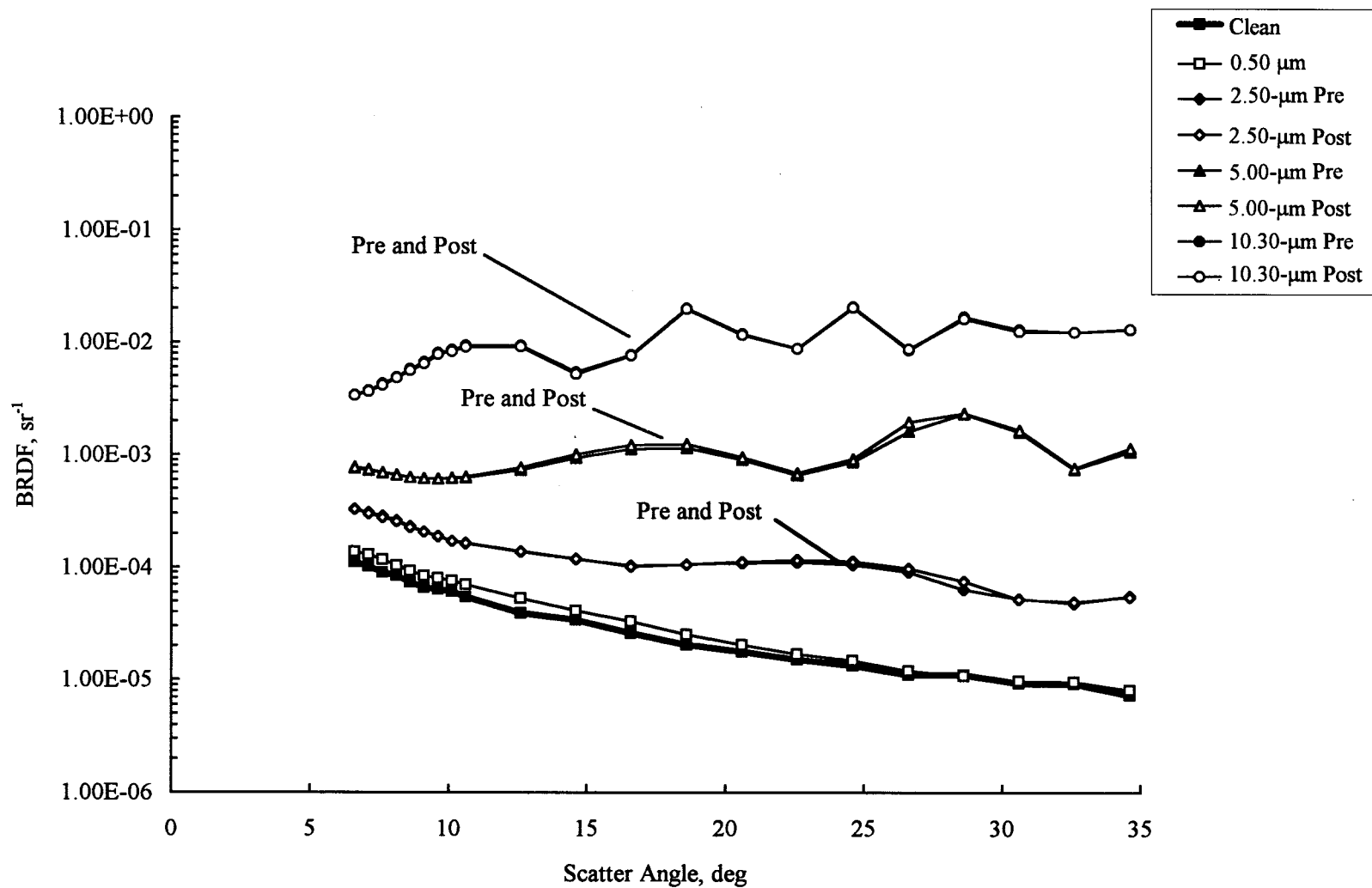
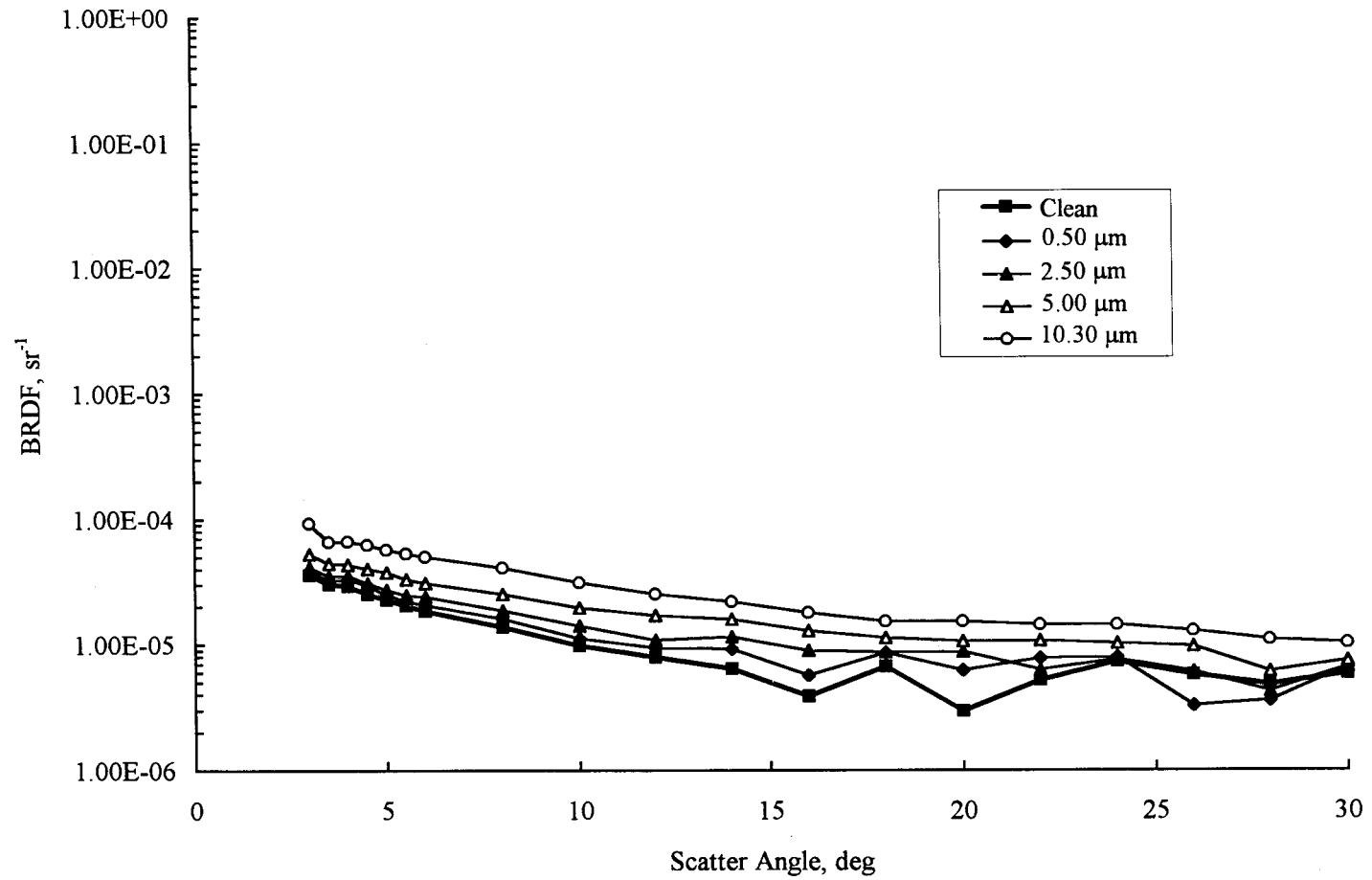


Figure 19. Superpolished mirror degradation at selected CO film thickness; 15 K surface, 0.63- $\mu\text{m}$  wavelength.



**Figure 20. Superpolished mirror degradation at selected CO film thickness; 15 K surface, 10.6-μm wavelength.**

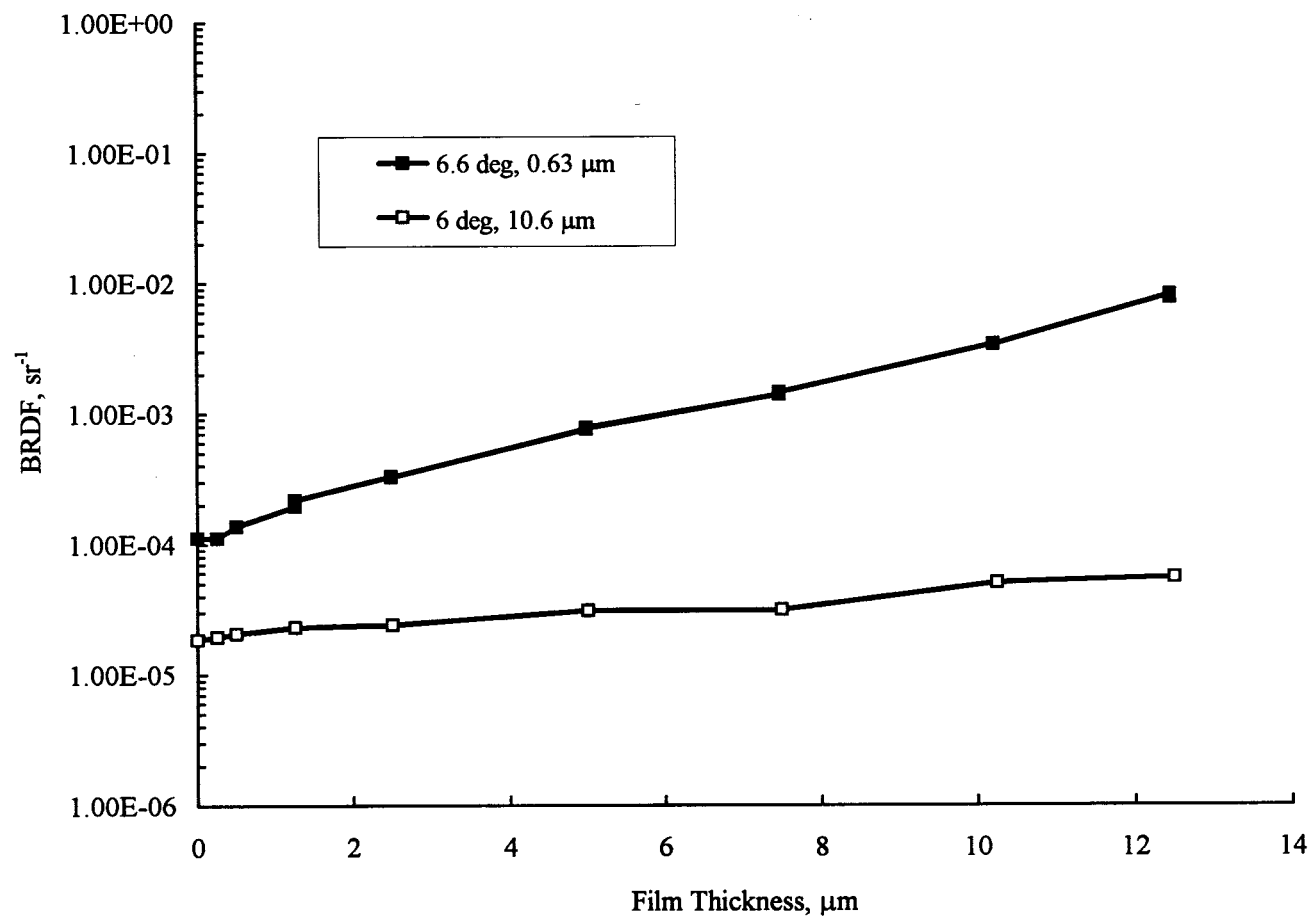


Figure 21. Superpolished mirror degradation with CO film thickness; 15 K surface, 6-deg scatter angle.



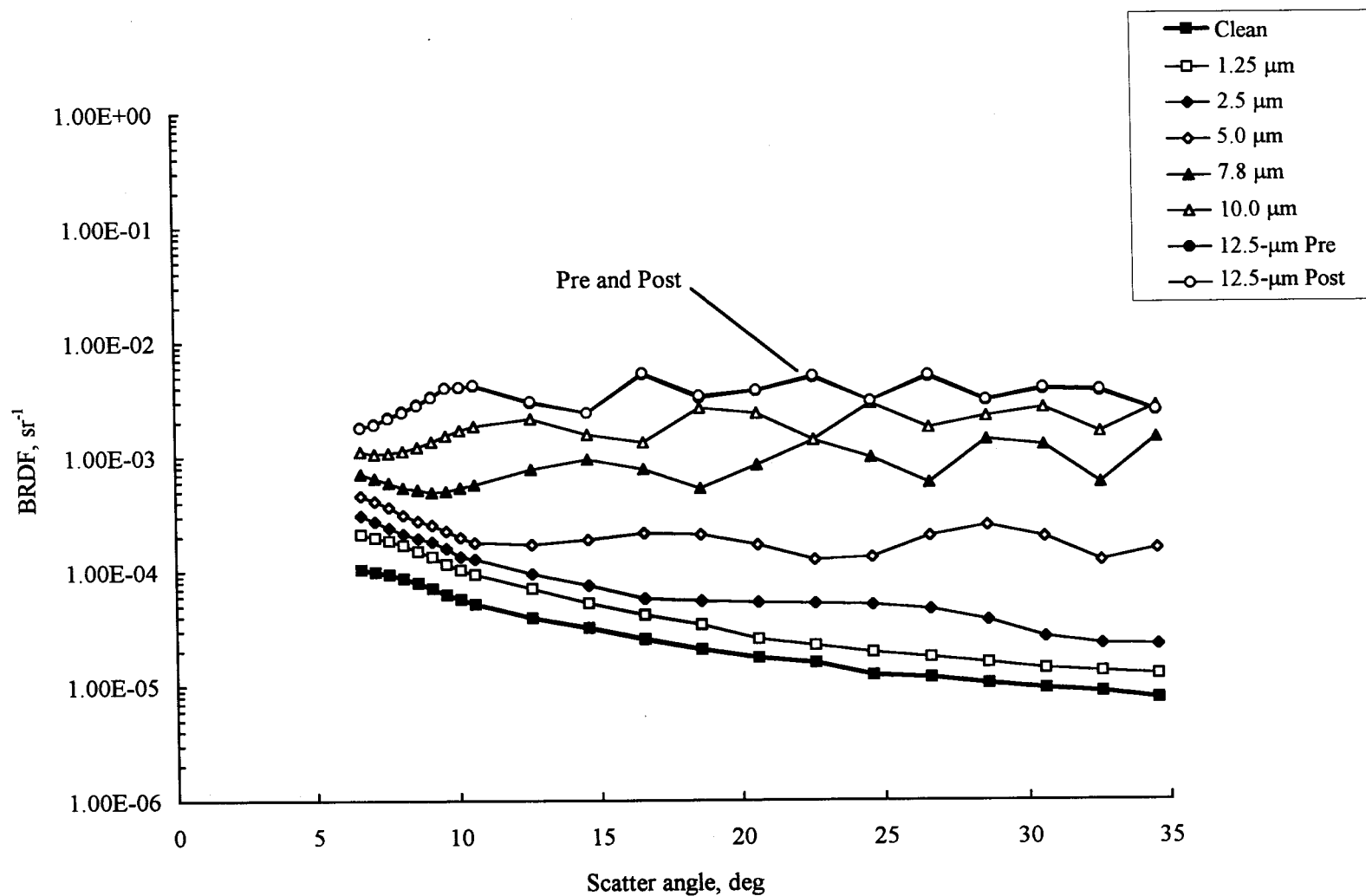


Figure 22. Superpolished mirror degradation at selected argon film thickness; 16 K surface, 0.63- $\mu\text{m}$  wavelength.

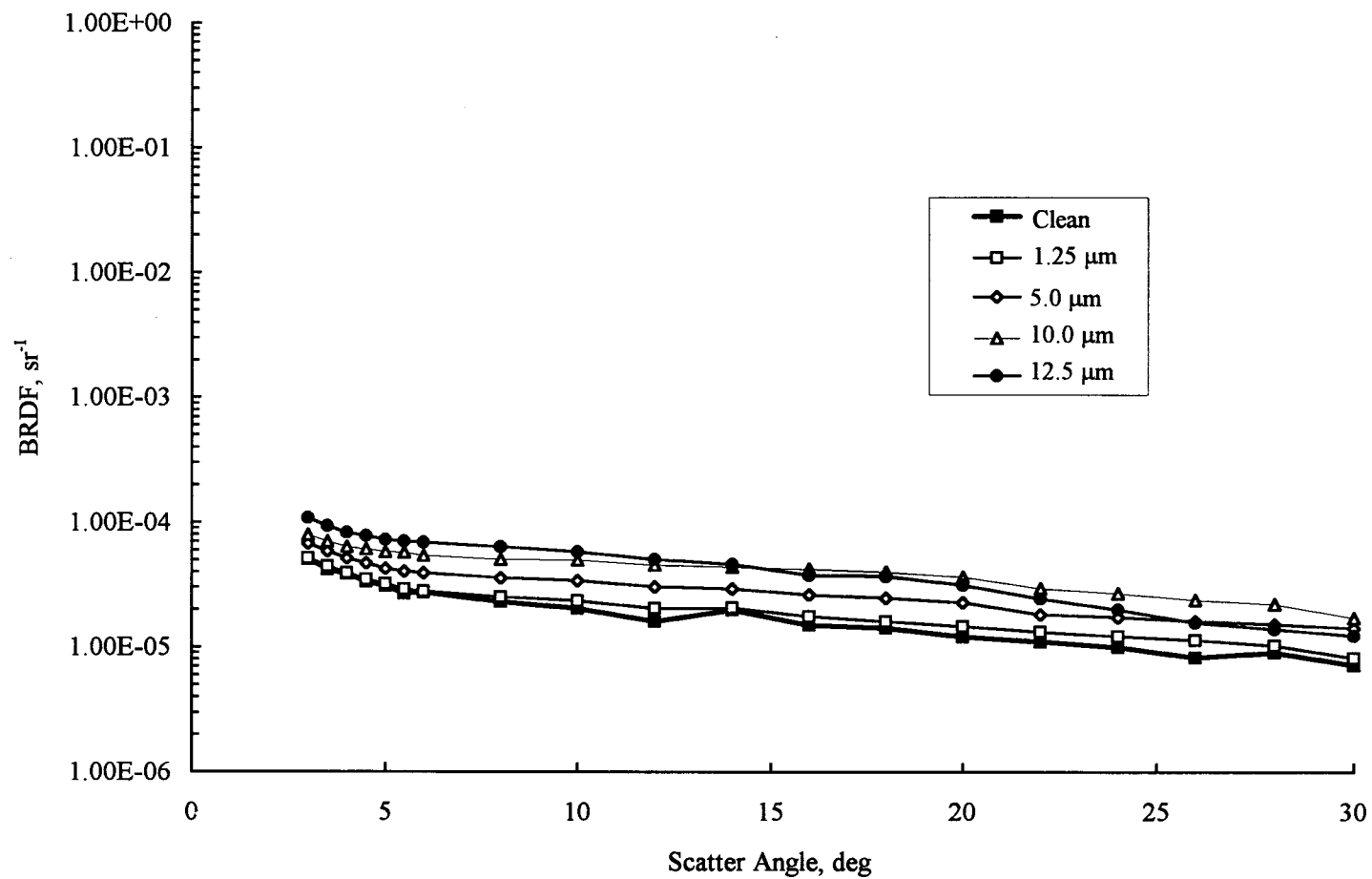
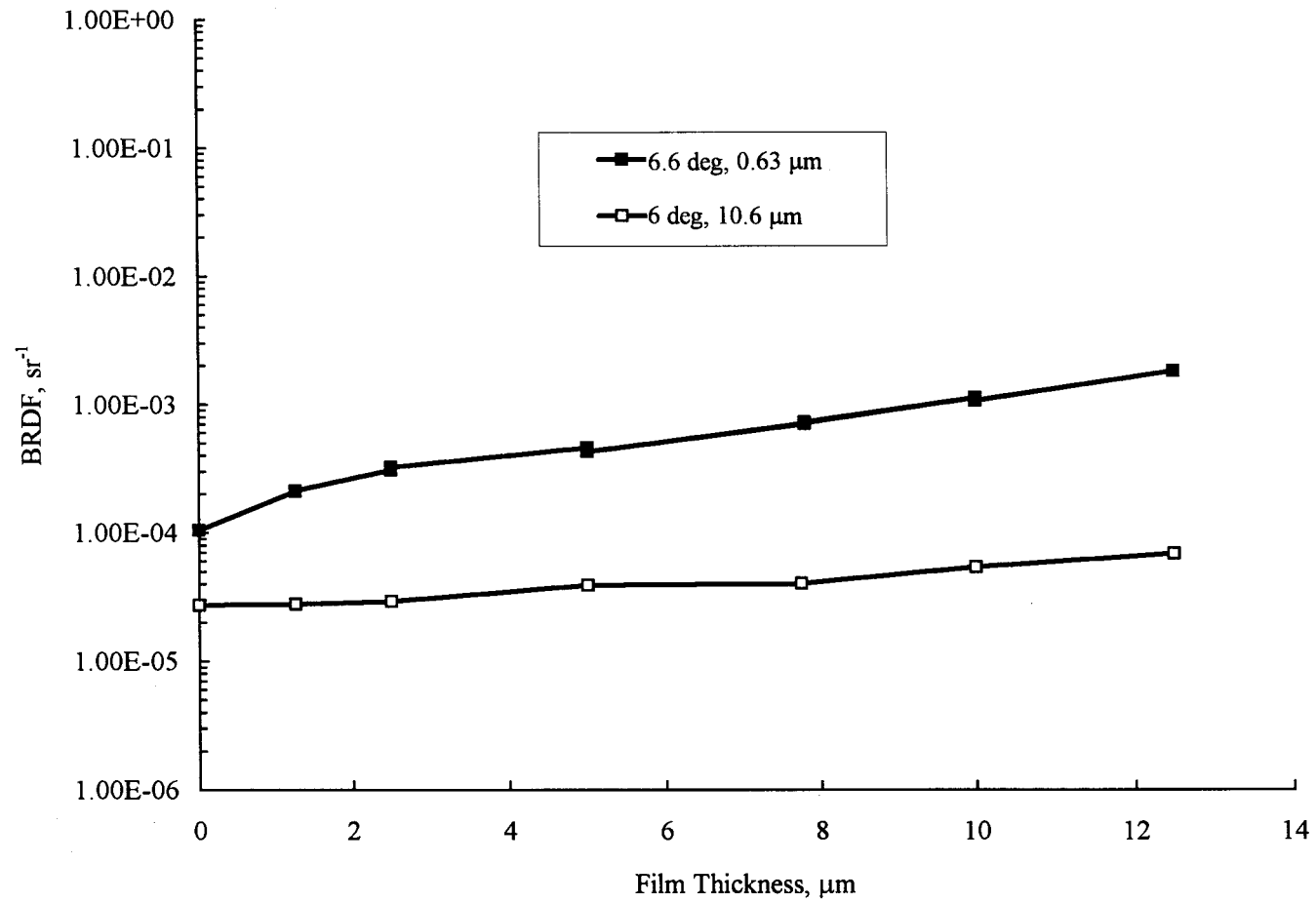


Figure 23. Superpolished mirror degradation at selected argon film thickness; 16 K surface, 10.6-μm wavelength.



**Figure 24. Superpolished mirror degradation with argon film thickness; 16 K surface, 6-deg scatter angle.**

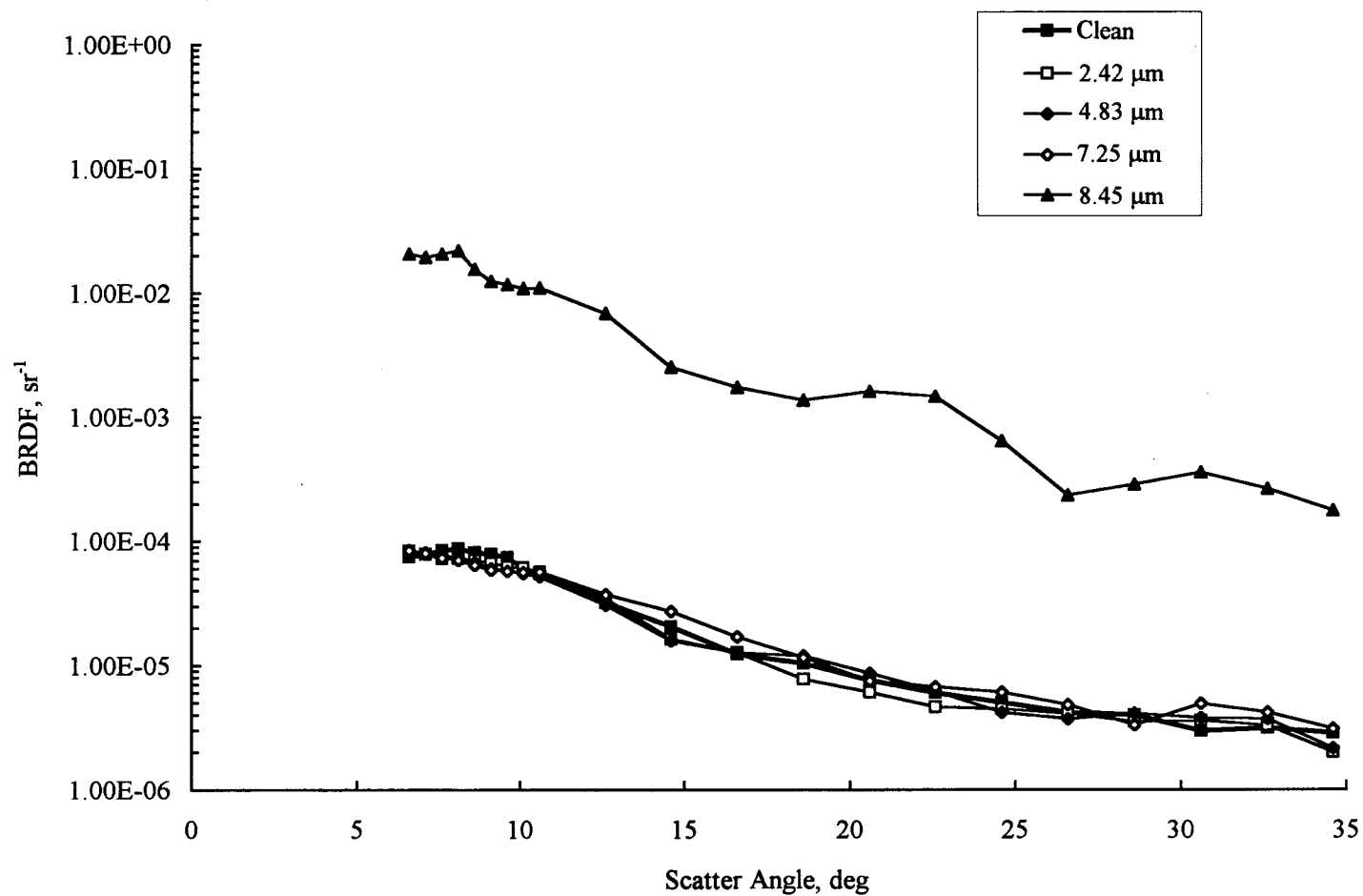


Figure 25. Superpolished mirror degradation at selected water film thickness; 88 K surface, 0.63-μm wavelength.

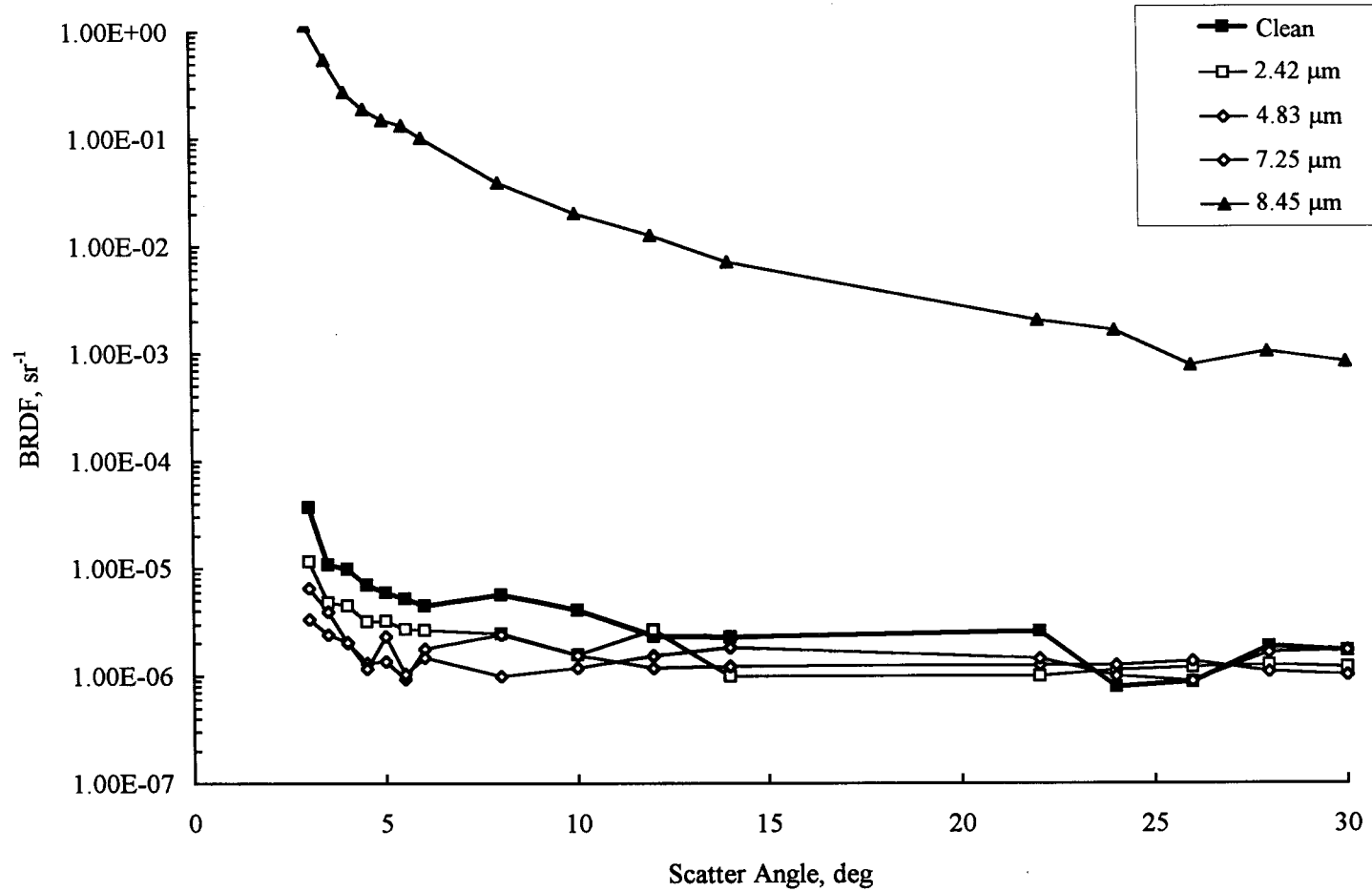


Figure 26. Superpolished mirror degradation at selected water film thickness; 88 K surface, 10.6-μm wavelength.

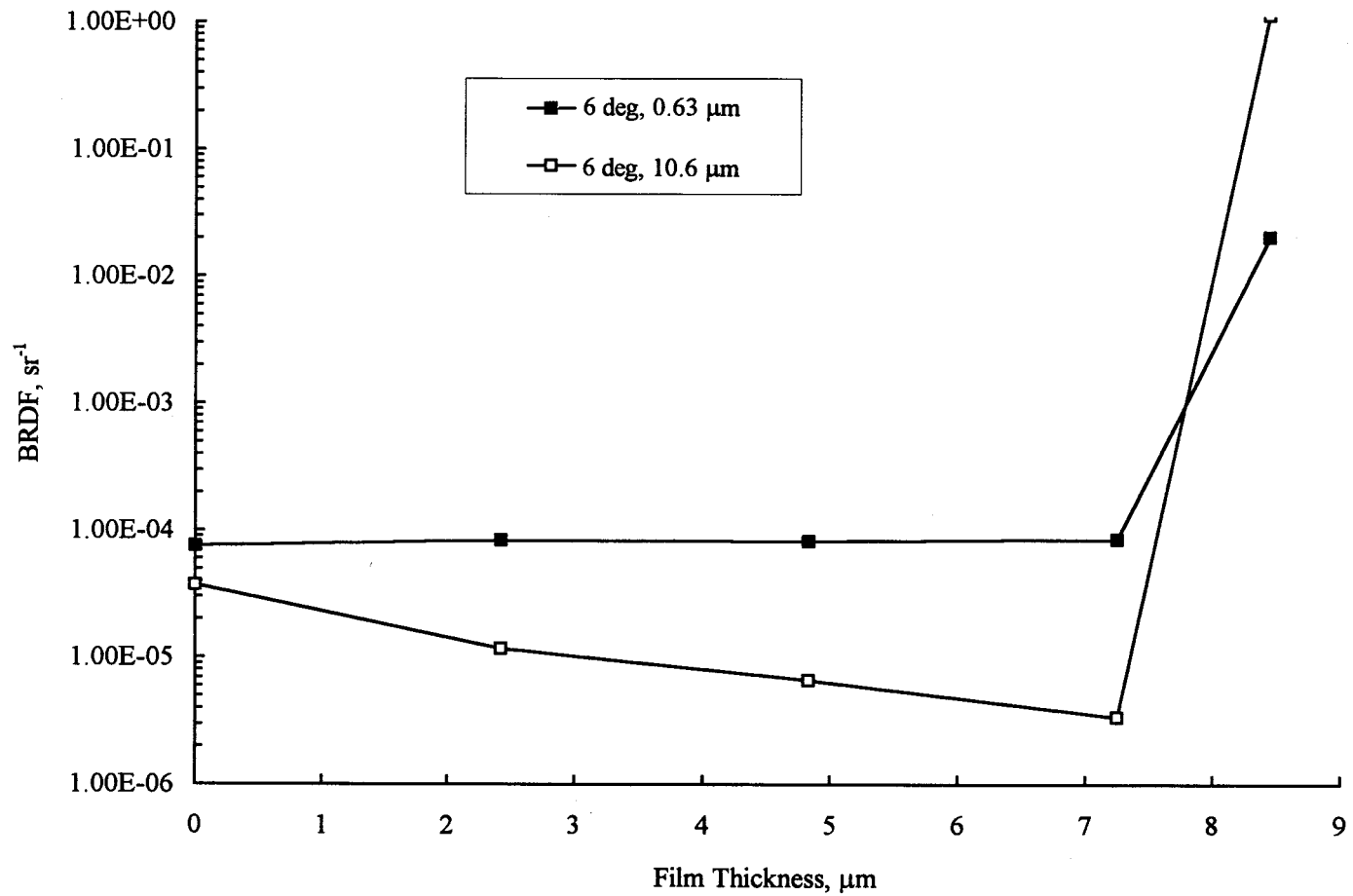


Figure 27. Superpolished mirror degradation with water film thickness; 88 K surface, 6-deg scatter angle.

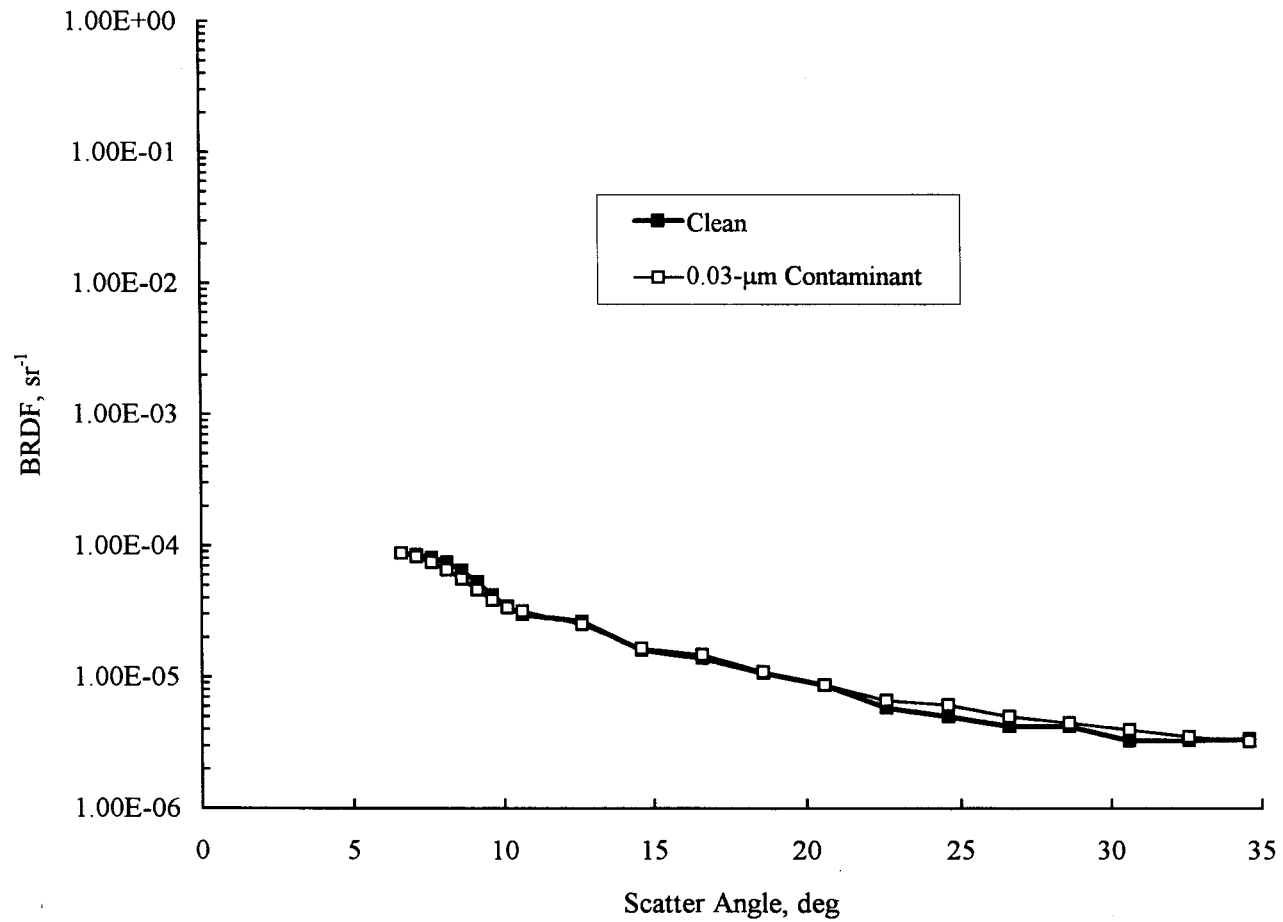
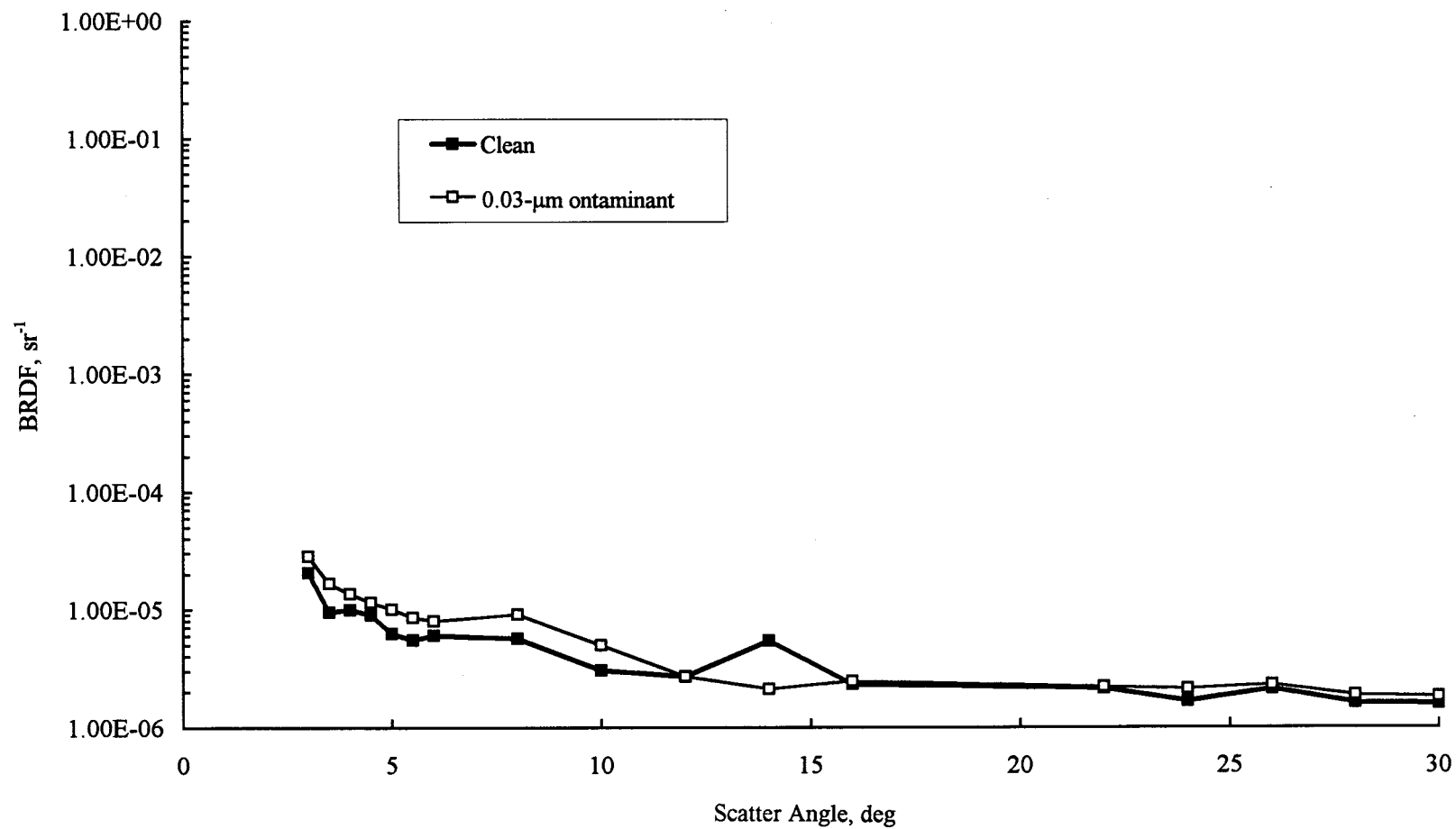


Figure 28. Superpolished mirror degradation with RS12M polycyanate resin effluent; 68 K surface, 0.63-μm wavelength.



**Figure 29. Superpolished mirror degradation with RS12M polycyanate resin effluent;  
68 K surface, 10.6-μm wavelength.**



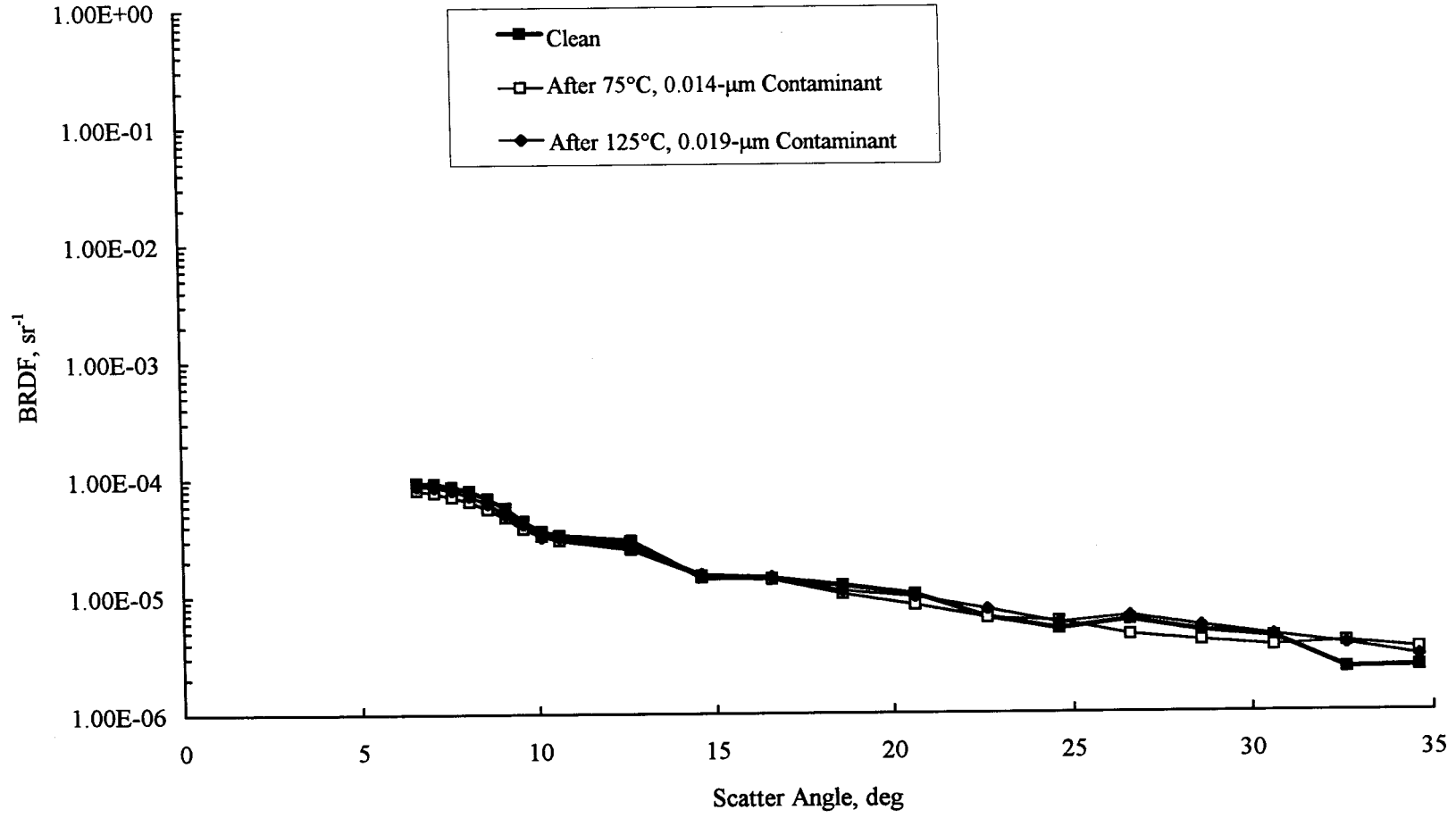
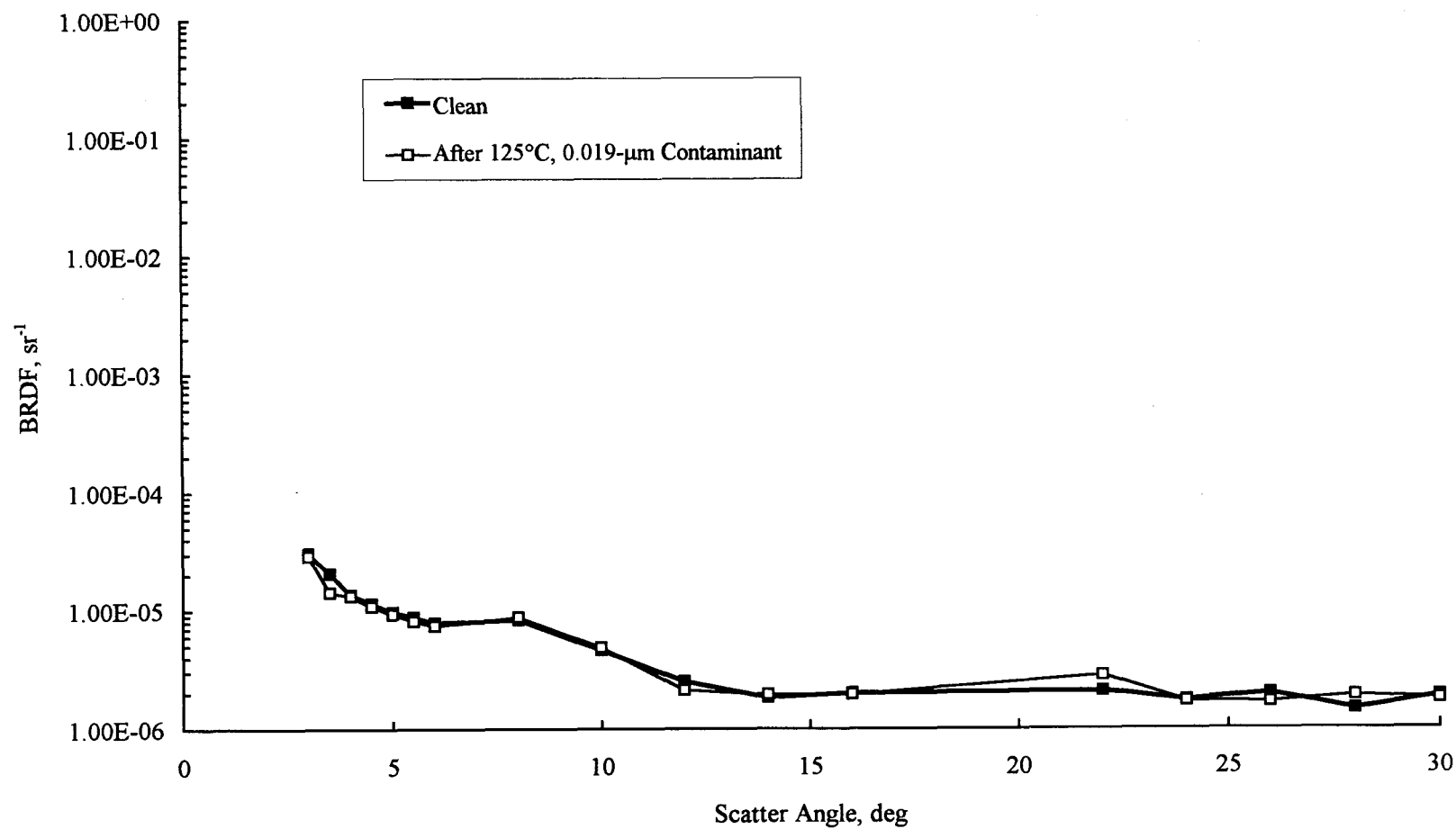


Figure 30. Superpolished mirror degradation with Nusil CV2500 silicone effluent; 68 K surface, 0.63-μm wavelength.



**Figure 31. Superpolished mirror degradation with Nusil CV2500 silicone effluent;  
68 K surface, 10.6-μm wavelength.**

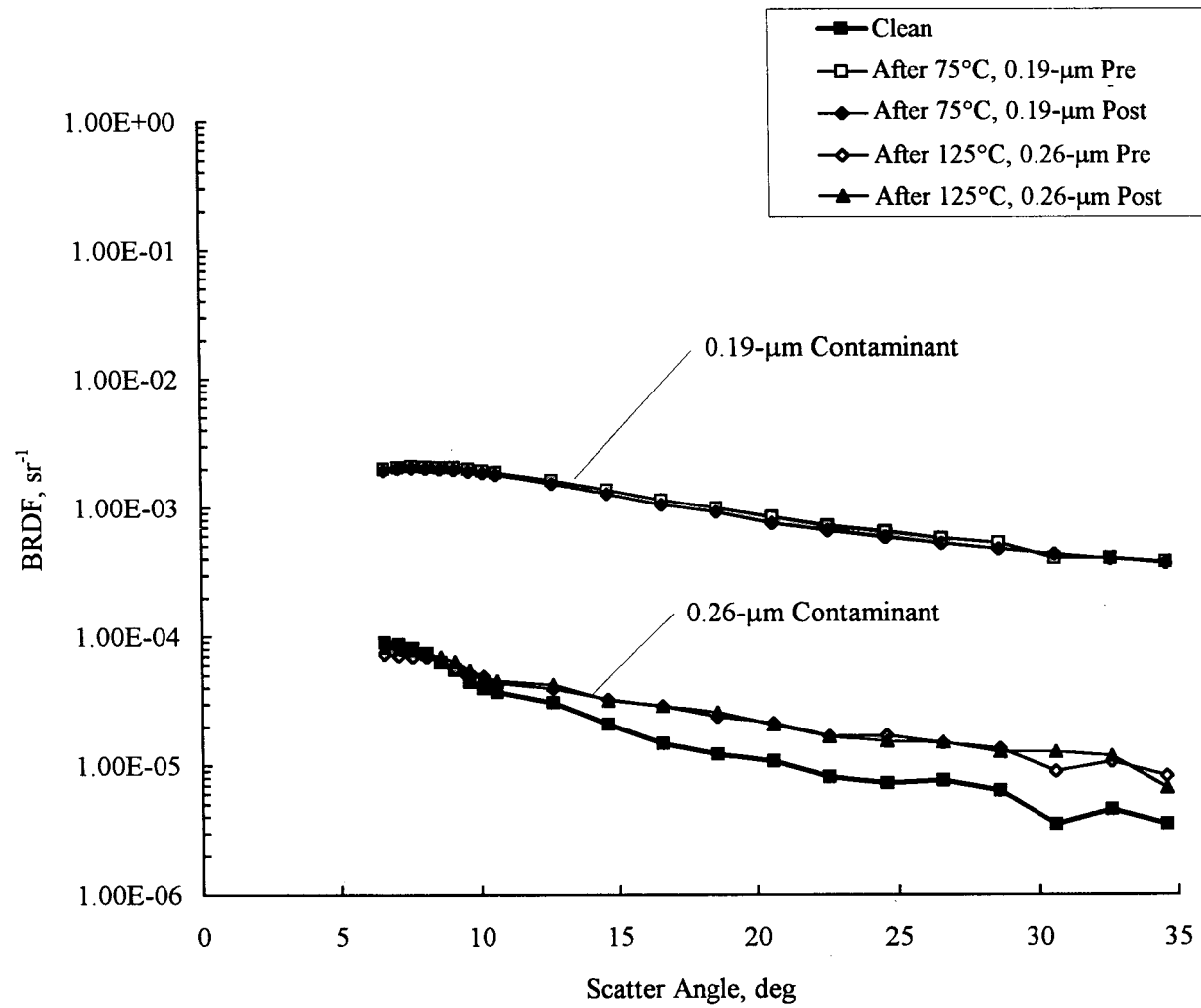
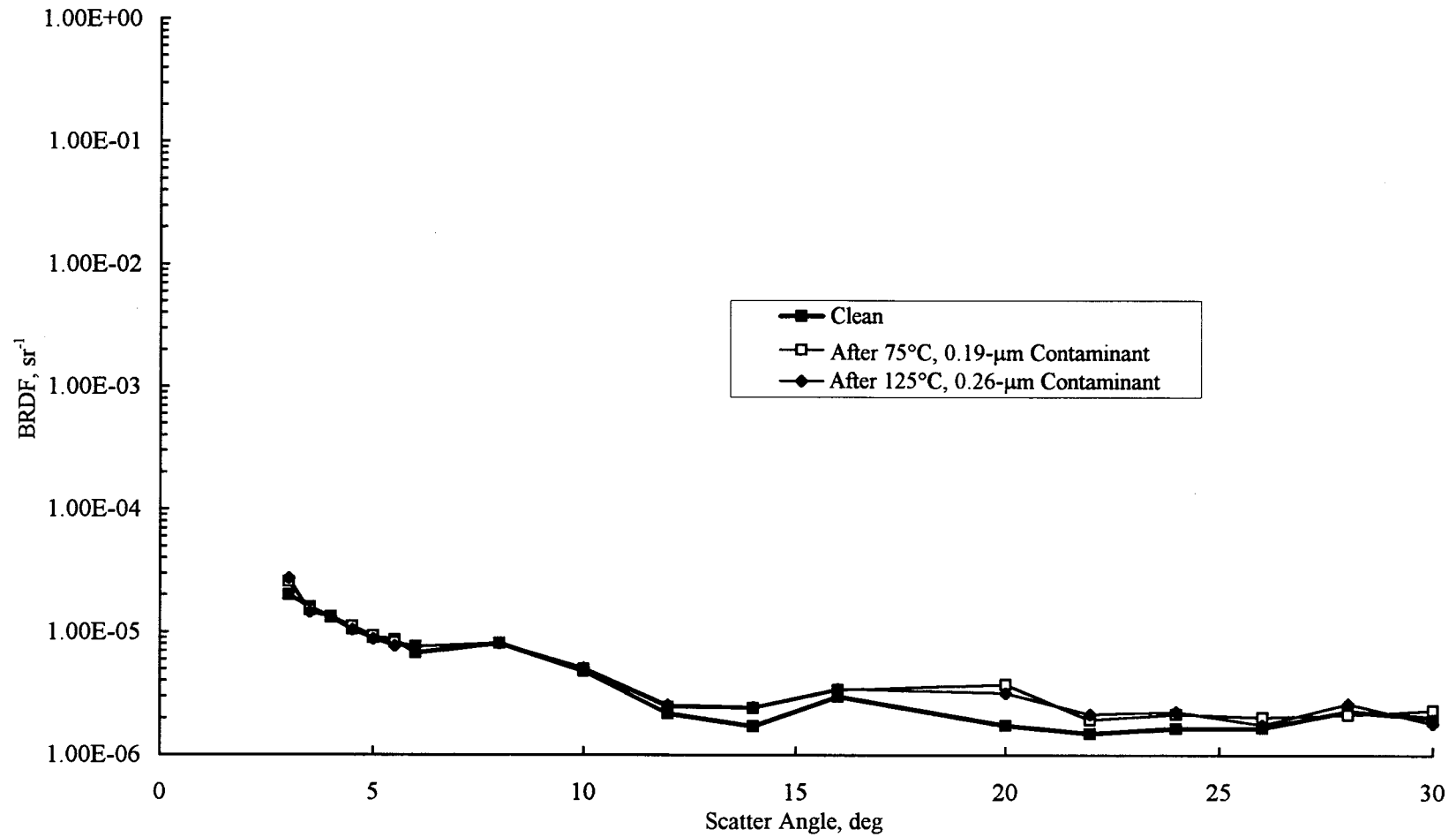


Figure 32. Superpolished mirror degradation with Solithane 113/C113-300 effluent;  
68 K surface, 0.63- $\mu\text{m}$  wavelength.



**Figure 33. Superpolished mirror degradation with Solithane 113/C113-300 effluent;  
68 K surface, 10.6-μm wavelength.**

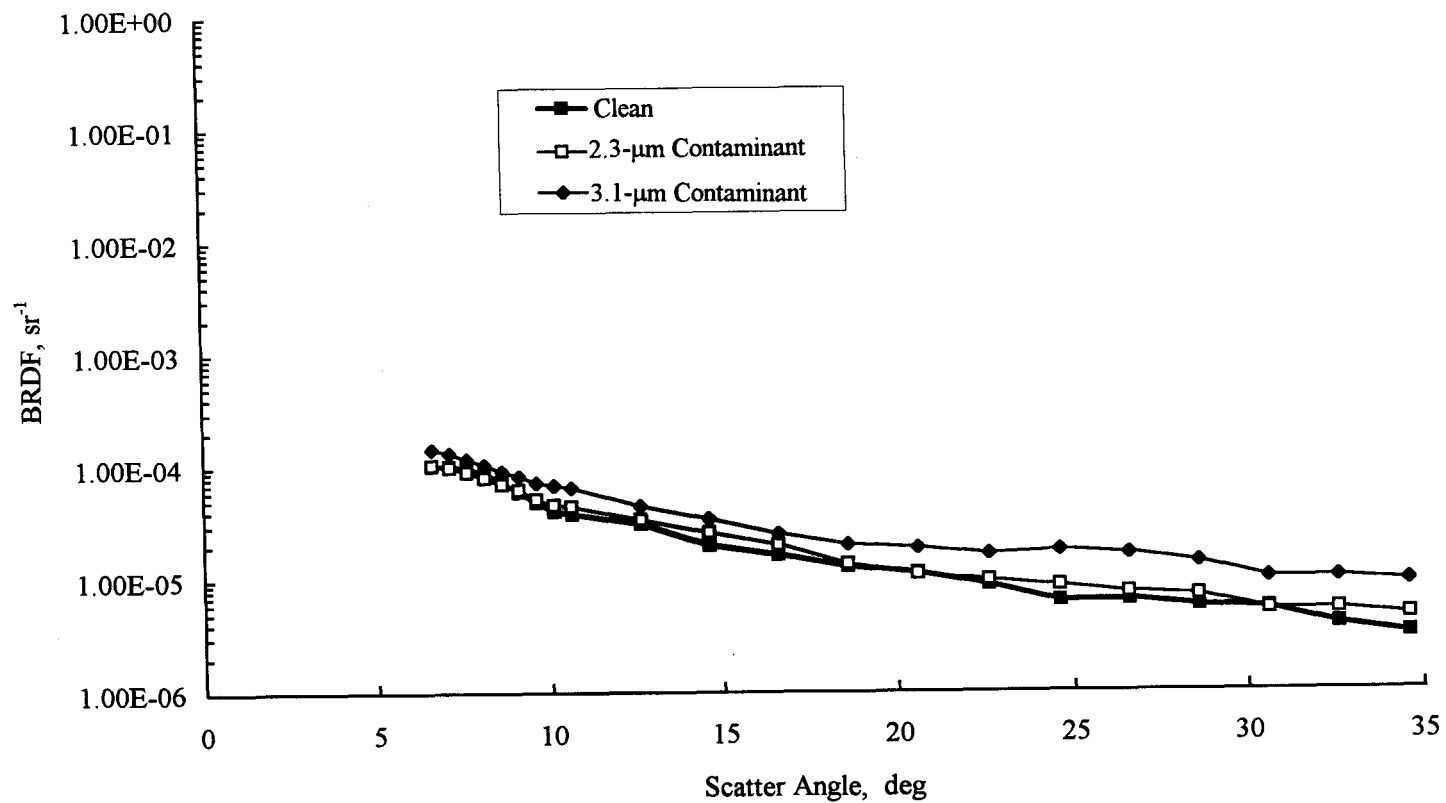
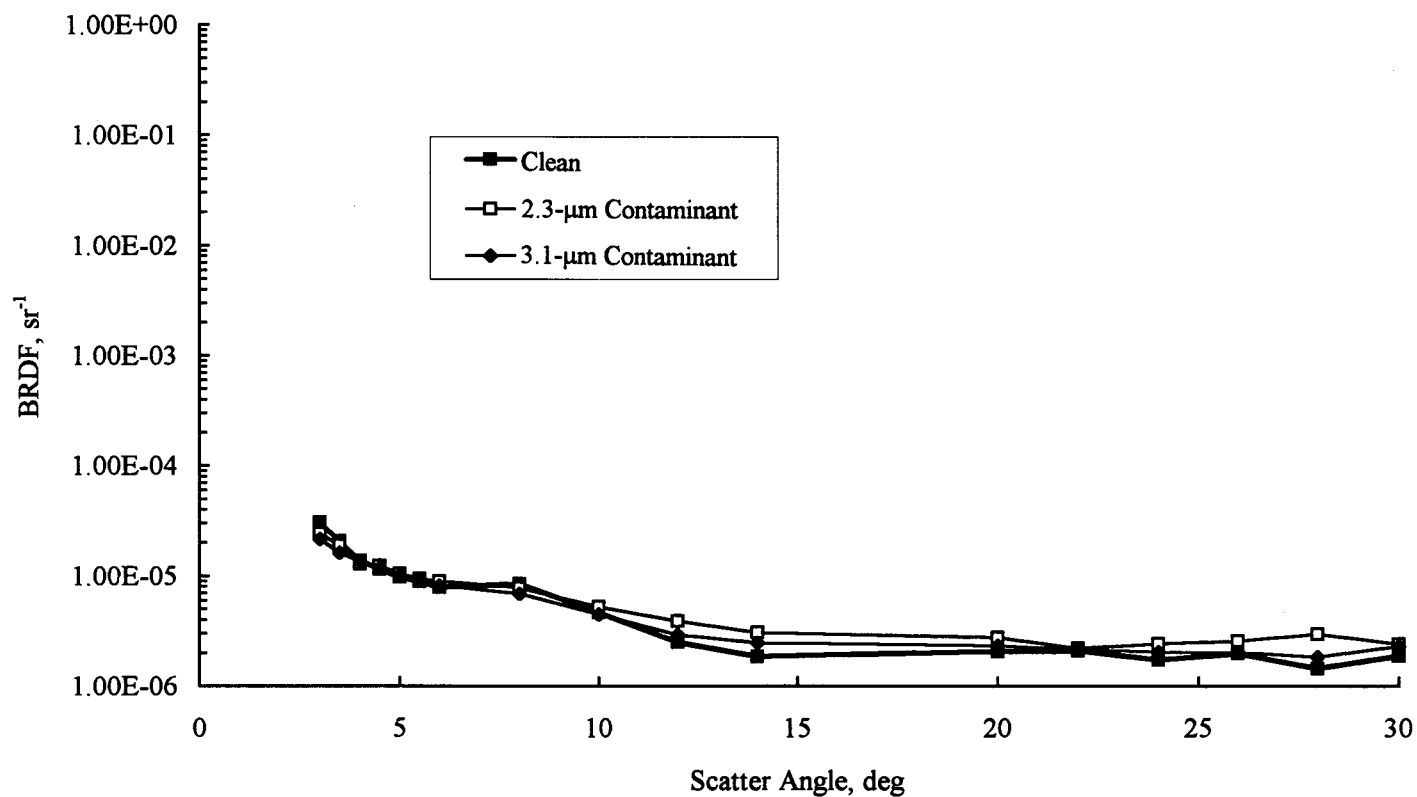
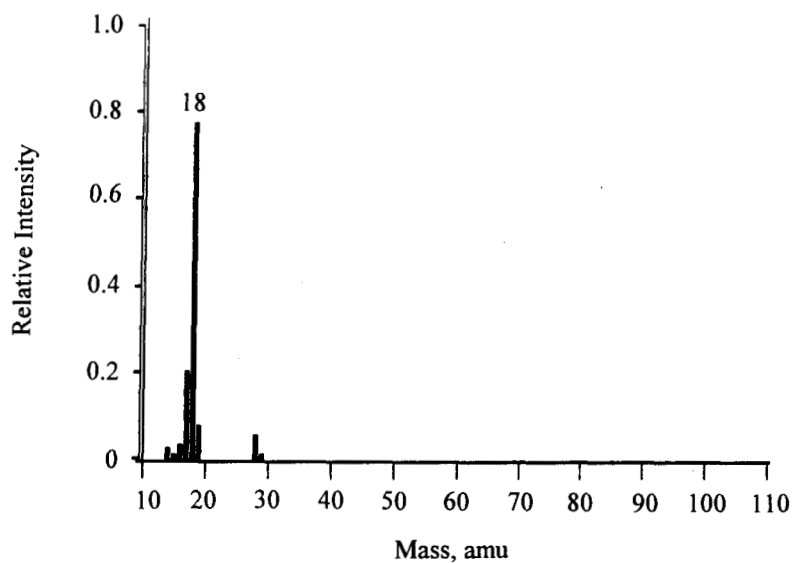


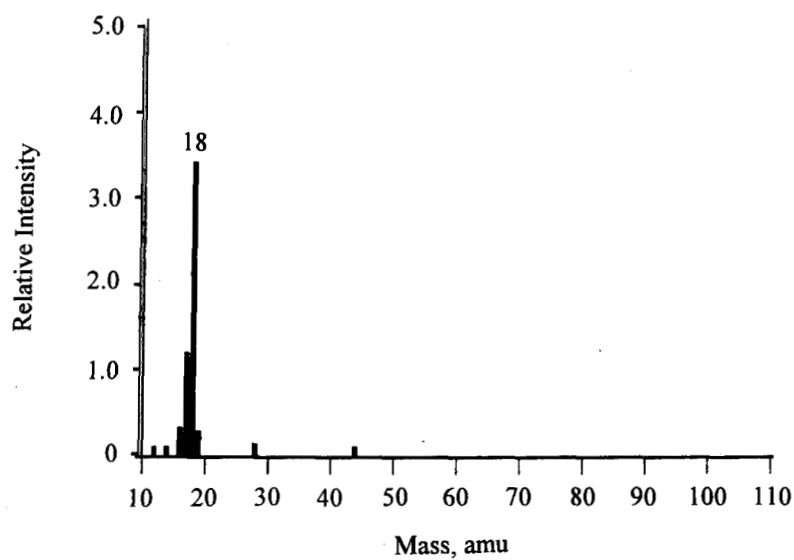
Figure 34. Superpolished mirror degradation with RTV560 silicone effluent; 68 K surface, 0.63-μm wavelength.



**Figure 35 Superpolished mirror degradation with RTV560 silicone effluent; 68 K surface, 10.6-μm wavelength.**

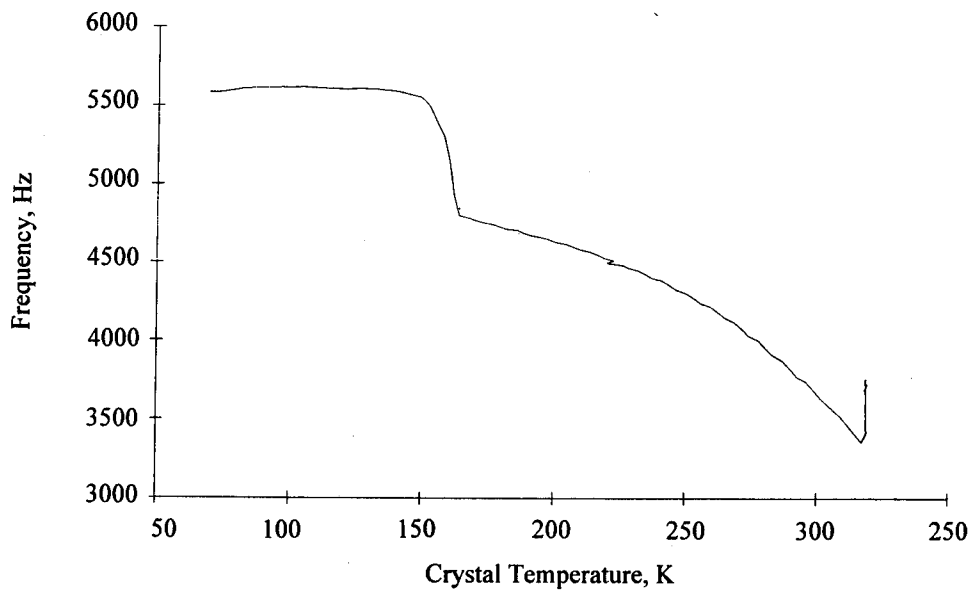


**a. Mass spectrum of effusion cell effluent at 75°C**

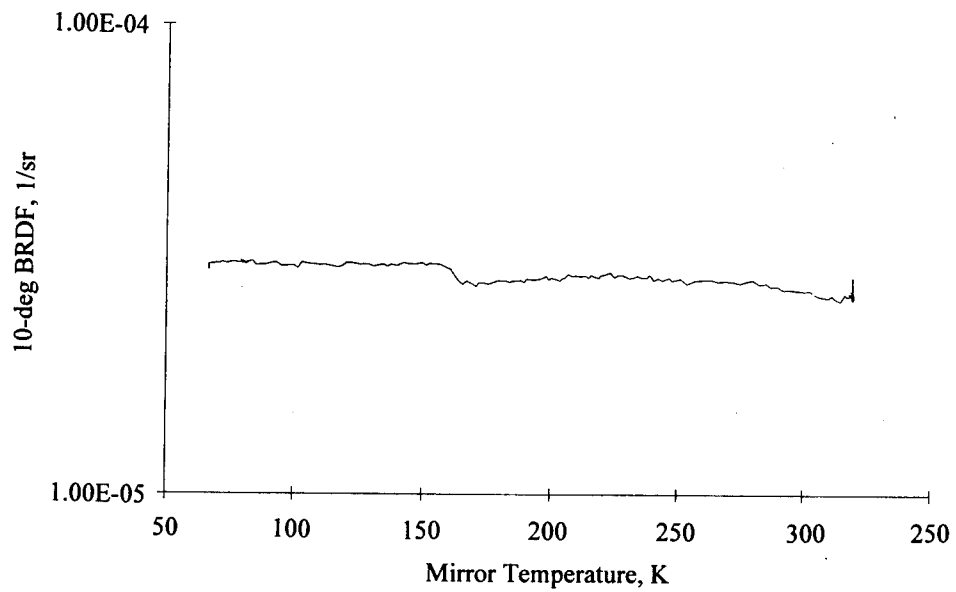


**b. Mass spectrum of effusion cell effluent at 125°C**

**Figure 36. RS12M polycyanate resin effluent mass spectrum.**



**a. QCM warmup**



**b. Mirror warmup, 10-deg BRDF, 0.63- $\mu$ m wavelength**

**Figure 37. QCM and superpolished mirror warmup, RS12M polycyanate resin.**



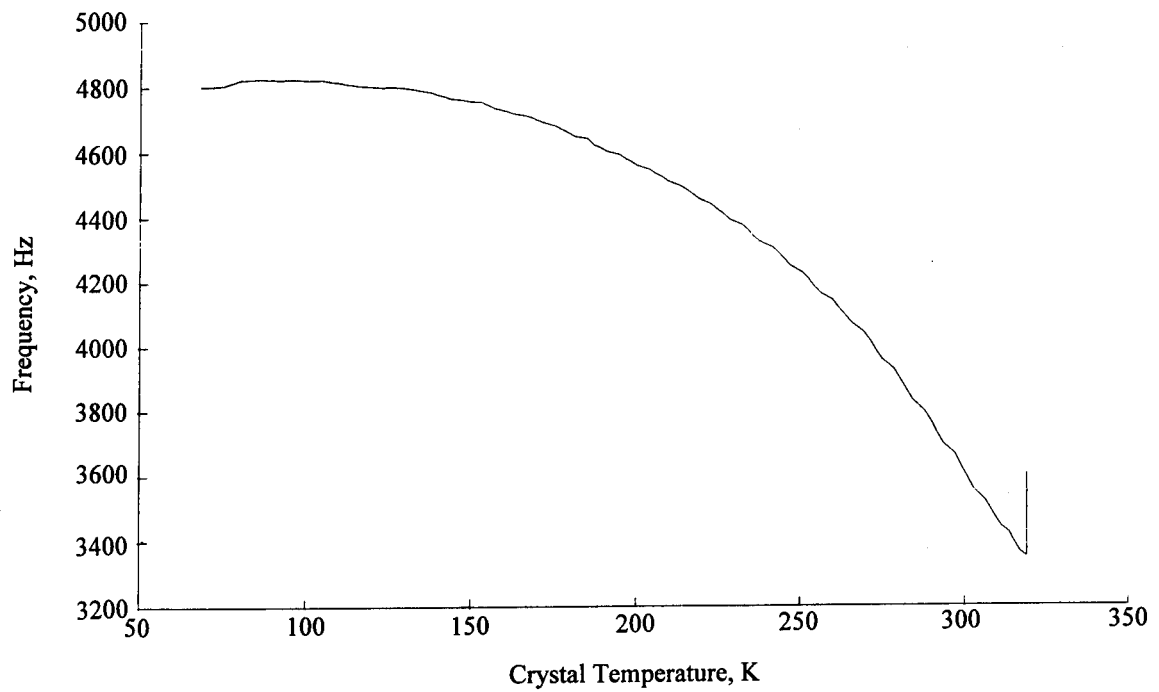
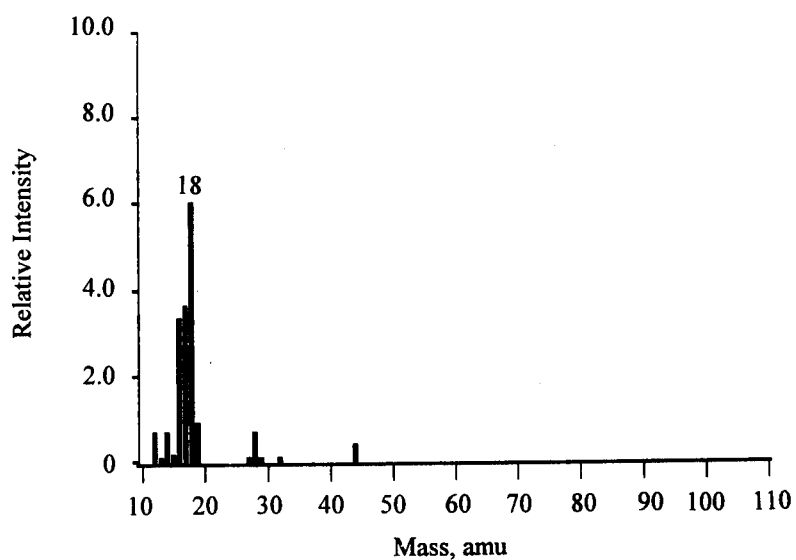
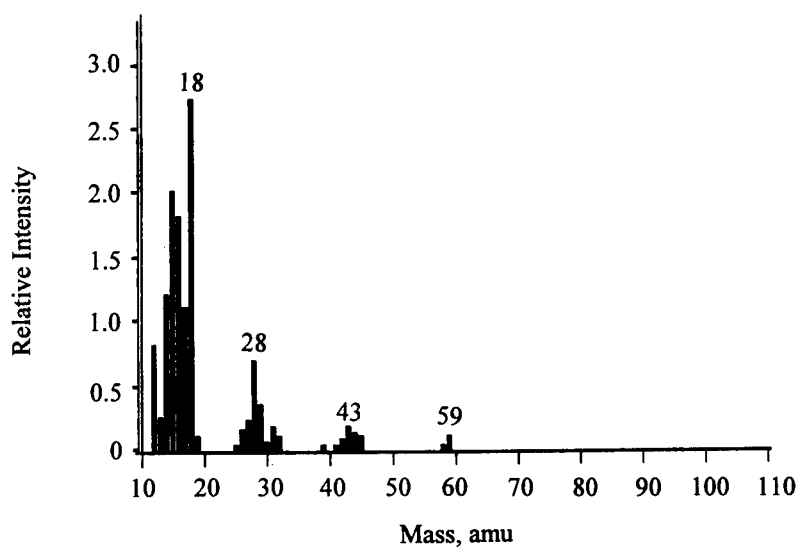


**Figure 38. QCM warmup with no contaminant, sn 588.**

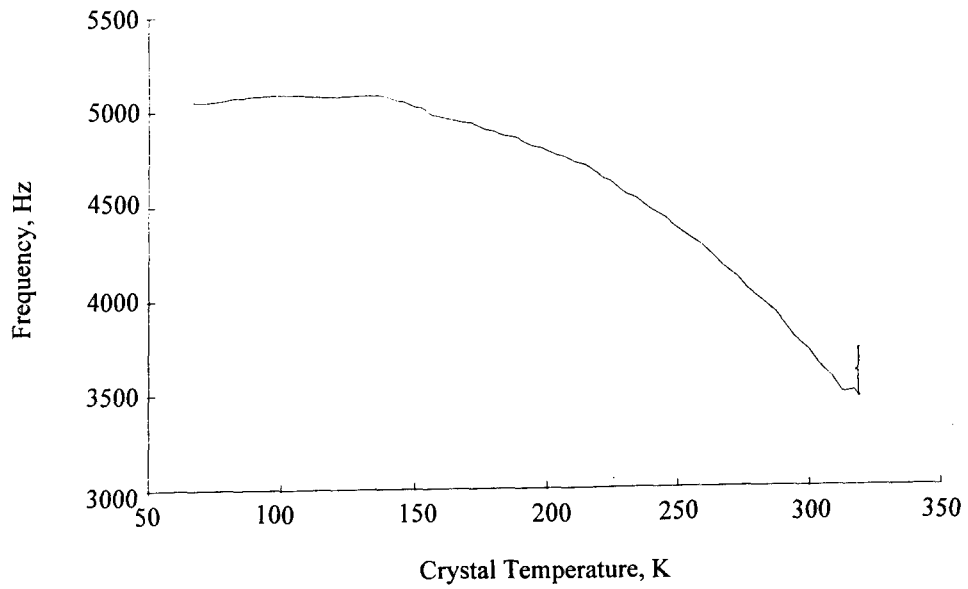


**a. Mass spectrum of effusion cell effluent at 75°C**

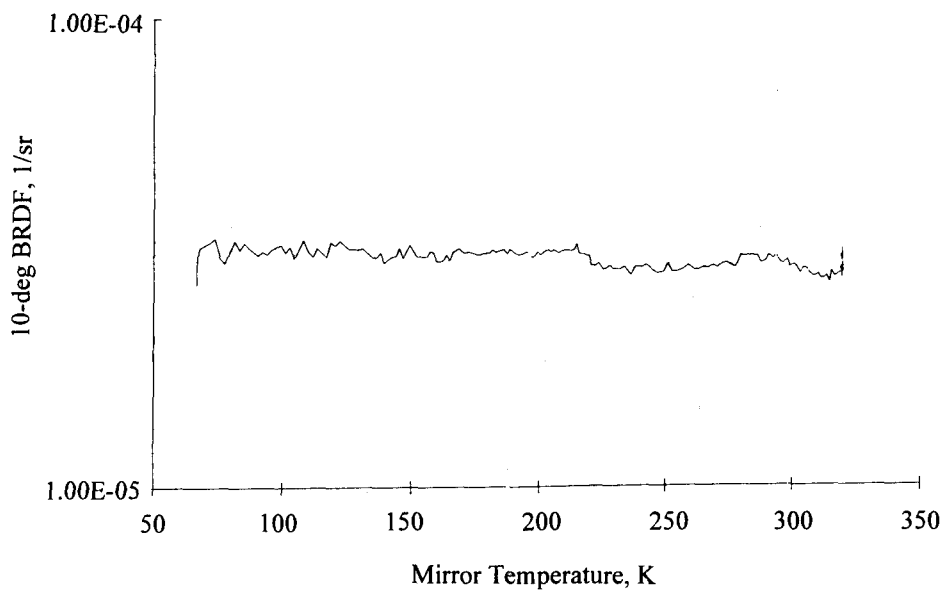


**b. Mass spectrum of effusion cell effluent at 125°C**

**Figure 39. Nusil CV2500 effluent mass spectrum.**

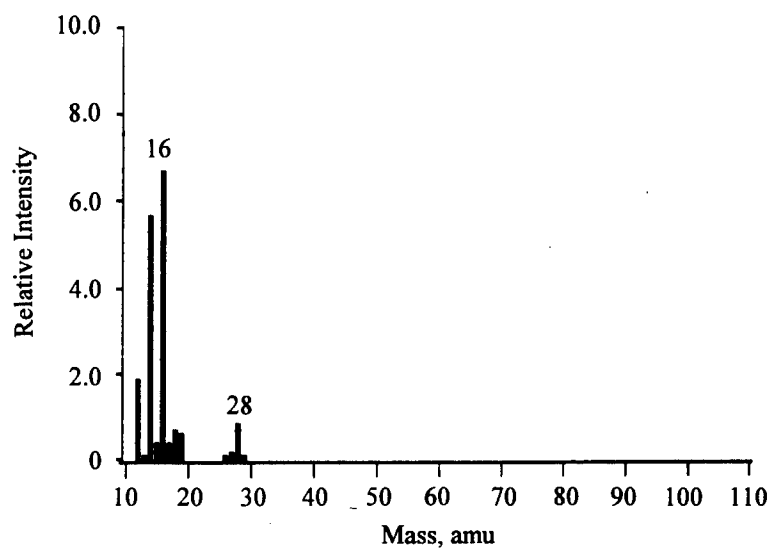


**a. QCM warmup**

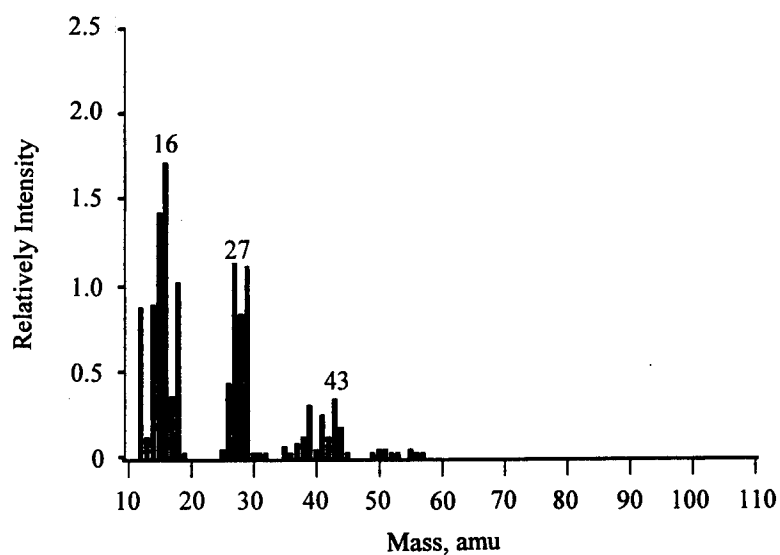


**b. Mirror warmup, 10-deg BRDF, 0.63- $\mu$ m wavelength**

**Figure 40. QCM and superpolished mirror warmup, Nusil CV2500.**

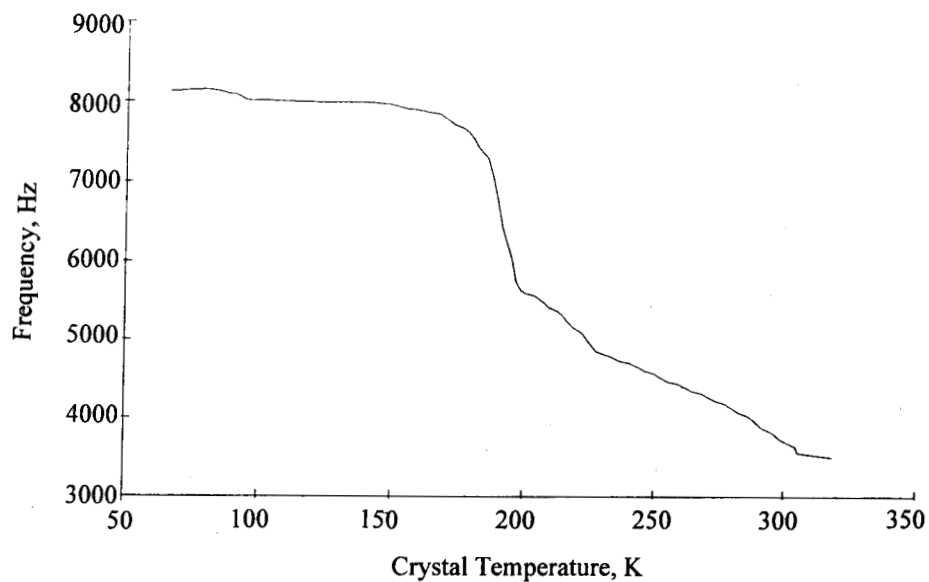


**a. Mass spectrum of effusion cell effluent at 75°C**

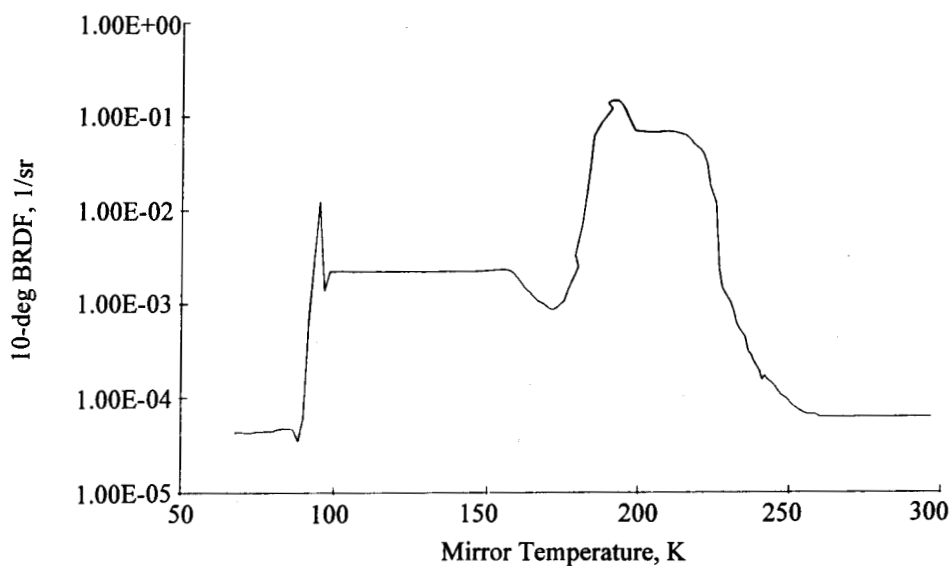


**b. Mass spectrum of effusion cell effluent at 125°C**

**Figure 41. Solithane 113/C113-300 urethane effluent mass spectrum.**

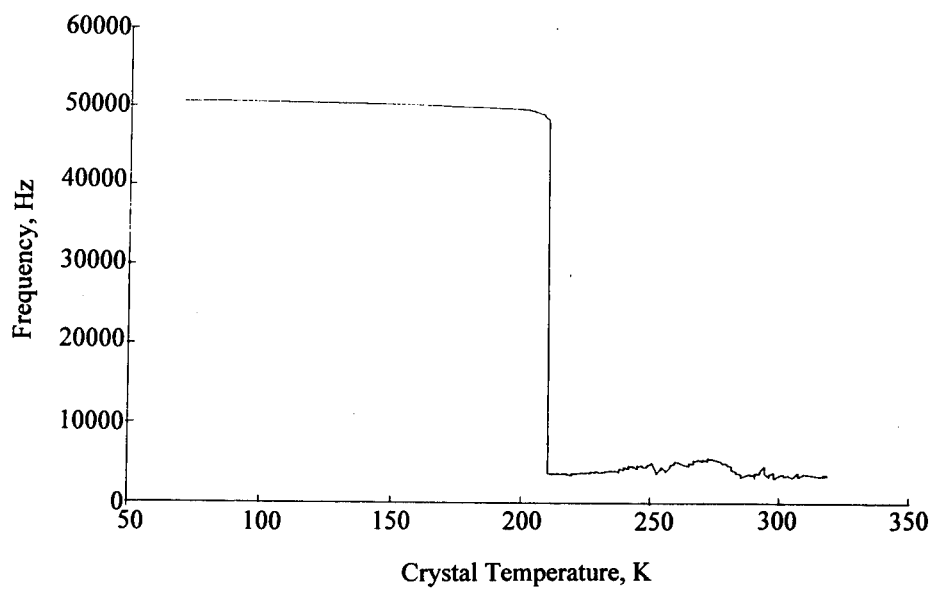


**a. QCM warmup**

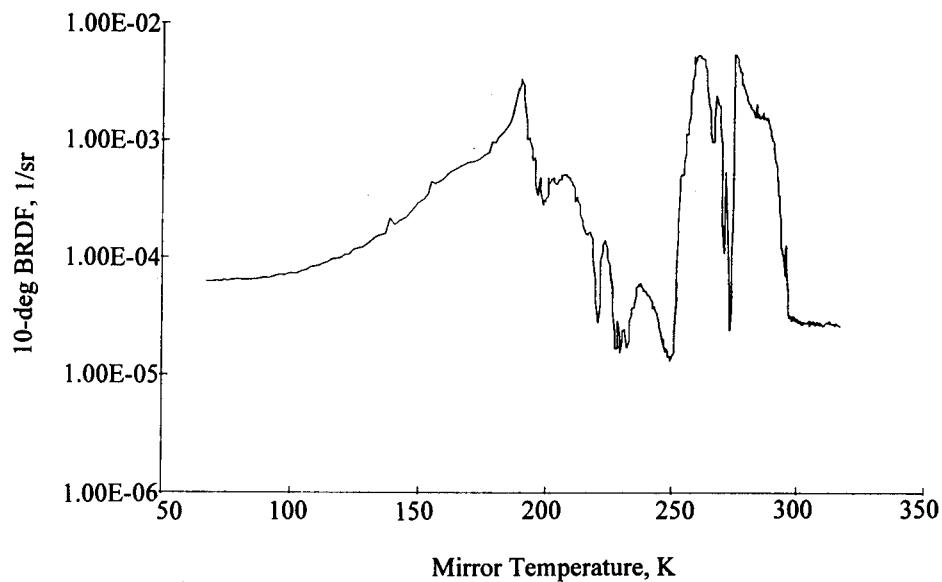


**b. Mirror warmup, 10-deg BRDF, 0.63- $\mu$ m wavelength**

**Figure 42. QCM and superpolished mirror warmup, Solithane 113/C113-300 urethane.**



**a. QCM warmup**



**b. Mirror warmup, 10-deg BRDF, 0.63- $\mu$ m wavelength**

**Figure 43. QCM and superpolished mirror warmup, RTV560 silicone.**

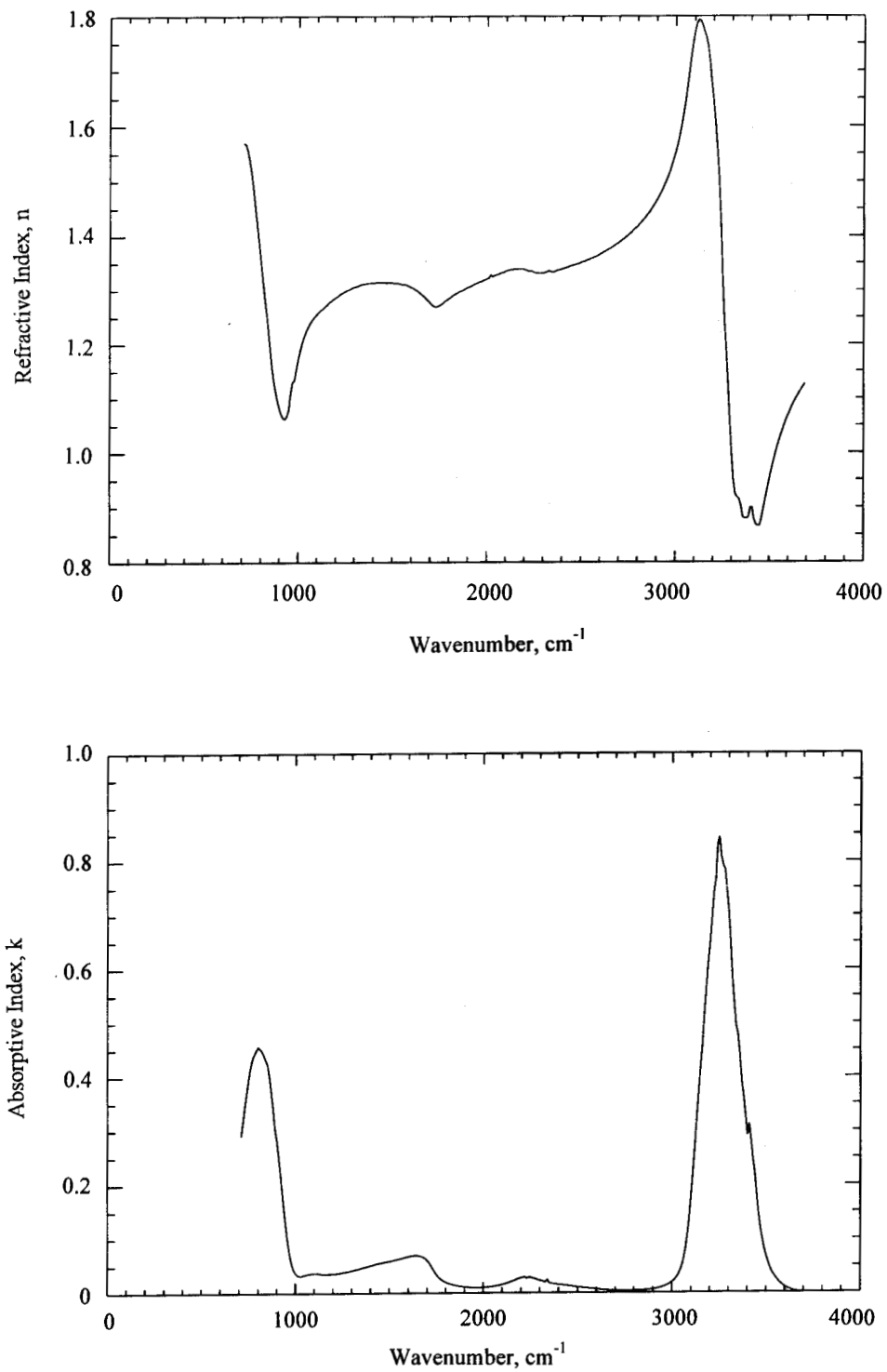


Figure 44. Optical properties of  $\text{H}_2\text{O}$  condensed on 80 K germanium.

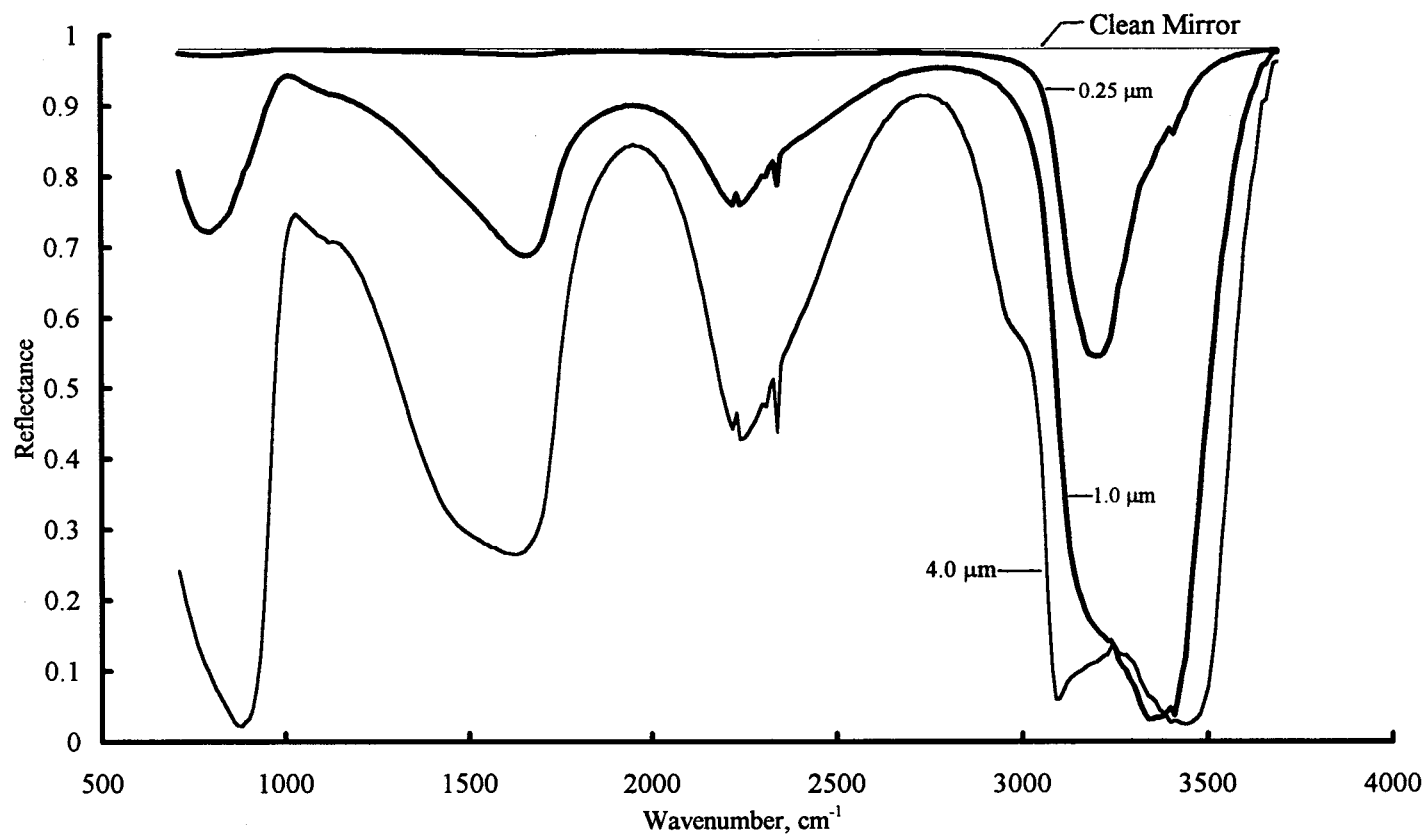
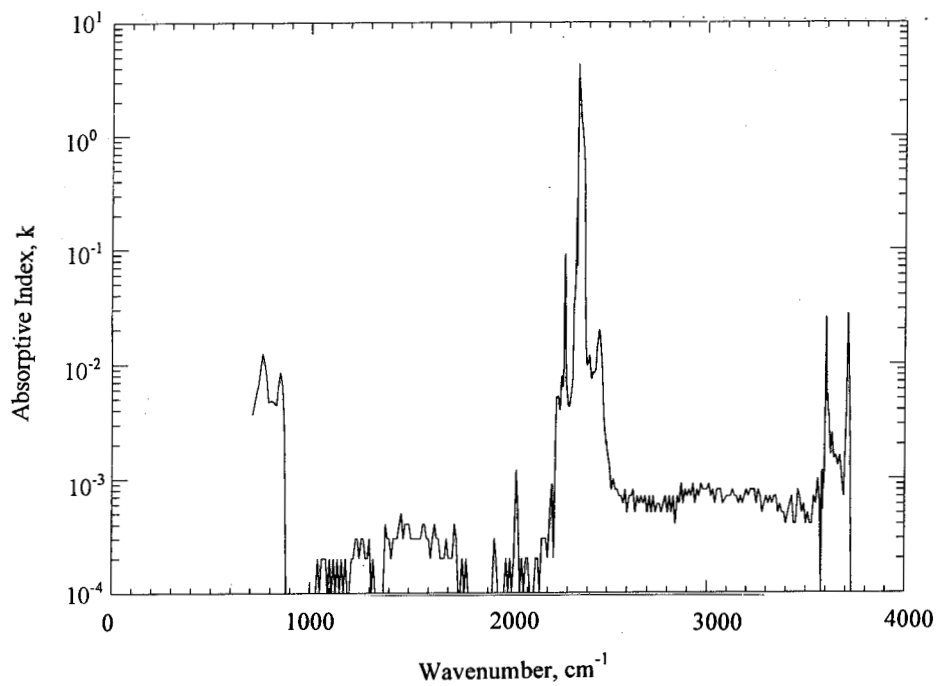
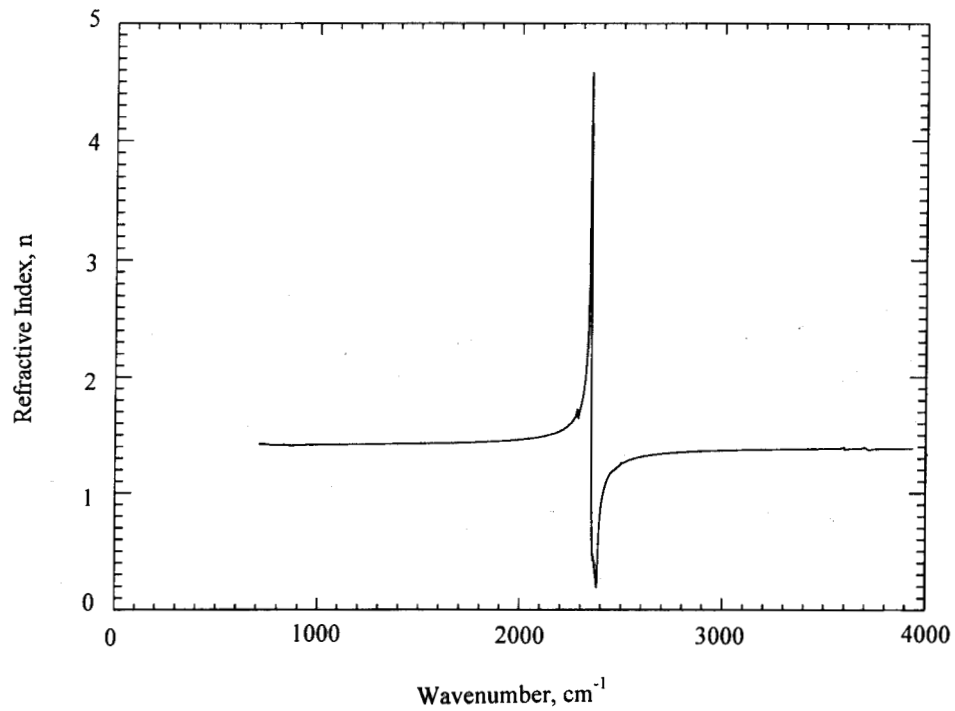
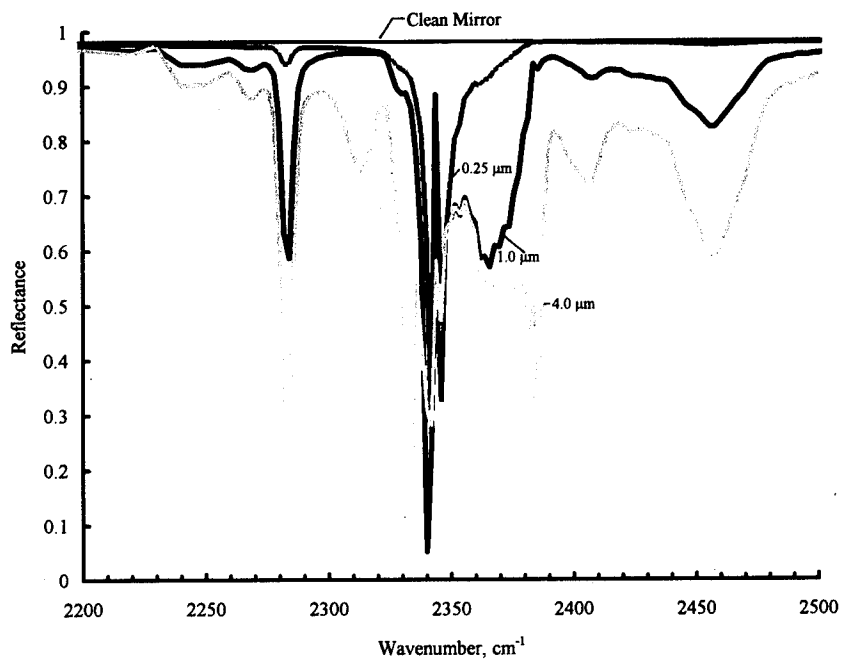
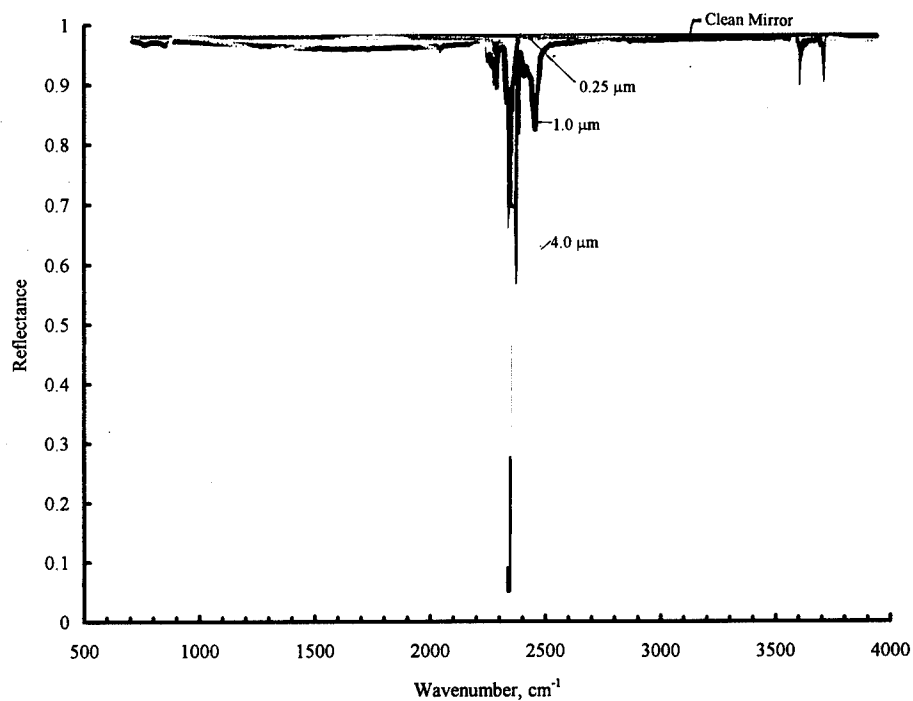


Figure 45. Calculated reflectance of 80 K aluminum mirror with  $\text{H}_2\text{O}$  contaminant films.





**Figure 46. Optical properties of  $\text{CO}_2$  condensed on 80 K germanium.**

**a. Expanded scale****b. Normal scale****Figure 47. Calculated reflectance of 80 K aluminum mirror with CO<sub>2</sub> contaminant films.**

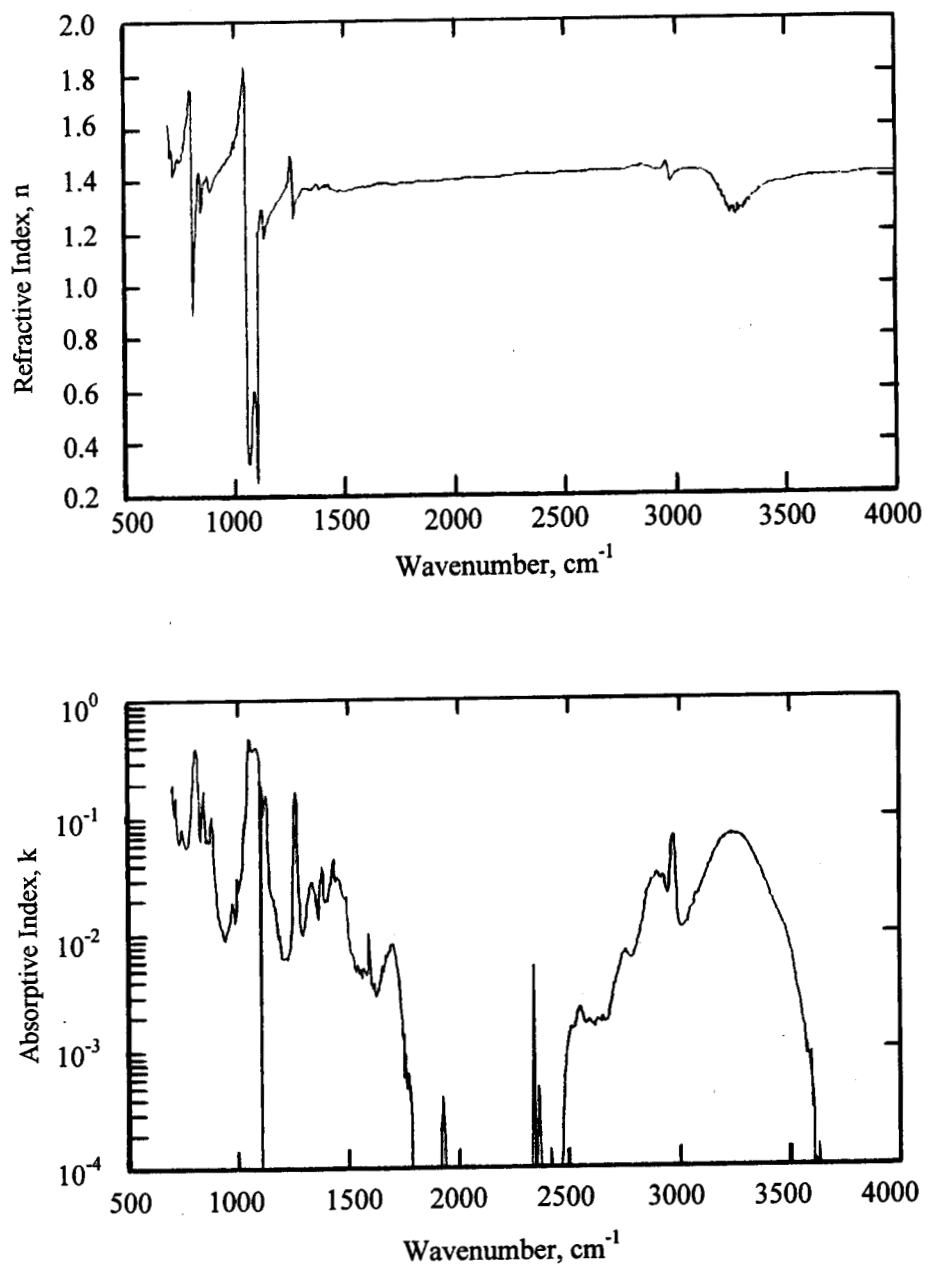


**Figure 48. Optical properties for RTV560 outgassing products condensed on 77 K germanium.**

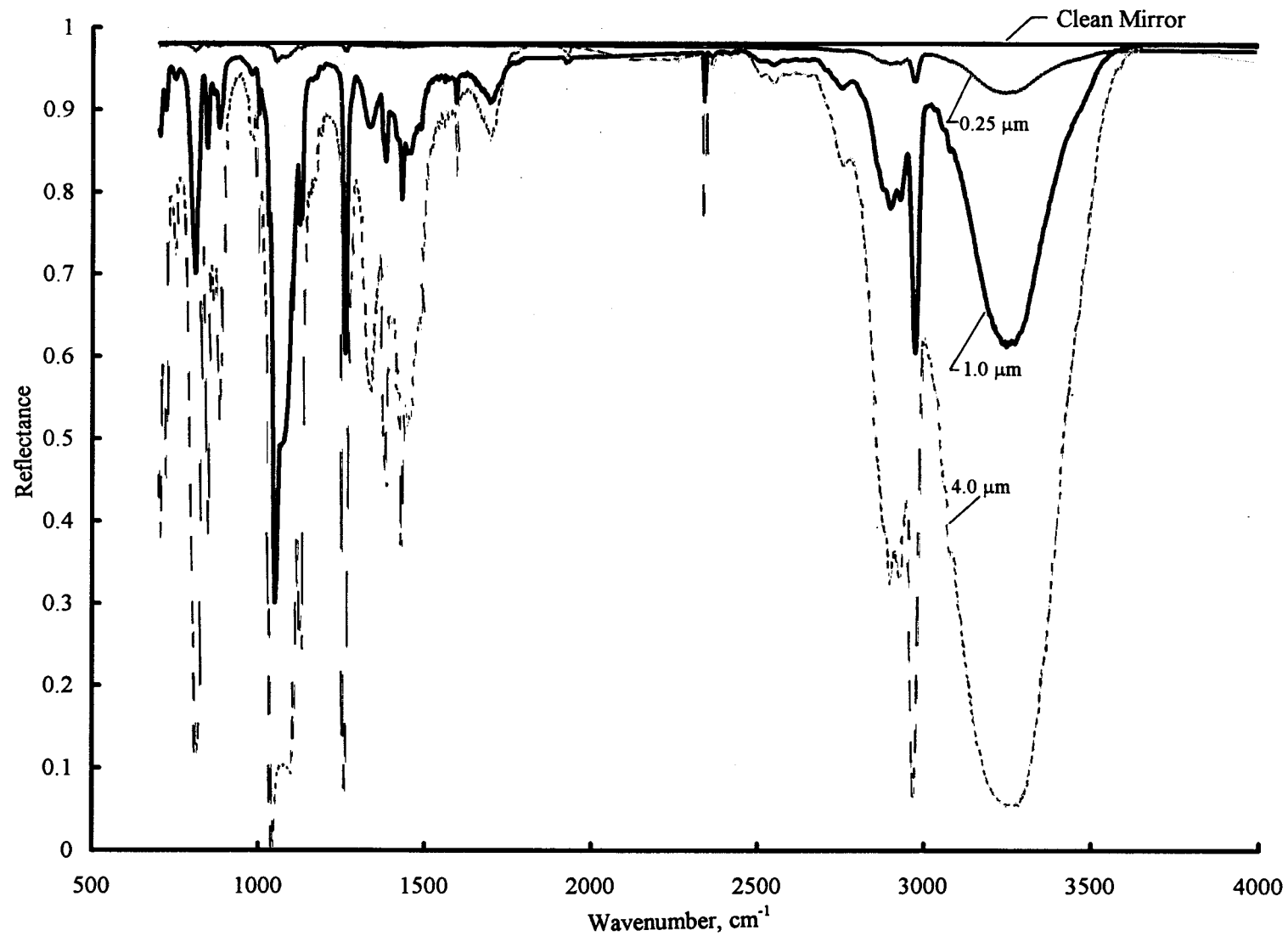
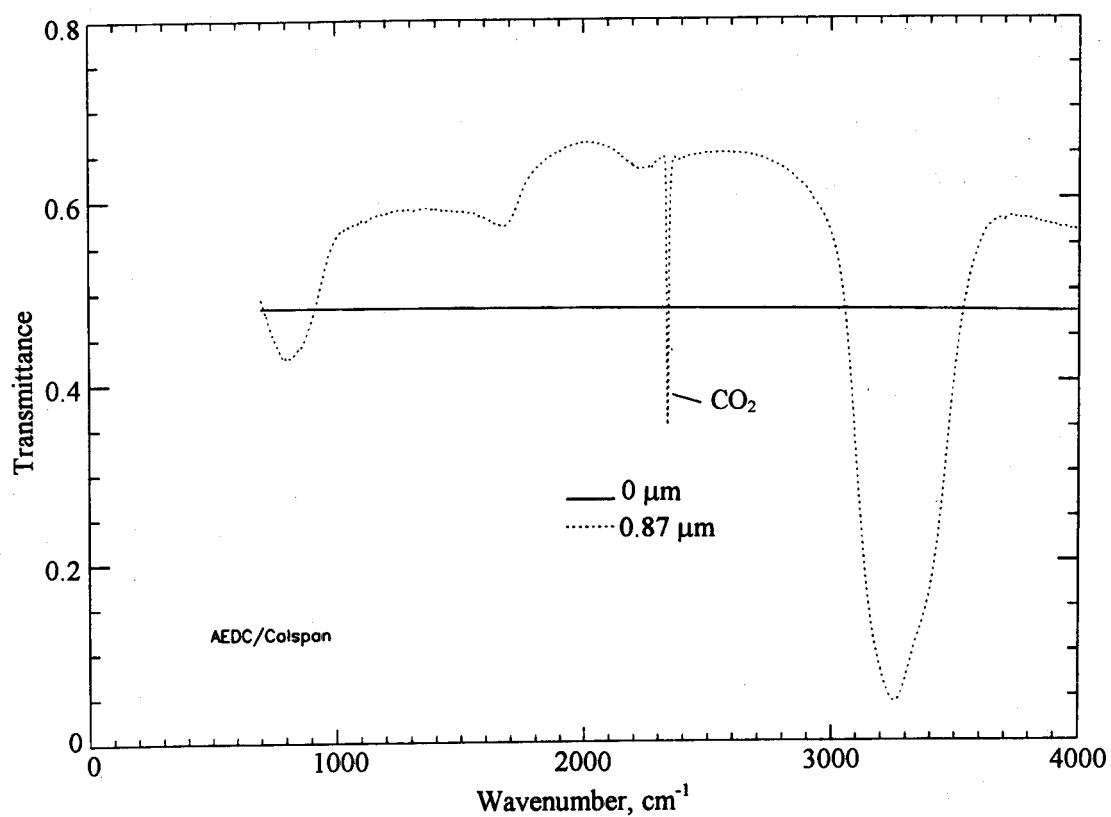
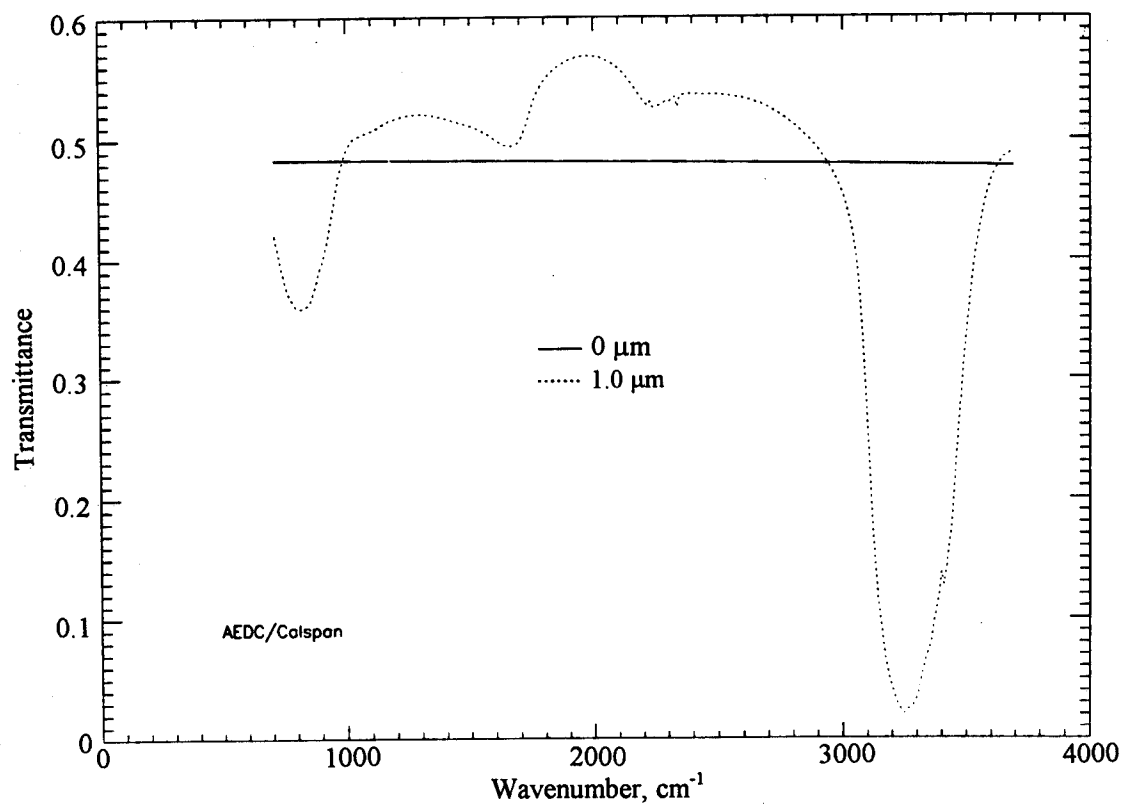


**Figure 49. Calculated reflectance of 77 K aluminum mirror with condensed RTV560 outgassing products.**

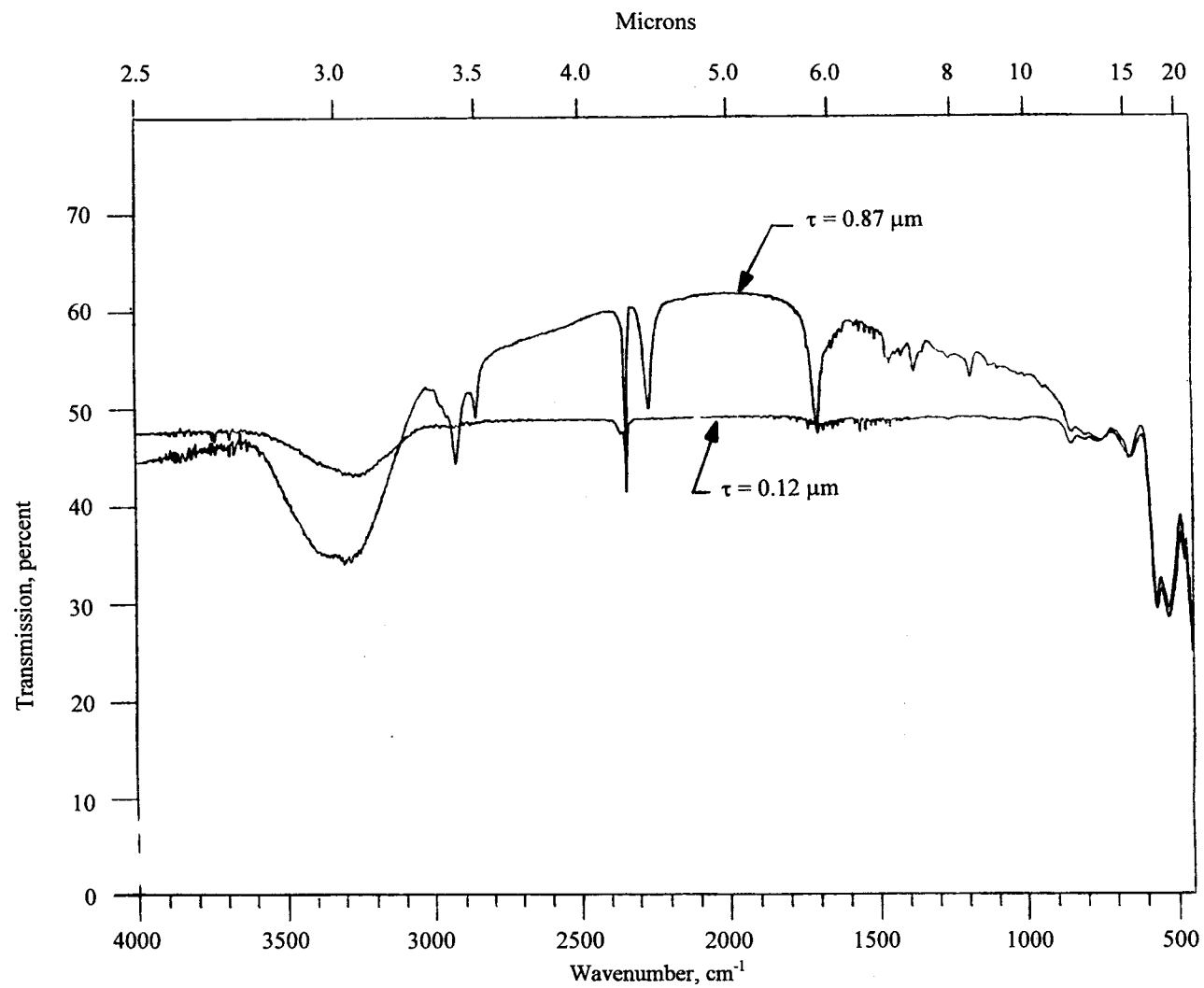


**a. RS12M polycyanate spectrum**

**Figure 50. Transmittance of 80 K germanium window with condensed RS12M polycyanate outgassing products.**

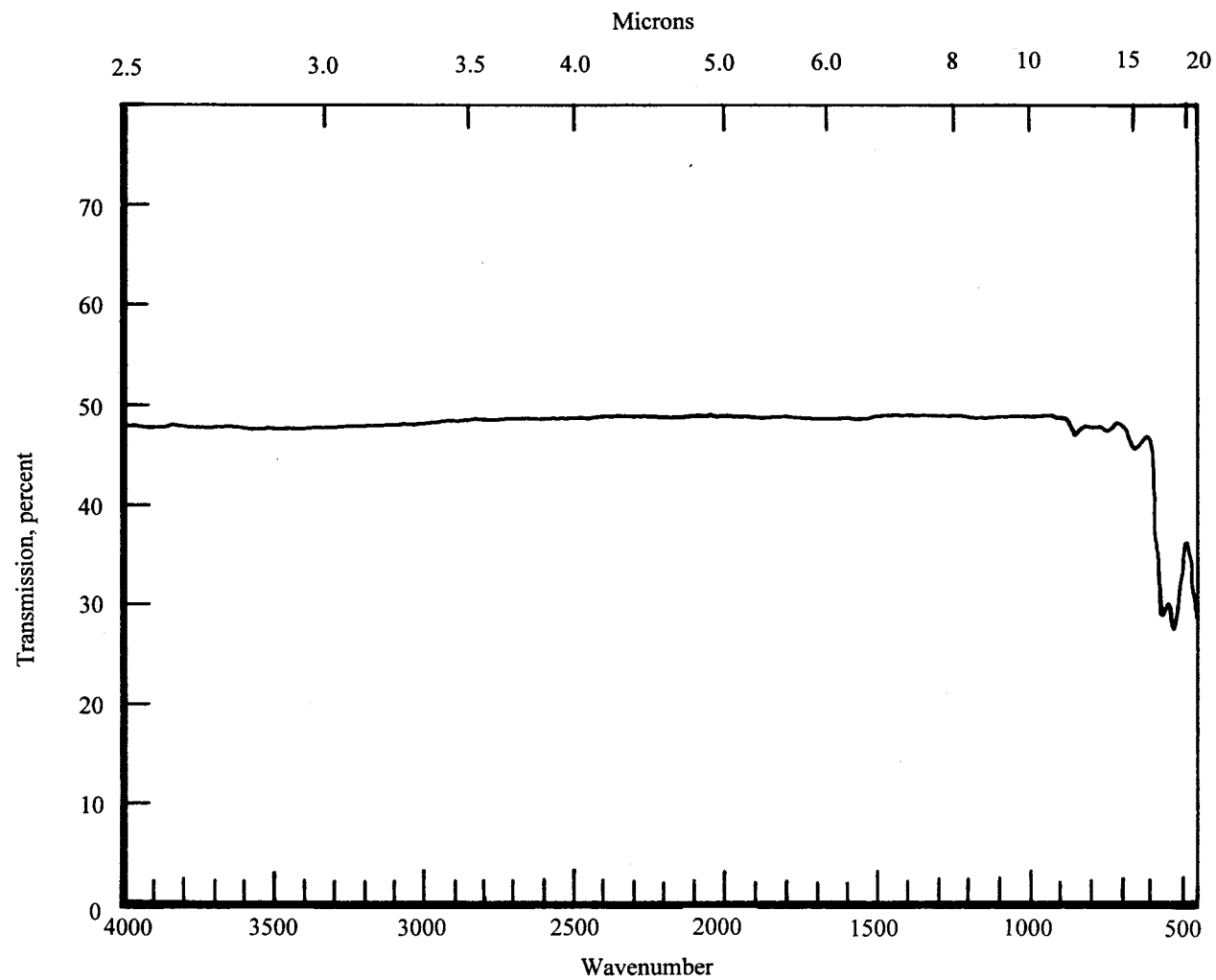


**b. Reference H<sub>2</sub>O spectrum**  
**Figure 50. Concluded.**



**a. Solithane 113 spectrum**

**Figure 51. Transmittance 77 K germanium window with condensed Solithane 113 outgassing products for film thickness of 0.12 and 0.87  $\mu\text{m}$ .**



**b. Reference spectrum for clean germanium window**  
**Figure 51. Concluded.**